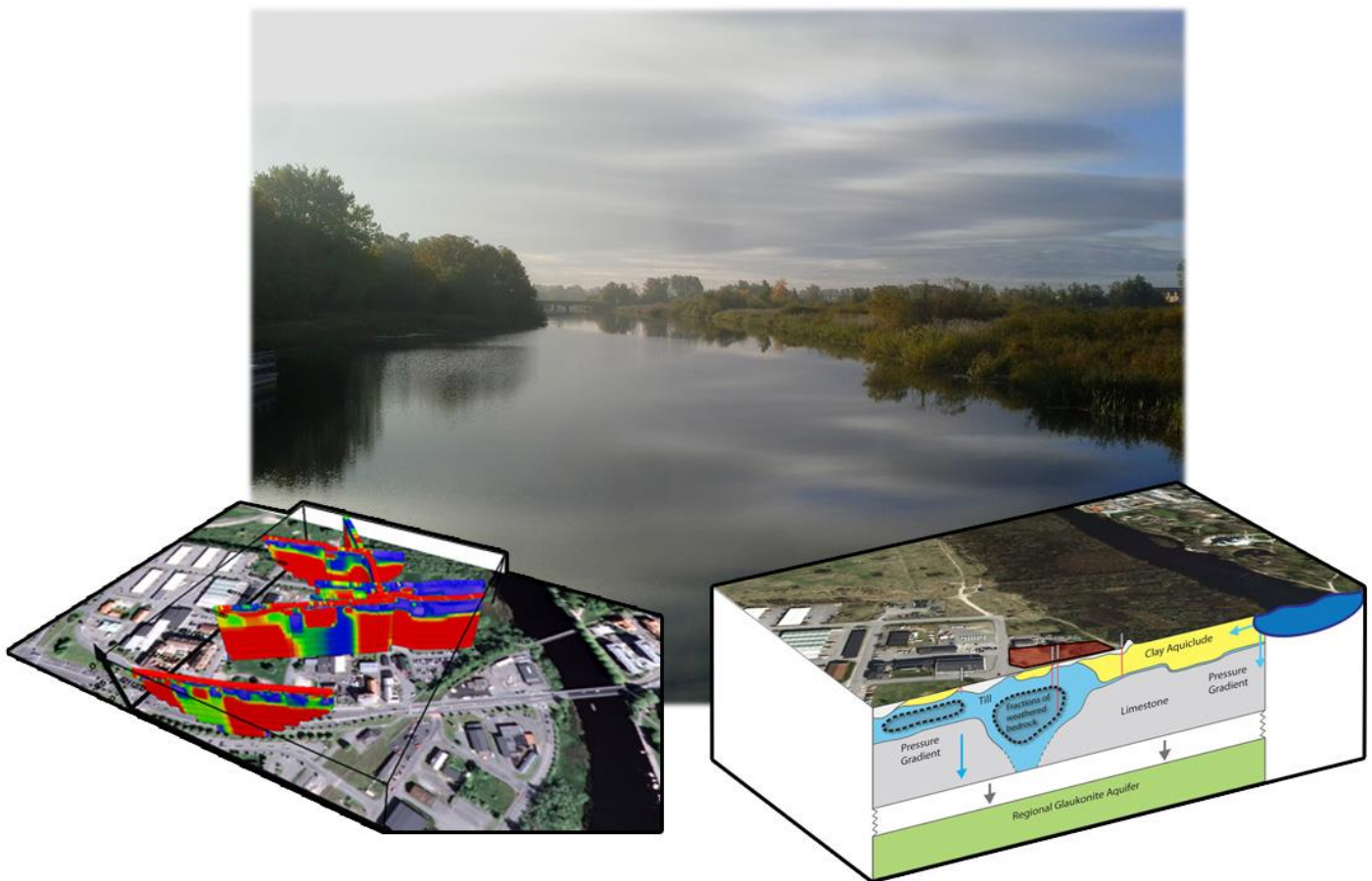




## Master's thesis

Mikael Lumetzberger

# 3-D and 2-D resistivity and IP mapping of geology and chlorinated aliphatics at Färgaren 3, Kristianstad



Academic advisor: Peter K. Engesgaard, Lars Nielsen, Torleif Dahlin

Submitted: 07/05/14

Name of department: Department of Geosciences and Natural Resource, KU

Title: 3-D and 2-D resistivity/IP mapping of geology and chlorinated aliphatics at Färgaren 3, Kristianstad

Author: Mikael Lumetzberger

Supervisors: *Associate Professor Peter K. Engesgaard* (Department of Geosciences and Natural Resource Management, KU)

*Associate professor Lars Nielsen* (Department of Geosciences and Natural Resource Management)

*Professor Torleif Dahlin* (Engineering Geology at Faculty of Engineering, Lund University)

ECTS credits: 45 ECTS points

Submitted: 7. May 2014

Cover image: Top: Photo of Helge Å River, Kristianstad, Sweden. Left: Modeled 2-D resistivity profiles. Right: Geological model.

## Abstract

A Terrameter LS instrument was used to map the subsurface of the field site: the vacant lot Färgaren 3 and surrounding area in the city of Kristianstad, Sweden. The soil and shallow groundwater at the field site is heavily contaminated with Tetrachloroethylene (PCE). The quaternary sediments, mainly a mix of till and postglacial clay, rest on Mesozoic limestone bedrock. Twenty-two electrical resistivity tomography (ERT) and induced polarization (IP) profiles were measured using a pole-dipole array. The data was modeled using inversion software Res2dinv and Res3dinv. Geology and contaminants were interpreted through comparisons with existing borehole documentation and soil samples available from previous studies.

The resistivity models were generally very consistent when compared to borehole logs and it was possible to interpret the geology of the Färgaren 3 field site and surrounding area in high detail.

The ERT results show that there is a 60 meters wide depression in the limestone bedrock under the heavily contaminated western section of the Färgaren 3 lot. Since PCE tends to sink through soils and accumulate on low-permeable surfaces like bedrock such a depression might facilitate a deeper spread of pollutants in the aquifer.

IP effects in the three-dimensional model indicate two major PCE soil concentrations in the western part of the Färgaren 3 lot, and an organic peat bed in the eastern section. The PCE IP effects correlate with the pollution sources of the previous dry cleaning business: spills from a large tank with concentrated PCE on the yard, and condensed PCE fumes accumulated under the exhaust pipes in the garden.

The extensive and accurate results from the Färgaren 2-D and 3-D models show the possibilities for urban ERT surveying as a non-intrusive, cost- and time-efficient method for subsurface imaging. ERT can be used in combination with traditional sampling methods to provide very extensive and detailed information about underground formations, greatly reduce the number of necessary boreholes, and guide a more effective placement of boreholes.

<b>1 Research Question and Aims.....</b>	<b>1</b>
<b>2 Procedure.....</b>	<b>1</b>
<b>3 Introduction .....</b>	<b>2</b>
3.1 TRUST Project .....	2
3.2 Pollutants.....	2
<b>4 Field Site: Färgaren 3, Kristianstad, Sweden.....</b>	<b>3</b>
4.1 Land Use .....	7
4.2 Regional Geology of the Kristianstad Basin.....	8
4.2.1 Bedrock and Mesozoic Deposits.....	8
4.2.2 Quaternary Sediments .....	9
4.2.3 Regional Glauconite Aquifer.....	9
4.3 Hydrogeological Conditions at Färgaren 3 .....	9
4.3.1 Glacial and Postglacial Sediments .....	11
4.3.2 Upper Sedimentary Bedrock .....	11
4.3.3 Current contamination and future risks at Färgaren 3.....	12
<b>5 Theory.....</b>	<b>13</b>
5.1 Resistivity Theory .....	13
5.1.1 The resistivity method and its applications.....	13
5.1.2 Electrical Resistivity .....	13
5.1.3 Resistivities of geological materials.....	13
5.1.4 Potential distribution and resistivity in a homogeneous half space .....	14
5.1.5 A homogeneous assumption in a heterogeneous reality and the 3-D Problem .....	17
5.1.6 Array Sensitivity.....	18
5.1.7 Electrode arrays and the pole-dipole array.....	18
5.1.8 Topography and topographic masking .....	19
5.1.9 ERT and multielectrode surveying.....	19
5.1.10 Limitations of resistivity modeling .....	20
5.2 Inversion Modeling.....	21
5.2.1 The inversion problem and difference modeling .....	21
5.2.2 Least squares inversion and Res3Dinv .....	22
5.3 Induced Polarization Theory.....	22
5.3.1 The induced polarization method and its applications .....	22
5.3.2 IP surveying and frequency domain .....	22
5.3.3 Time domain IP.....	23
5.3.4 Electrode and membrane polarization, IP effects of various materials .....	23

<b>6 Field Procedure .....</b>	<b>25</b>
6.1 Field Equipment.....	25
6.2 Field Work .....	26
<b>7 Results .....</b>	<b>28</b>
<b>8 Interpretation.....</b>	<b>31</b>
8.1 Hydrogeological model.....	31
8.2 Model Fit and Borehole Log Correlation .....	32
8.2.1 Boreholes as an independent control method.....	32
8.2.2 Borehole - 2-D line fit and model interpretation .....	33
8.2.3 3-D Model Fit.....	34
8.2.4 Numerical Fit and Model Resolution.....	36
8.3 Soil resistivities and layer characteristics .....	37
8.3.1 Filling .....	37
8.3.2 Clay .....	37
8.3.3 Till .....	37
8.3.4 Limestone.....	38
8.4 Local model formations and anomalies .....	39
8.4.1 External reference survey profile .....	39
8.4.2 Buried postglacial river banks .....	41
8.5 IP interpretation and contaminants .....	41
8.5.1 PCE extent and pollution sources.....	43
8.5.2 Why do borehole samples and IP show different pollution extents? .....	44
<b>9 Discussion .....</b>	<b>45</b>
9.1 Decontamination and future plans for Färgaren 3.....	45
9.2 3-D ERT and infrastructure: Färgaren 3 and Apennine (Italy) .....	46
9.2.1 Urban surveying and alternate geophysical methods .....	46
9.2.2 Three-dimensional ERT – Advantages and procedure .....	47
9.3 Observing and modeling PCE degradation in aquifers: Dover, Delaware (US) .....	47
9.3.1 PCE degradation and Chloride – Färgaren Chemical Samples and Resistivity.....	47
<b>10 Conclusions .....</b>	<b>49</b>
<b>11 Acknowledgements .....</b>	<b>50</b>
<b>12 References .....</b>	<b>51</b>
<b>Appendices .....</b>	<b>53</b>

# 1 Research Question and Aims

This study is a part of the project TRUST which aims to collect geoelectrical data in urban environments as a step to improve subsurface imaging techniques and increase the cost efficiency of infrastructure work. This study aims to find:

- Is it possible to efficiently, and with high data quality, map the geology and PCE contaminants at the Färgaren 3 field site (Kristianstad, Sweden) by collecting, modeling and interpreting three-dimensional induced polarization (IP) and electrical resistivity tomography (ERT) data, in an urban environment where infrastructure and electrical interference complicates geoelectrical surveying?

The quality of the geoelectrical model will be validated against borehole data from previous and ongoing hydrogeological surveys of the site.

## 2 Procedure

This 45 ECTS-points study consists of the following:

### i) Field Work

- An assessment of the field site was followed by a three-dimensional (3-D) resistivity & IP survey of the Färgaren 3 field site in Kristianstad.
- Field work was carried out in two steps to allow for intermediary evaluation and changes (electrode patterns, area of interest etc.).

### ii) Data Processing & Interpretation

- Collected data was processed and modeled in the inverse modeling software Res3Dinv.
- A hydrogeological model interpretation with regards to material from previous site investigations was made. The extent of the contaminants was interpreted based on the geoelectrical resistivity and IP data.

### 3 Introduction

There is an ongoing risk assessment of polluted sites across Sweden. This is a response to the large number of harmful local deposits from previous businesses, industries and small waste dumps left neglected during the 20<sup>th</sup> century (Nordin 2014).

The field site “Färgaren 3” in Kristianstad has been prioritized as a highly harmful polluted site in an environmental risk assessment. The soil has great concentrations of Tetrachloroethylene (or PCE, a chlorinated aliphatic that is a strong carcinogen) which originates from a dry-cleaning business that operated on site during 1906-1988. The pollution has dispersed from the site through the shallow groundwater. There is a concern for further pollution spread to the deep groundwater which is part of a regional aquifer used for drinking water (Engdahl et.al. 2011).

#### 3.1 TRUST Project

This thesis’s survey is a part of the TRansparent Underground STructure (Trust) project (TRUST 2014).

The Trust project aims to improve technology for construction of underground infrastructure, and as a subproject Trust 2.1 aims to improve geoelectrical methods for gathering data in urban environments. Trust 2.1 main objectives are:

- Developing technique for handling of urban noise and obstacles
- Developing procedure for 3-D surveys in urban area
- Improving knowledge on how to interpret contaminated soils from geoelectrical methods
- Improving detailed interpretation of geological features

As a part of that, this survey is a prototype procedure for surveying and interpreting 3-D resistivity and IP data in a contaminated, urban environment.

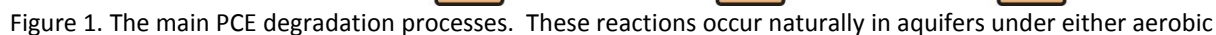
Resistivity and induced polarization surveying is commonly applied as a fast, non-intrusive method to detect contaminants in soil and groundwater (Butler 2005).

#### 3.2 Pollutants

Tetrachloroethylene (PCE) is a chlorinated aliphatic that is a very strong carcinogen through genotoxic metabolites. In studies on rats it has been shown to cause tumors in the kidneys, blood, testicles and the brain. At high temperatures, e.g. during welding, PCE oxidizes into phosgene – an extremely poisonous gas that reacts with water and forms hydrochloric acid in the lungs (Guha et.al 2012, ATSDR 2013).

PCE was commonly used as a solvent in dry cleaning and degreasing of metal parts for the majority of the 20<sup>th</sup> century. It still sees use for stain removal but with minimized exposure level to humans. It is also an intermediate chemical used for chlorofluorocarbon production (Guha et.al 2012).

PCE is a dense, colorless, non-aqueous phase liquid (DNAPL) i.e. it is a liquid that sinks through water and dissolves in water at a slow rate. These physical properties have important implications for how fast a PCE contamination spreads in an aquifer. PCE generally sinks through soil and accumulates at less-permeable surfaces such as bedrock.





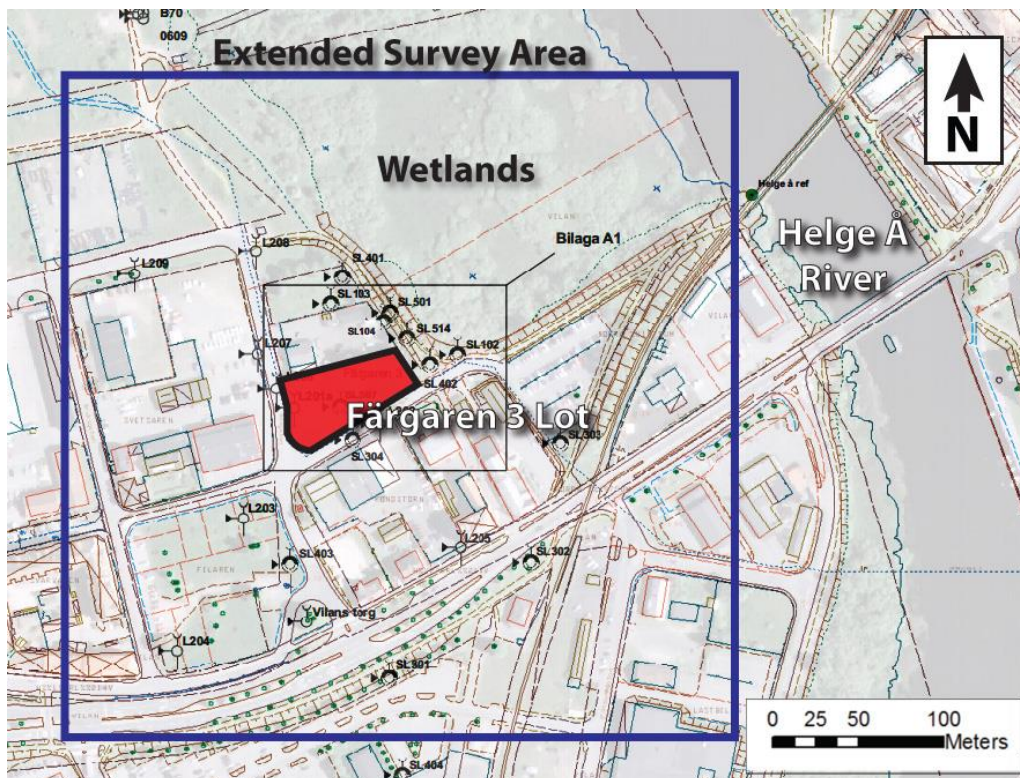


Figure 2. Field site Färgaren 3 and surrounding extended survey area. The river Helge Å runs to the east of the field site. The wetlands are the vegetated area in the north-eastern part of the picture. The circles mark the location of boreholes.

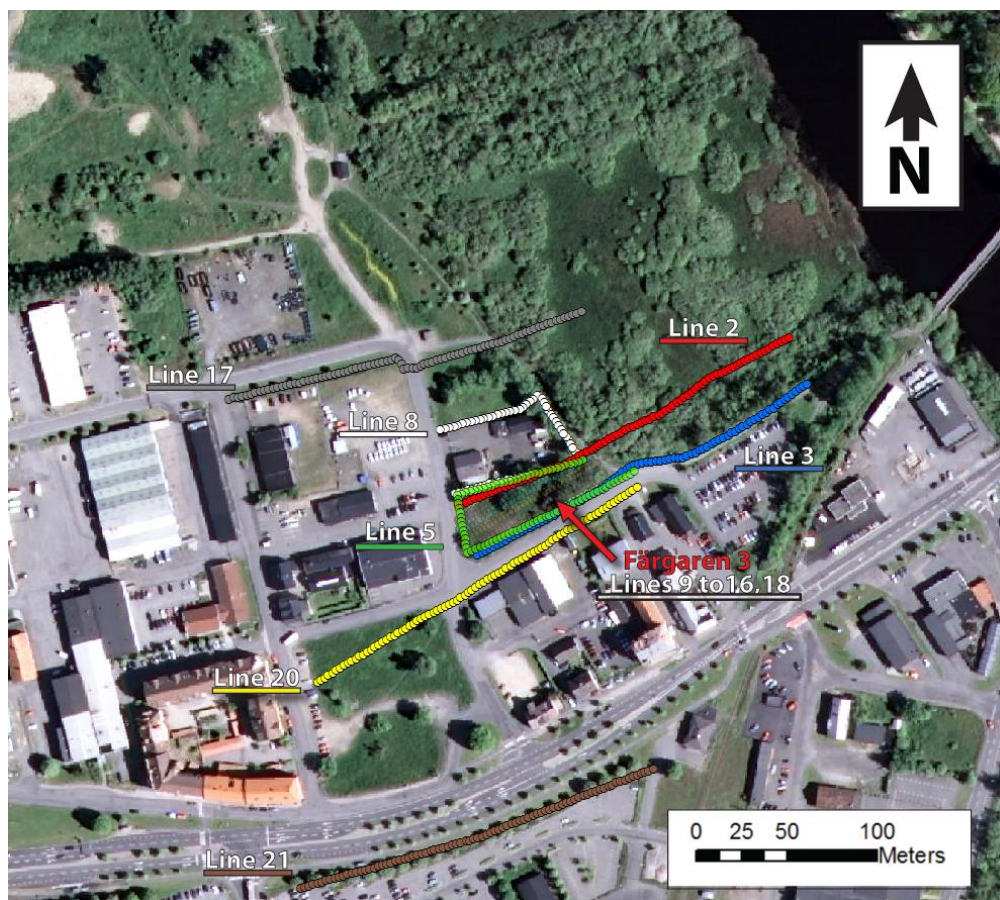


Figure 3. All field site survey lines. Each dot marks an electrode position (some missing GPS points beneath foliage have been interpolated). The wetlands are the vegetated area in the north-eastern part of the picture.



The lot is empty apart for some remaining tree stubs (cut down to avoid poisoning through fruit). During the years since it has stood vacant, the lot has become covered with grass, shrubs and various undergrowth (figure 4).

At the time of the field work, there was one mobile cabin module and one large garbage container stationed at the eastern end of the lot next to the gravel road (figure 4B).

There were four wells with metallic casing remaining from the previous surveys (Engdahl et.al. 2010, Johansson et.al 2013). In addition to these four wells there were also a large number of non-metallic sampling wells covering the lot at the time.

The wetlands and surrounding areas are shown with some illustrations figure 5.

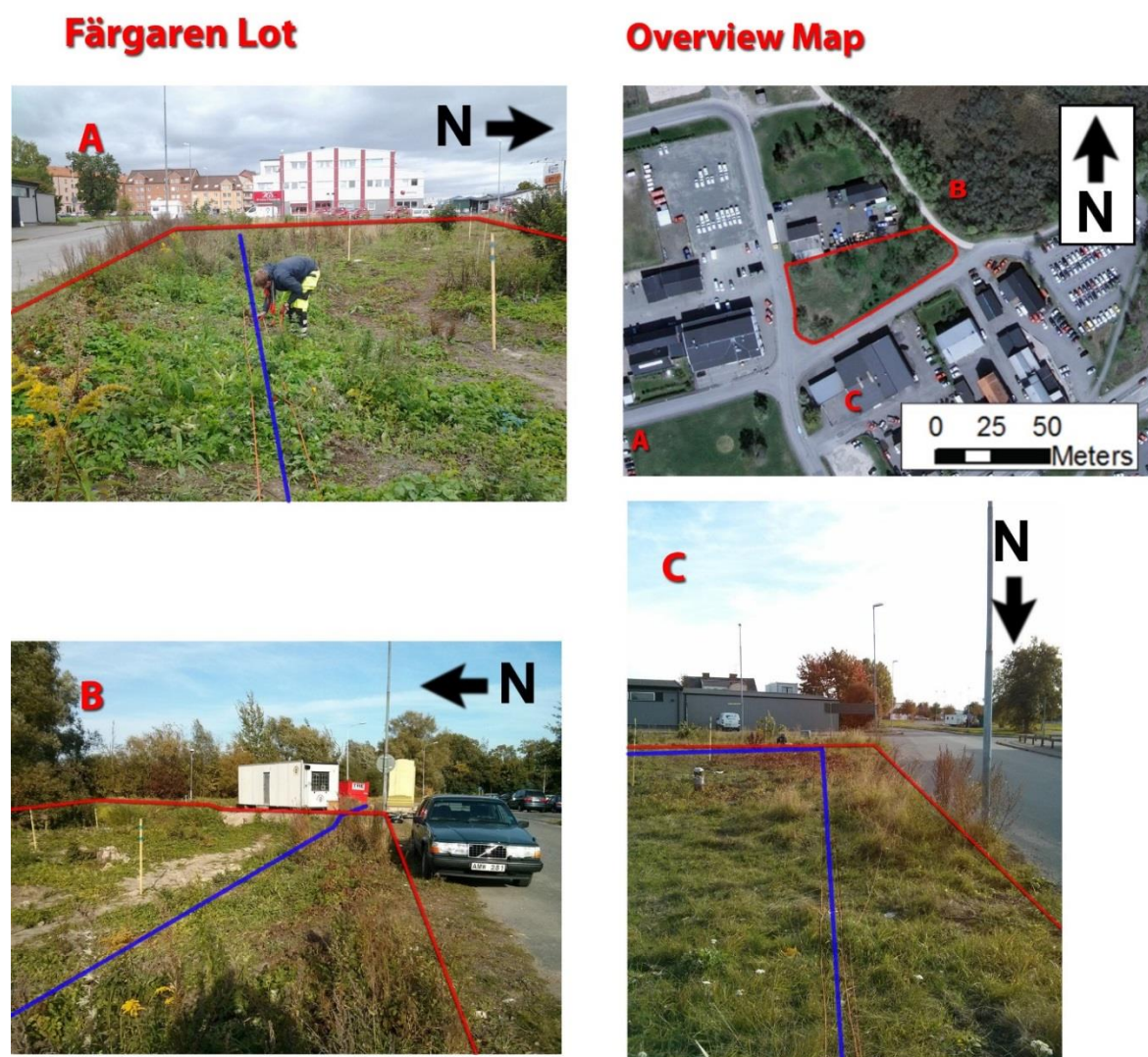


Figure 4. Photos of Färgaren 3 lot (A, B, C) and a satellite overview map. Red lines show lot borders. Survey profiles are highlighted in blue.

- *A: Picture overlooking the western part of the Färgaren 3 lot and some of the surrounding industrial and residential buildings. Survey line is shown. The sticks mark groundwater sampling wells from an ongoing consultant investigation.*

- *B: Picture overlooking the eastern part of the lot including a temporary cabin module. The vegetation behind the cabin marks the location of the flooding levy and the wetlands behind it. The head levels in the wetlands and the river is higher than at Färgaren 3.*
- *C: Picture showing northeast corner of the lot. The picture showing survey line 5, a U-shaped line bending at the western corners of the lot. The picture also showing one of the four metal cased wells (middle left) on the property that was used for the diver logging.*

## Surrounding Areas



Figure 5

- *A. Picture overlooking the first (western) section of survey line 17 (marked with blue). It is located north of the Färgaren 3 lot.*
- *B. Termination point (eastern point) of survey line 17 in the wetlands in the vicinity of the lot. The buildings are on the opposite (eastern) side of Helge Å.*
- *C. Picture overlooking the termination point (northern point) of survey line 4, located to the north of the lot.*
- *D. Picture overlooking Helge Å taken from a bridge roughly 550 meters from the Färgaren 3 lot. The remote electrode was located in the wetlands under this bridge during all surveys.*



## 4.1 Land Use

The ongoing consultant surveys and evaluations of Färgaren 3 and the surrounding area are in preparation for a decontamination of the site. The goal is to reduce the contamination and have the area assessed suitable for planned future residential buildings (Nordin 2014).

The dry cleaning business “Anders Perssons Kemiska Tvätt & Färgeri” was founded by Anders Persson in 1882 (Engdahl et.al. 2011). In 1906 it was moved to the plot at Färgaren 3 where a new building was erected for the purpose (figure 6 and 7). The business was run by the family until 1964 when it was sold to Raoul Wangel. “Wangels Kemiska Tvätt & Färgeri” operated until 1988. During the larger part of the 20<sup>th</sup> century the carcinogen tetrachloroethylene was a common solvent used e.g. during washing, and the Färgaren 3 business was among the first adopters in Sweden (Engdahl et.al. 2011).

The building was demolished in 2001 and the lot has been vacant ever since (Engdahl et.al. 2011).

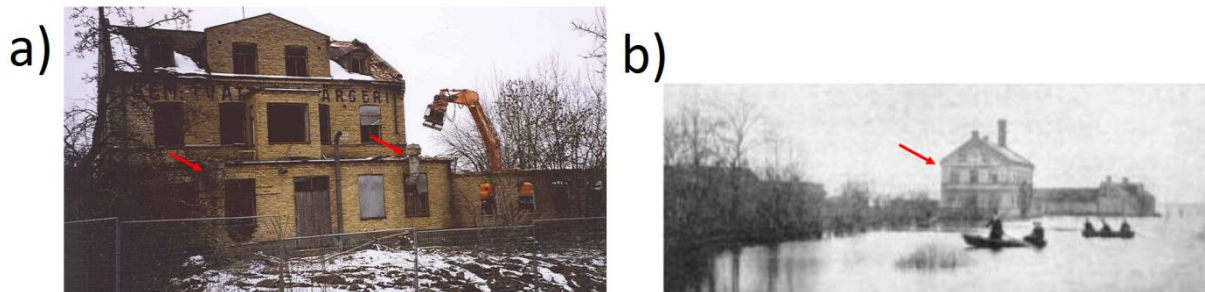


Figure 6. Färgaren dry cleaning business a) prior to demolition and b) during flooding of Helge Å in 1916 (Engdahl et.al. 2011).

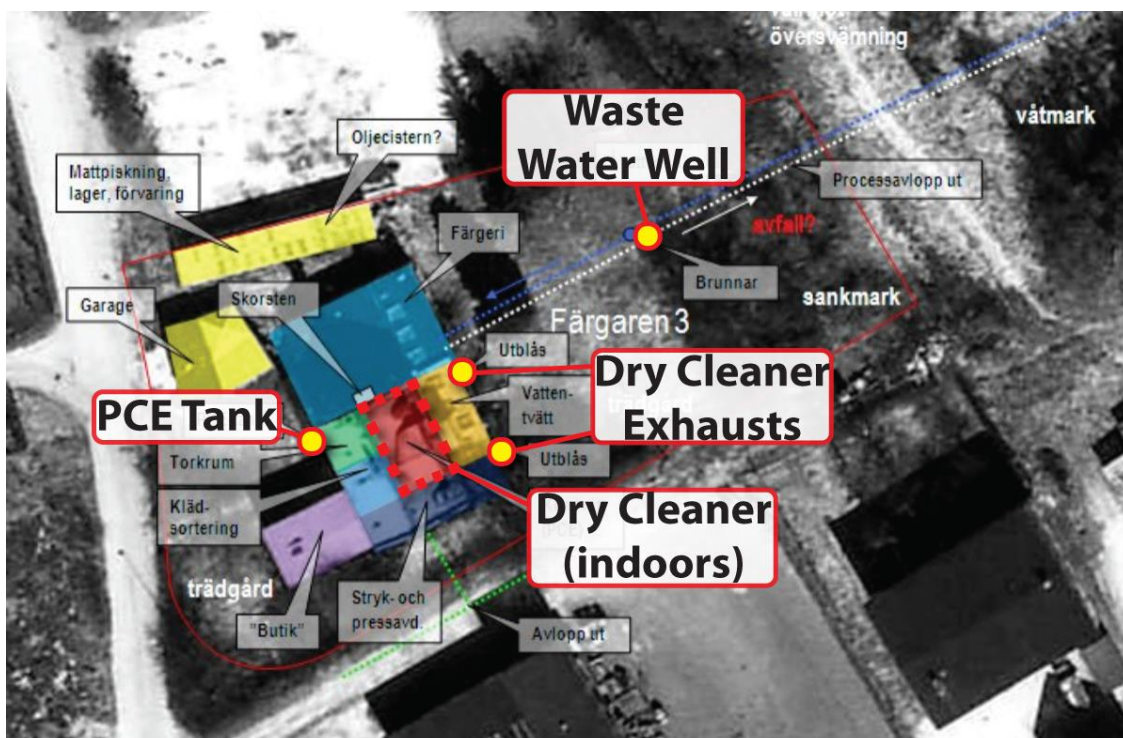


Figure 7. Photograph of the building. Site for PCE storage (left), dry cleaner exhausts, dry cleaner machine room and possible PCE waste water discharge (right) are marked in red (modified from Engdahl et.al. 2011).

## 4.2 Regional Geology of the Kristianstad Basin

### 4.2.1 Bedrock and Mesozoic Deposits

The Kristianstad basin was formed through tectonic activity during the Cretaceous period in the Mesozoic era (figure 8). The crystalline bedrock (the Fennoscandian shield) of what is today the Kristianstad plain was tilted downwards Southwest, where a fault zone forming the Linderödsåsen and Nävlingeåsen horsts were created – forming a regional basin-range formation (Christensen 1984).

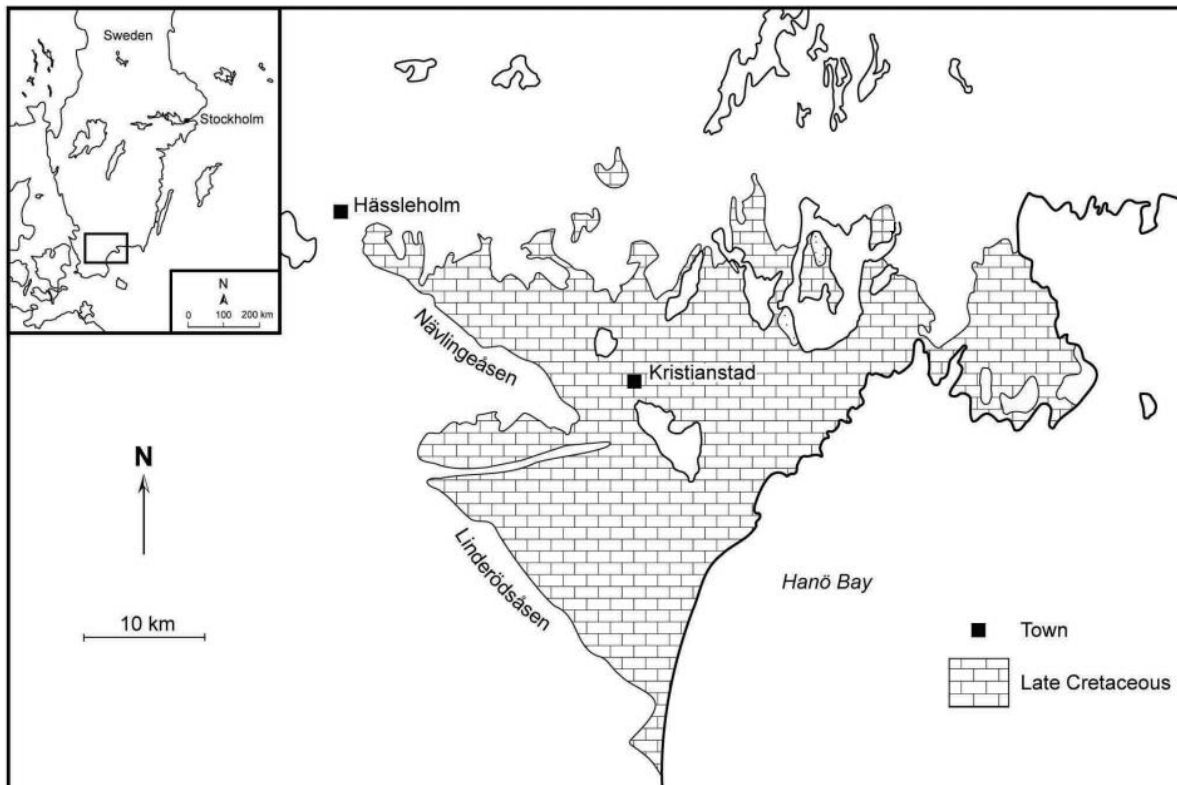


Figure 8. Map showing the distribution of calcareous deposits in the Kristianstad basin, bordered in the southwest by the Linderödsåsen and Nävlingeåsen horsts. Modified from Lindgren and Siverson, 2002.

In the warm near shore environment during the cretaceous there was a continuous sedimentation in the basin, and the limestone and sand deposits are rich in fossils. The topography of the crystalline and sedimentary bedrock in the area is heterogeneous and uneven. The humid climate and transgressing shorelines in the area during the Mesozoic era caused extensive erosion (Christensen 1984).

The oldest Cretaceous sediments are calcareous glauconitic sands overlain by limestone. The thickness of the cretaceous deposits are up to 200 m in the southwestern part of the basin. They generally become thinner towards to the northeastern part of the basin (Christensen 1984).

#### *4.2.2 Quaternary Sediments*

Till is the dominating quaternary sediment. The thickness of the quaternary sediments vary between 0-15 m. In the regions of the plains where they are thickest, the stratigraphy reflects the development during the late ice age and the Holocene: From bottom to top, after crystalline rock and cretaceous sediments it consists of, till, glaciofluvial deposits (gravel and sand), postglacial clay and postglacial sand. The estimated local sea level maximum is up to 55 maml and the postglacial sand is several meters thick in many places in the region. These sands mark locations of old shorelines and waterways. Organic sediments are found in proximity to present lakes and waterways such as Helge Å (Ringberg 1991).

At the Färgaren 3 site the quaternary sediments are 15-20 m thick, followed by cretaceous limestone with an estimated thickness of c:a 80 m. Below the limestone the cretaceous glauconite sand layer is estimated to be c:a 35 m thick, followed by crystalline bedrock (Z3).

#### *4.2.3 Regional Glauconite Aquifer*

The glauconite sands of the lower cretaceous stratigraphy forms a large continuous aquifer below the Kristianstad plains. There is a large extraction for drinking water and public utilities as well as for industrial use. The aquifer is an important environmental resource to the region and is to be protected from potential contamination (Engdahl et.al. 2011).

### **4.3 Hydrogeological Conditions at Färgaren 3**

This project report has utilized existing documentation from extensive field surveys carried out by consultancy companies for the township of Kristianstad. These consultancy studies have been used for risk assessments and form the basis for a planned near-future decontamination of the field site (Engdahl et.al. 2011).

Below is a list of the methods used to collect data in the previous field studies (Engdahl et.al. 2011, Johansson et.al 2013):

- Extensive borehole drilling and borehole logging
- Soil and tree chemical sampling
- Extensive groundwater chemical sampling
- Sinkers and divers measuring continuous groundwater head levels
- Hydraulic conductivity estimations through slug tests
- Hydraulic conductivity estimations through pumping experiment

From this data, a geological model of the soil stratigraphy (figure 10) has been interpreted by Engdahl et.al. 2011 (Hifab AB):

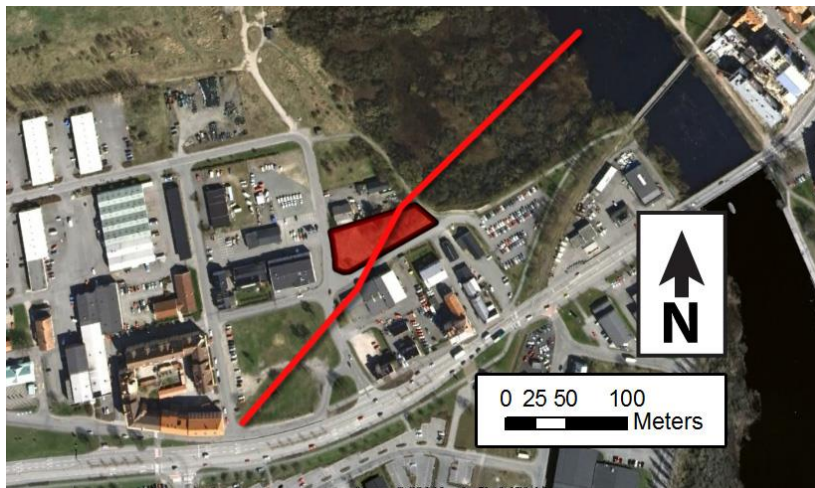


Figure 9. Path for model section figure 10 shown below. The highlighted red area marks the Färgaren 3 lot (modified from Engdahl et.al. 2011).

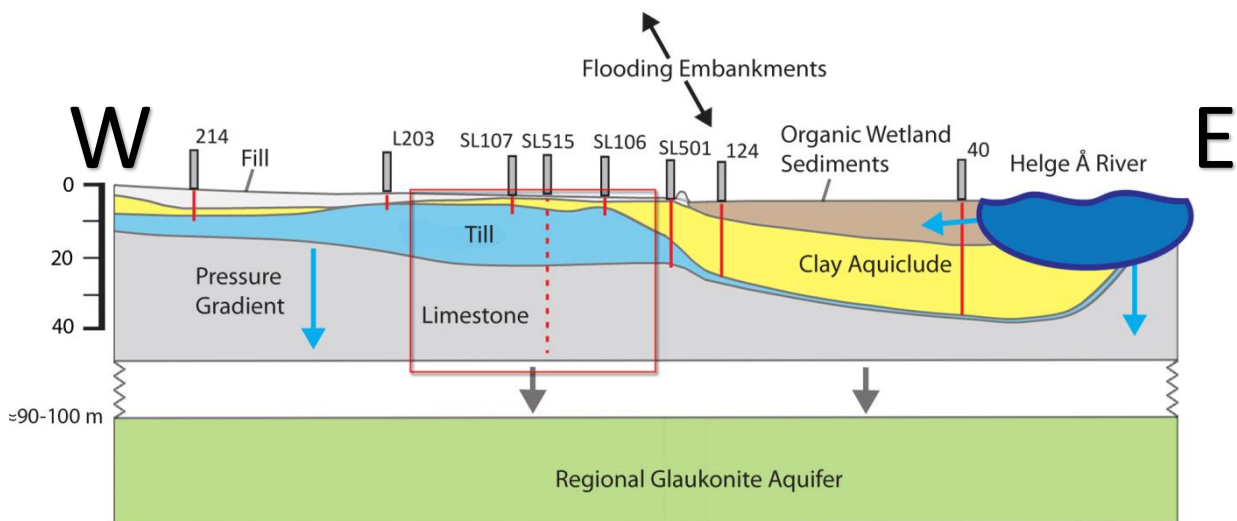


Figure 10. Hifab's geological model of the Färgaren area. The highlighted red area marks the Färgaren 3 lot (modified from Engdahl et.al. 2011).

The till is relatively thick compared to the clay in the western part of the lot. In the eastern section this distribution between till and clay starts to change and shows similarities to the wetland environment as the cross section approaches the river. The groundwater table has been observed to vary between 2 to 4 meters below the surface of the lot, which is lower than the corresponding head level measurements of the Helge Å River. A relationship between the head levels in the till and glaukonite sand aquifer and nearby industrial pumping outtake has been observed.

Estimated hydraulic conductivities of the till and limestone are presented below.

Lithology	Conductivity ( $\text{ms}^{-1}$ )
Till	$1\text{-}4 \cdot 10^{-5}$
Upper Limestone (23 m depth)	$3,6 \cdot 10^{-6}$

There are also regional estimates of vertical conductivity which are roughly one magnitude lower for both till and limestone (Engdahl et.al. 2011).

#### *4.3.1 Glacial and Postglacial Sediments*

The surface layer is a heterogeneous mix of construction fill (occasional broken bricks) and dirt. The layer is found to be somewhat thicker in the western part of the lot (up to 2 m deep where the basement was located), but varies across the entire lot between a few decimeters to ca. 1 m. Immediately east of the lot, the fill material of the embankment, which also underlies the gravel road, is 4-5 m deep.

Below the filling material there is a layer described as varved silty clay with a thickness mostly between 1 to 3 meters in the western part of the lot, although in some locations it is thinner or not observed at all (Engdahl et.al. 2011).

The postglacial clay is followed by a section of till that is relatively thick, between 8 and 14 meters in the western part. Its character is generally described as silty sandy chalk till, though the ratio between coarse and fine material and the grain size composition of the sediment varies between the different boreholes in the lot. Cobble, coarse gravel and in one borehole occasional boulders were also present in the soil (Engdahl et.al. 2011). Infiltration to these more permeable sediments is likely reduced to a small leakage in most of the local area due to the confining clay layer (Johansson et.al 2013).

In the easternmost 15 meters of the plot, the thickness of the clay increases greatly, and instances of coarser sediments are found within it, padded with peat sediments. In Hifab's model, this has been interpreted as a historical shoreline from a postglacial period when the river had a wider span (Engdahl et.al. 2011)

#### *4.3.2 Upper Sedimentary Bedrock*

The soils rest on an approximately 80 m thick limestone formation overlying a deeper glauconite sandstone aquifer.

The limestone immediately beneath the till was found to be heavily fractured and weathered to a point where it was difficult to extract in situ samples with the drill. The till contains a lot of eroded limestone, and since the drill crushed and mixed the limestone, it was difficult to distinguish a boundary between soil and bedrock in the weathered transition zone. The Hifab report (Engdahl et.al. 2011) notes that this makes their estimate of the bedrock position somewhat uncertain.

The solid pieces of rock extracted from a few meters below the weathered boundary zone show medium to fine grain size sand consolidated in a finer material. These core samples do not show any large fractures or pore networks, although the survey does not directly investigate the character or fracturing of the deeper sections of the limestone.



#### 4.3.3 Current contamination and future risks at Färgaren 3

When dimensioning a risk assessment, there are three main concerns: i) pollution concentrations, ii) proximity to sensitive areas, and iii) potential pathways of exposure needs to be considered.

In 2010 the PCE concentration on the Färgaren 3 lot had concentrations up towards 9100 times higher than what is deemed safe for the desired land use, and the shallow groundwater concentration in the upper aquifer had concentrations up to over 3700 times above what is considered very harmful. In addition to these concentrations, the derivative products (figure 1) were also present in toxic concentrations (Engdahl et.al. 2011). Products of PCE decomposition spreading through the shallow groundwater aquifer was estimated by Hifab in 2011 (figure 11).

Furthermore, the underlying glauconite aquifer is considered to be a valuable national natural resource, and it is of crucial interest to prevent any contamination (Engdahl et.al. 2011).

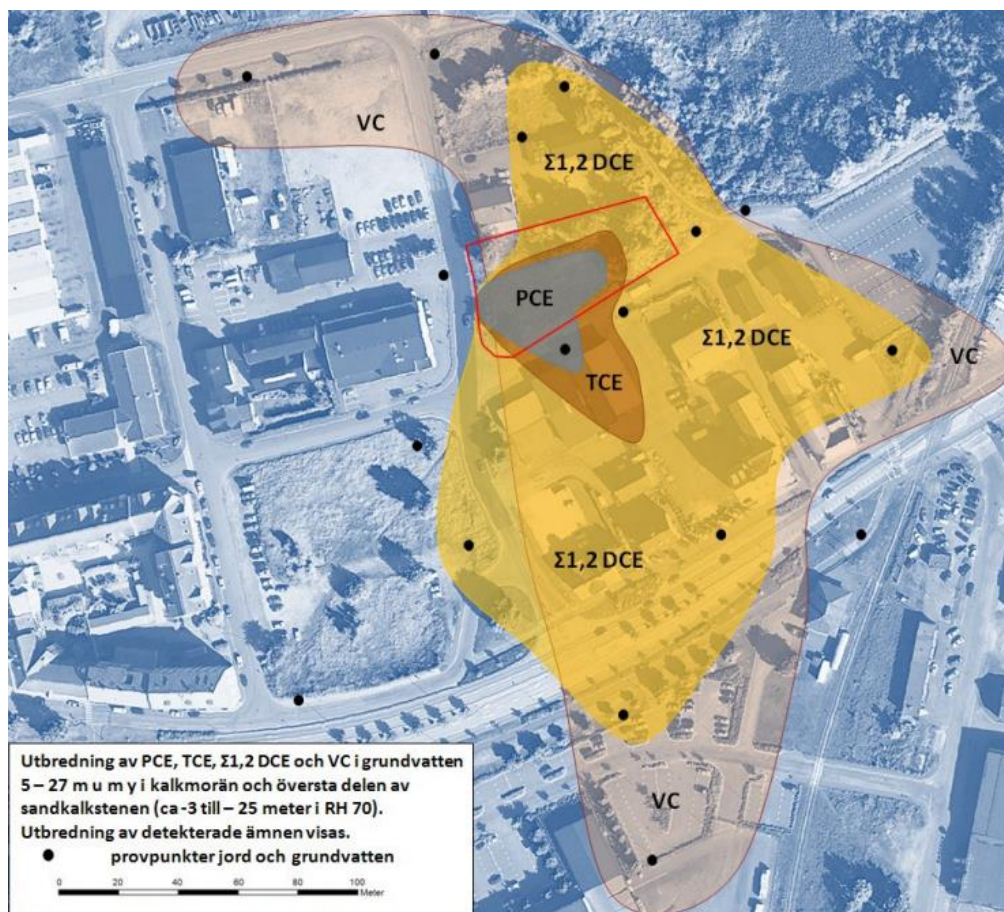


Figure 11. Hifab's estimated contamination plume of PCE and decomposition products around the Färgaren 3 lot (marked in red). Figure from Engdahl et.al. 2011.

## 5 Theory

### 5.1 Resistivity Theory

#### 5.1.1 The resistivity method and its applications

Resistivity survey techniques have been used since the early 20<sup>th</sup> century by e.g. Frank Wenner and the Schlumberger brothers (who also founded the Société de Prospection Electrique) (Loke 2004, Barker 2004). The method has become more widely adopted in the last decades as improved instruments and increased computational power have become available. Modern geoelectrical instruments are used for mineral and oil prospecting, geothermal exploration, pollution mapping at contaminated sites, in construction projects, archeological prospecting and for various hydrogeological purposes (Loke 2004, Butler 2005).

#### 5.1.2 Electrical Resistivity

Resistivity  $\rho$  ( $\Omega m$ ) is the vector form of resistance  $R$  ( $\Omega$ ) and the reciprocal of conductance ( $S$ ) – the opposition to the passage of an electric flow.

Resistivity surveys rely on Ohm's law (equation 1, 1827) which states that the potential and current in an electrical field are linearly related through the resistance of the conducting material. Resistivity surveying is a galvanic geoelectrical method, where current mainly flows electrolytically.

$$\begin{bmatrix} I = R^{-1} \cdot V \\ J = \rho^{-1} \cdot E \end{bmatrix}$$

Equation 1. Ohm's law stating the relationship between current ( $I$ ), resistance  $R$  and potential  $V$ . Below it is formulated in vector form where  $J$  is current density ( $A \cdot m^{-2}$ ),  $\rho$  is resistivity ( $\Omega \cdot m$ ) and  $E$  is electric field intensity  $V \cdot m^{-1}$  (Loke 2004).

The aim of resistivity surveying is to gather information about the physical properties of the subsurface. Different geological materials have different resistivities, and from the values it is possible to infer geological boundaries and structures. (Loke 2004, Butler 2005).

#### 5.1.3 Resistivities of geological materials

The resistivities of different geological materials vary greatly (figure 12). Igneous rocks generally display the highest values. Sedimentary rocks, which are more porous, can be expected to be some orders of magnitude lower. Unconsolidated soils have the lowest resistivities. A high (saturated) porosity and clay content will significantly increase the conductivity of a soil (Loke 2004). Clays have the capability to adsorb large amounts of ions, and even a small clay presence can lower the electrical resistivity of a soil significantly (Waxman 1968).

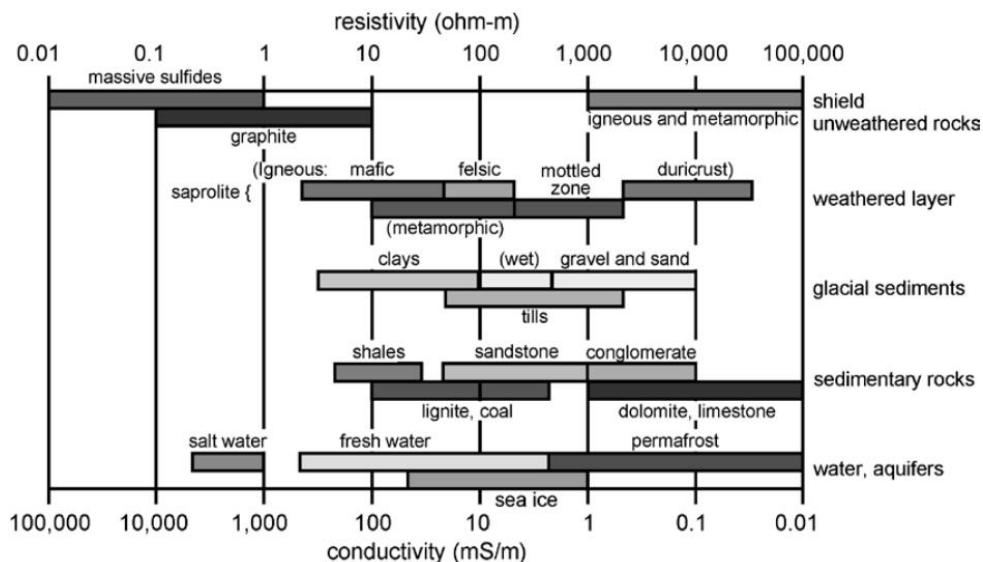


Figure 12. Typical ranges of earth material resistivities for various materials. Conductivity (Siemens) is the reciprocal of resistivity. Note the logarithmic scale and the resistivity ranges of water and salt water (Palacky 1987).

Generally, most geological materials are poor conductors (sulfide ore and graphite are two notable exceptions). The saturated porosity and resistivity of the pore fluid (mainly the chloride concentration) has a decisive impact on the resistivity. This causes the resistivity intervals between several sedimentary rocks and soils to overlap. If the pores are filled with air, the geological material will show a high resistivity. This is an important consideration when interpreting the results. There is no direct correlation between a resistivity value and a lithology (JEP, Butler 2005).

Other factors such as mineral content will cause the resistivity of e.g. different igneous rocks to differ from each other. Local resistivity changes may also reflect fracture zones filled with pore water, ore bodies or other structures (JEP, Loke 2004).

#### 5.1.4 Potential distribution and resistivity in a homogeneous half space

A hypothetical homogeneous one-layered earth model is useful to illustrate the fundamentals behind the geoelectrical surveying techniques.

In the simplest case, a single electrode injecting current the ground will create an electric field in the form of a half sphere, or circle if seen in 2-D. Current will flow from the source electrode. The potential will decay radially with increasing distance from the electrode, perpendicular to the current flow (figure 13) (Loke 2004).

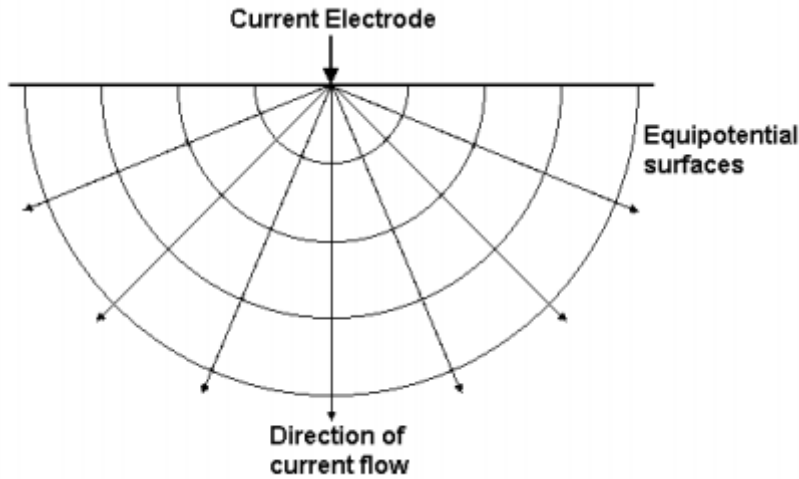


Figure 13. Current flow and potential distribution from a single source in a material with a uniform resistivity (Loke 2004).

The potential  $V$  at a certain location in such a field is given by eq V where  $\rho$  is the resistivity of the earth,  $I$  is the current injected through the electrode,  $r$  is the location's distance from the electrode.

By using equation 3 and measuring  $r$ , it is possible to investigate beyond the point's resistance, which is location dependent, and normalize for path length to solve for the resistivity, which is a material property.

$$V = \frac{\rho \cdot I}{(2\pi r)} \rightarrow = \frac{\rho \cdot I}{(k)}$$

Equation 2. Potential  $V$  for a point in a half space at a distance  $r$  from one current source. Equation 2 expressed with the geometric factor  $k$  (equation 4) is shown to the right (Loke 2004).

$$\rho = \frac{V \cdot (2\pi r)}{I} \rightarrow \rho = (k) \cdot \frac{V}{I} \rightarrow \rho_a = (k) \cdot R$$

Equation 3. Resistivity  $\rho$  for a point in a half space at a distance  $r$  from one current source. Equation 3 expressed with the geometric factor  $k$  (equation 4) is shown to the right (Loke 2004).

In practice two current electrodes are normally used in geoelectrical surveys: a positive current source electrode and a negative current “sink” electrode. Figure 14 shows the elongated ellipsoid shaped potential distribution resulting from a pair of source (C1) and sink (C2) electrodes.

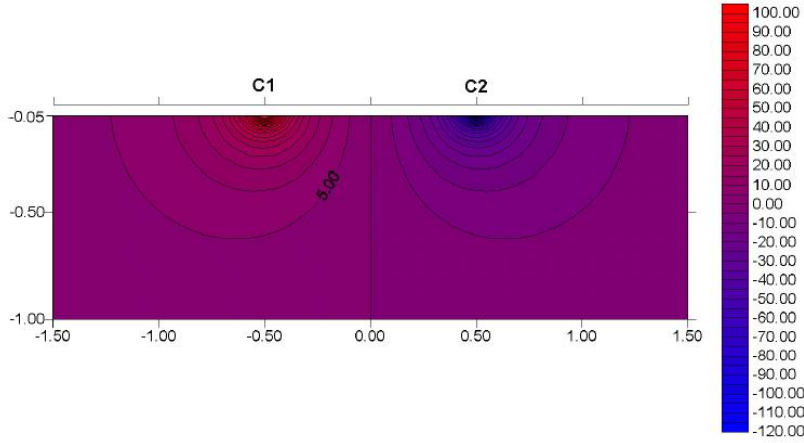


Figure 14. The polarized potential distribution caused by a pair of source (C1) and sink (C2) current electrodes in a homogenous half-space with a resistivity of 1 Ohm-m and a current of 1 ampere. Figure from Loke 2004.

At any one location in the model, the potential is now a sum of i) the positive contribution from the source electrode ii) subtracted with the negative potential generated by the sink electrode. The total value thus depends on a location's relative distance to C1 and C2.

A third important consideration is that resistivity surveys commonly seek to measure the voltage difference between a pair of potential electrodes. This requires that the potential at two different points need to be calculated (P1 and P2). The relative location of these two potential electrodes depends on the array type used in the survey (in the most conventional arrays they are located inside the pair of current electrodes) (Loke 2004).

This consideration is called the geometric factor (equation 4) and the geometric factor is introduced in equation 2 and 3. The geometric factor can be simplified for convenience depending on the electrode setup and is different for more complex arrays (equation 5).

$$k = 2\pi([r_{C1P1} - r_{C2P1}] - [r_{C1P2} - r_{C2P2}])$$

Equation 4. Geometric factor describing potential normalization (figure 15). The potential difference is calculated between electrode P1 (red) and P2 (blue) (Loke 2004).

$$k_{pole\ dipole} = 2\pi(n(n + 1)a)$$

Equation 5. Geometric factor describing potential normalization for the pole-dipole array (figure 16) (Loke 2004).

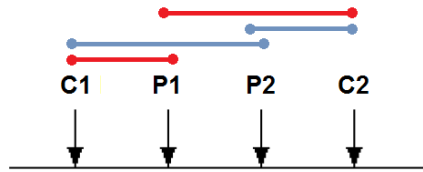


Figure 15. Illustration of equation 4: potential contribution to potential (P) electrodes from current (C) electrodes in conventional arrays (e.g. the Wenner array) (modified from Loke 2004).

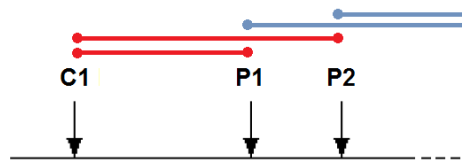


Figure 16. Illustration of equation 5: potential contribution to P electrodes from C electrodes in a pole-dipole array (modified from Loke 2004).

#### 5.1.5 A homogeneous assumption in a heterogeneous reality and the 3-D Problem

In a homogeneous model equation 3 calculates the resistivity based on how the voltage would decay in a homogeneous conductive material where current from one electrode flows in a perfect half-sphere (figure 13).

In a heterogeneous reality this is never true. The current density in the half space will be higher in the paths of lower resistance (figure 17). This “distorts” the potential distribution and equation 3 will represent a flawed assumption regarding the resistivity – an apparent resistivity  $\rho_a$  that is not representative of the real resistivity.

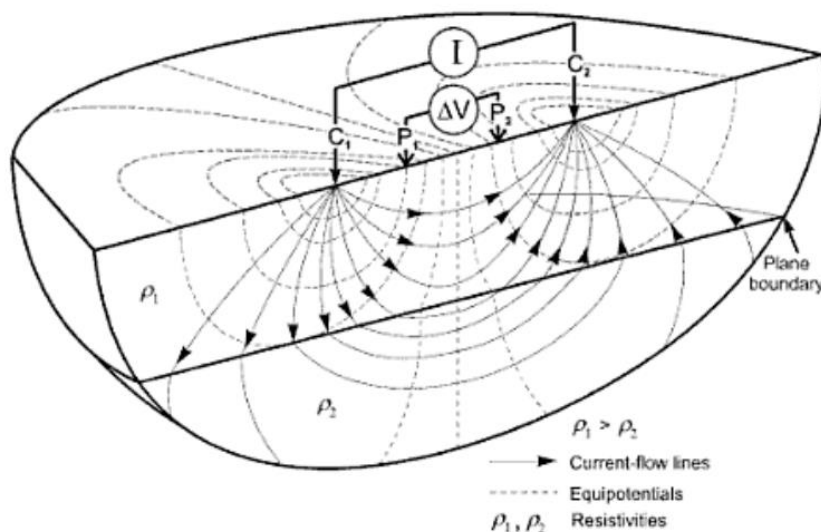


Figure 17. Traditional Wenner array quadrupole showing electrical current and potential distribution in a two-layer half-space. Notice the refraction of current flow at the resistivity layer boundary (Knödel et.al. 2007).

Apparent resistivity is “the resistivity of a homogeneous ground that will give the same resistance value for the same electrode arrangement” (Loke 2004).

The potential difference measured for one data point (figure 17) is influenced by 3-D resistivities, which the model must replicate in a two-dimensional (2-D) grid.

Trying to fit 3-D generated observation data into a (2-D) model grid introduces some discrepancies compared to the real resistivity values of the ground, especially if there are large lateral resistivity variations along a line. This inherent flaw of 2-D inversions is called the 3-D problem or the 3-D effect” (Loke 2004).

#### *5.1.6 Array Sensitivity*

Introducing heterogeneity in a homogeneous conductor e.g. figure 14 will change the potential distribution and the measured apparent resistivity. Depending on where the change in resistivity is introduced, the impact on the measured apparent resistivity value will vary.

The relative positioning between i) the heterogeneities ii) the current electrodes and iii) the potential electrodes determine the effect on the apparent resistivity. This means the sensitivity towards heterogeneities is array dependent (Loke 2004). Due to this fact, different array types display different pseudosection appearances for similar models.

- The closer to the potential electrode heterogeneities get, the larger the effect on the measured potential field value, i.e. this is where the array is the most sensitive.
- If the block is too deep below, or too far to the sides of the array it will not affect the measurement. The survey will be insensitive to it, i.e. it will be below the depth of investigation. Physical properties of the earth outside the sensitivity range will not affect the survey (Furman et.al. 2004 E, Loke 2004).

#### *5.1.7 Electrode arrays and the pole-dipole array*

Depending on the expected background noise and the structures to be mapped, different array types can be chosen for any particular survey at hand (Butler 2005). Array setups - the relative internal placement in an electrode quadrupole (i.e. two current electrodes and two potential electrodes, figure 17) - differ in their maximum depth of investigation, their sensitivity with regards to detecting vertical or horizontal structures and their signal strengths (Loke 2004, Butler 2005).

In this field study the pole-dipole array was used (figure 18). Pole-dipole is a popular array for multichannel measuring with a good compromise between signal strength, lateral and vertical resolution and practicality. Compared to a dipole-dipole which does not require a remote electrode array, pole-dipole has improved signal strength, a greater lateral resolution and an increased depth of investigation (Butler 2005, Dahlin and Zhou 2004).

The pole-dipole array relies on a receiver dipole of potential electrodes at an “a spacing” separated by an n-factor from one current electrode on the survey site and a remote electrode at “infinity” distance (at least greater than 10 a spacings). Data points are plotted directly beneath the receiver dipole.



Figure 18. Pole-dipole array. Red shows current “pole”, blue shows potential “dipole”. Lateral resolution  $\approx 1/2$  a-spacing. Depth of investigation for  $n = 6$  is  $d > 2,5$  a-spacings (modified from Butler 2005).

### 5.1.8 Topography and topographic masking

Unless corrected for, terrain can severely distort resistivity profiles (figure 19). Topographical peaks will cause a localized dispersion of flow lines and potential distribution, creating terrain induced anomalies even in a homogeneous model. Topographical data should be included with the survey data to address the issue during the inversion (Loke 2004, Fox et.al. 1980).

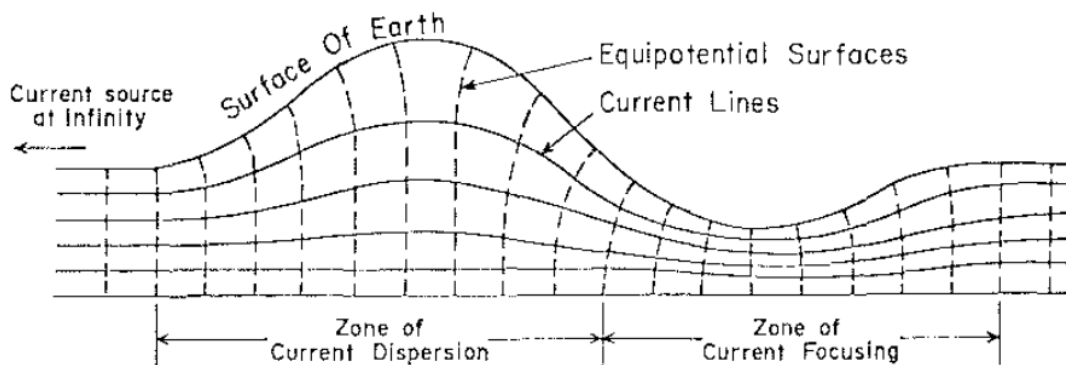


Figure 19. Figure showing a terrain affected potential distribution (Fox et.al. 1980).

### 5.1.9 ERT and multielectrode surveying

A single electrode quadrupole such as the one shown in figure 17 results in one data point. A typical resistivity section for a 2-D or 3-D survey consists of several thousand data points. Multi take-out cables connects dozens of electrodes to a resistivity meter (a Terrameter LS was used in this survey) that automatically switches quadrupole combinations (figure 20) (Loke 2004). An example of data from an ERT profile exported from the Terrameter LS is shown in Appendix B. The data is in the res2Dinv .dat format.



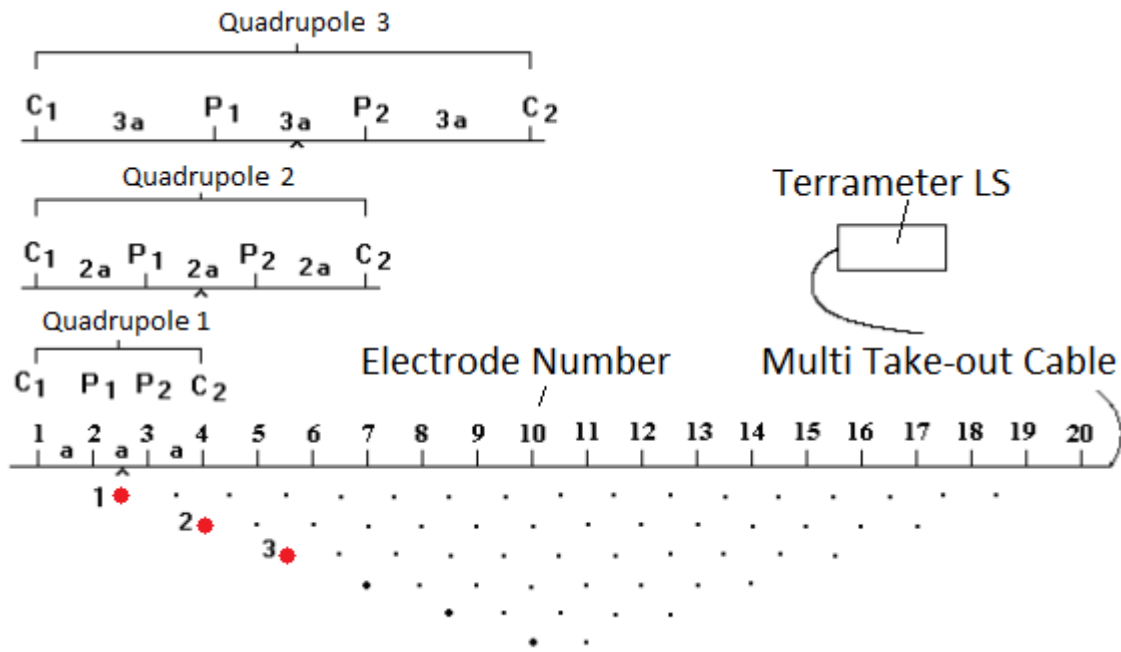


Figure 20. 2-D survey section showing three electrode quadrupole combinations (using the Wenner array). The quadrupoles with greater internal a-spacings have data points plotted at greater depths (modified from Loke 2004).

#### 5.1.10 Limitations of resistivity modeling

Due to the time consuming data gathering and computationally intensive modeling of 3-D resistivity data, 2-D tomographic modeling is the most commonly adopted approach during surveys. Models are plotted in 2-D sections but the recorded data points are influenced by data in 3-D half-spaces. There can also be elements of anisotropic resistivity in lineated materials such as shales, clays and certain minerals (Furman et.al. 2004, Loke 2004)

There is a wide overlap between the resistivity ranges of different lithologies (figure 12). This is an important consideration when interpreting results (Butler 2005). There is no immediate correlation between a resistivity value and a lithology, and complementary methods such as borehole logs are required to validate models.

## 5.2 Inversion Modeling

### 5.2.1 The inversion problem and difference modeling

The generation of **model parameters (i.e. resistivity)** from **observed values (i.e. a measured pseudoresistivity profile)** is the inverse problem (equation 6) and is a critical aspect of resistivity and IP tomography (Loke 2004).

The inverse problem is solved through iterative finite difference or finite-element modeling. There are several software programs for this purpose. This project has used Res2Dinv and Res3Dinv.

$$\mathbf{d} = g(\mathbf{m})$$

Equation 6.

- i) The forward problem: given the model  $\mathbf{m}$ , predict the data  $\mathbf{d}$ .
- ii) The inverse (i.e. reverse) problem: given the data  $\mathbf{d}$ , predict the model  $\mathbf{m}$ .  $g$  is the forward operator.

The spatial extent of a forward difference model can be defined as a grid of cells. Boundary conditions and constraints in the model are defined, and initial parameter conditions are set. The model runs until it reaches the maximum number of iterations or other set end conditions e.g. when a misfit threshold is reached, or when the iterative change becomes too low (Loke 2004).

In a forward modeling resistivity problem, the resistivity distribution of the model grid is specified and the model's purpose is to calculate the apparent resistivity distribution, or pseudosection (figure 21a). Generating synthetic apparent resistivities (measurement data) from a user defined model can be a useful tool to investigate how different parameters, e.g. different electrode arrays, affect the data output (Loke 2004).

In a real world survey, the pseudosection data of apparent resistivities are known, but the spatial resistivity distribution of the ground is unknown i.e. the inversion problem. It can be solved by reversing the modeling process: reverse difference modeling.

Instead of obtaining data from a set template model (forward modeling), the inversion process will calibrate the model parameters to fit the data (figure 21b).

New iterations of the model will be generated within a restricted parameter space until a model reaches max number of iterations or another defined end criteria (this usually includes a good fit with the observed pseudosection or a low rate of change between model iterations).

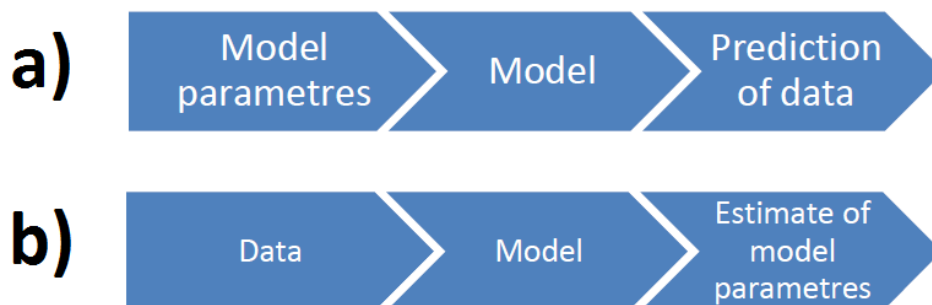


Figure 21. Illustration of a) Forward modeling and b) Inverse modeling (Menke 1989).

### *5.2.2 Least squares inversion and Res3Dinv*

Least squares inversion is a computational approach to fit a geophysical resistivity model to observed survey data (figure 21b). It is commonly adopted in inversion software, for example in Res3Dinv which has been used to model the Kristianstad field data in this project. Least squares inversion minimizes the sum of square differences between the observed data values and corresponding calculated model data values for successive model iterations.

The response in apparent resistivity due to the iterative change in resistivity is computed for the entire model grid using a Jacobian matrix (a derivative matrix). Observed data is compared with computed apparent resistivities to deduce model data fit (Loke 2004).

The modelling is solved towards a compromise between observed data fit and model complexity. The complexity is a series of numerical smoothness constraints set by the user previous to the inversion. This is a matter of adapting the inversion algorithm's tendencies to suit the expected geology (mainly regarding the degree of heterogeneity) (Loke 2004).

## **5.3 Induced Polarization Theory**

### *5.3.1 The induced polarization method and its applications*

The induced polarization (IP) method is very closely related to the resistivity survey. The IP-method was patented in 1912 by Conrad Schlumberger (Butler 2005). IP is more sensitive to noise and requires stronger currents than resistivity surveying but has seen increasing use due to improved instruments and its ability to detect certain minerals and pollutants that resistivity measurements cannot (Loke 2004). IP has previously been applied mainly in the mineral exploration business since the first half of the 20th century. It has recently been adopted for a wider range of uses such as mapping groundwater contamination plumes, landslides & structurally sensitive clays and the detection of buried landfills, (Butler 2005, Dahlin et.al. 2010).

### *5.3.2 IP surveying and frequency domain*

The induced polarization effect is a material's ability to temporarily retain a residual charge from an induced current, essentially forming a capacitor (Butler 2005). It is quantified either over a time window (time-domain IP) or a frequency spectrum (frequency domain IP).

If a remaining current is still present during a following resistivity measurement, it will disturb the potential field generated by the array and affect the resistivity value. Varying the frequency of the AC resistivity signal will vary the magnitude of the induced residual charge (if a chargeable material is present).

In other words, resistivity is frequency dependent in chargeable materials. The relation between the frequency-dependent resistivity (complex resistivity) and the material's properties are described in the Cole-Cole model (equation 7) (Loke 2004, Butler 2005).

$$\rho_s(f) = \rho_0 \left[ 1 - m \cdot \left( 1 - \frac{1}{1 + (i\omega\tau)^c} \right) \right]$$

Equation 7. The Cole-Cole model describes spectrally induced resistivity i.e. complex resistivity ( $\rho_s$ ) as a function of frequency ( $f$ ) where  $\rho_0$  is resistivity,  $m$  is chargeability,  $\tau$  is the time constant of the material and  $c$  is the relaxation constant (Butler 2005).

An advantage of the AC frequency domain method has been that it allows the recording of phase shift patterns across frequency spectrums to distinguish particular materials' IP signatures.

### 5.3.3 Time domain IP

Chargeability can also be measured in the time domain. The chargeability is then quantified as the residual potential in a specified time window after current has been switched off (equation 8). Thus the chargeability value depends on the chosen time-window (usually 0,45 to 1,1 s) (Butler 2005).

$$V_o/V_a$$

Equation 8. Applied voltage  $V_a$  is compared with observed residual voltage  $V_o$  in the chosen time window (Butler 2005).

### 5.3.4 Electrode and membrane polarization, IP effects of various materials

Materials are believed to be polarized by two main mechanisms i) electrode polarization and ii) membrane polarization (figure 22 and 23).

Electrode polarization occurs in relation to highly conductive minerals where current flow is both electrolytic (ionic) and electronic (through the mineral itself). Electrochemical reactions take place at the interface between the conducting metal and the ionic pore fluid and create a charged layer. This is thought to take place at instances where the metallic grains block the ionic current flow (figure 22). Pore water ions build up on each side of the grain diffuse over time when the current is suspended (Butler 2005).

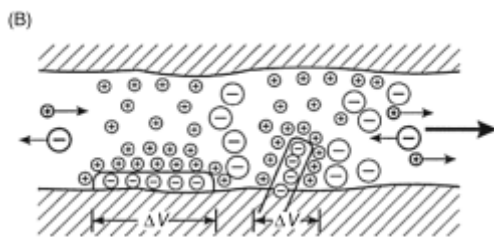


Figure 22. Electrode polarization. Polarized grain blocking the flow of ions (Reynolds 2011).

Membrane polarization is closely tied to the presence of clay minerals in soils or rocks. It has also been observed in decaying organic material. The IP-effects due to membrane polarization are much smaller than electrode polarization IP effects. Clays are normally in the range of 10-50 mV/V (figure 24) (Loke 2004). Cations in the pore fluid bind to negative surfaces on the edges of clay particles. In narrow passages, the layer of cations at the interface can become thick enough to block the electrolytic flow, building up a charge (figure 23) (Butler 2005, Reynolds 2011).

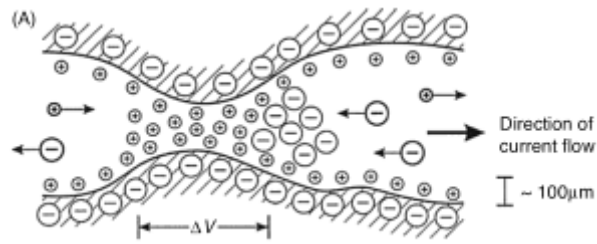


Figure 23. Membrane polarization constricting a pore channel and blocking the flow of ions (Reynolds 2011).

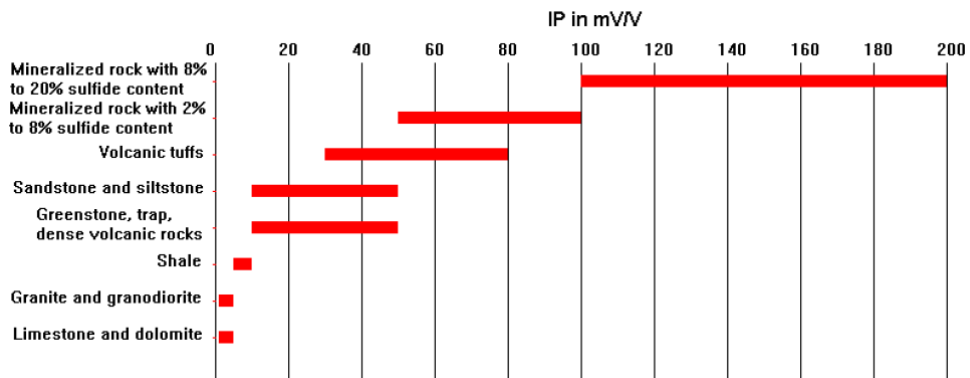


Figure 24. Some chargeability ranges in common polarizable geological materials. Note the high values in IP-effects due to conductive minerals (Loke 2004).

## 6 Field Procedure

### 6.1 Field Equipment

Resistivity and IP data were recorded using a 12-channel Terrameter LS connected to an ES10-64 Relay switch (figure 25). The relay allows parallel cable pairs which separates the potential and current signals. This is a way to avoid electromagnetic coupling and improve the signal quality which is particularly important when measuring IP effect (Dahlin and Leroux 2012).

- Electrode cables with 21 take-outs at 5 meter spacings were used:

i) 207,5 m (102,5+2,5+102,5 m) long lines using: Four cables in total with two pairs of parallel cables at each end of the instrument, connected to a total of 84 electrodes, and one 85th remote electrode connected directly to the instrument.

ii) 102,5 m long lines using: Two cables in total with one pair of parallel cables connected to the instrument, connected to a total of 42 electrodes, and one 43rd remote electrode connected directly to the instrument.

- Electrodes and cable jumpers (21 per cable)
- 12 Volt batteries.



Figure 25. Terrameter LS and ES10-64 relay. Red lines represent multielectrode cables (ABEM 2013).

Other miscellaneous equipment used:

- Electrode hammers
- Compasses
- Saws for vegetation
- Water and electrode contact slurry
- Headlights

## 6.2 Field Work

- Prior to the field survey, the site and the surrounding area was visited to plan the location and extent of the survey lines.
- The remote electrode was placed beneath a bridge  $\approx 0,6$  km from the Färgaren 3 lot. A first survey line at the edge of the property was prepared and measured. The data were evaluated and a modified protocol was created to be used for the remainder of the field survey. It is important that the remote electrode is placed at a sufficient distance from the survey area and that it has a good contact with the ground. The remote electrode cable reel should ideally be completely extended to avoid induction effects.
- The first week started with a series of long 2-D-sections (table 1). The sections originated from the property and extended into surrounding fields and wetlands to get a geological overview of Färgaren 3 and its surroundings. Divers recording water pressure levels were installed in the four metal cased wells at the Färgaren 3 lot. Complementary induced electromagnetic (VLF) and magnetometric surveys were made on the lot (these results are not included in this report).
- Two u-shaped sections stretching around the property were measured for diagonal 3-D-inversion.
- During the second week 9 single length (102,5 m) parallel sections were measured inside the Färgaren 3 lot for high resolution 3-D-inversion. Since only one cable pair was required, the relay switch was redundant, and a new protocol was designed for these sections, increasing the data acquisition rate. Some parallel lines cross the Färgaren 3 boundaries (paved road and wire fence). These external electrode segments were excluded.
- Two external long sections (205 m) were measured in the vicinity of Färgaren 3 near the estimated fringe areas of the pollution plume.
- A second series of measurements with three additional survey lines shown in table 2 was measured four months later in week 6, 2014.
- A reference survey line was measured c:a 3,7 km from the field site.
- A 2-D section providing deeper information about the conditions directly beneath the Färgaren 3 lot was measured. A power drill was used to place electrodes through the sidewalk concrete where necessary.
- A 2-D section was measured at the very southwest fringe of the estimated pollution plume to provide more information about the geology in the extended survey area.

Date	Survey Day	Survey Line
2013-09-30 – Monday	1	1
2013-10-01 – Tuesday	2	2
2013-10-02 – Wednesday	3	3
2013-10-03 – Thursday	4	4
2013-10-04 – Friday	5	5
2013-10-05 – Weekend Saturday	6	–
2013-10-06 – Weekend Sunday	7	–
2013-10-07 – Monday	8	8
2013-10-08 – Tuesday	9	9,10,11,12
2013-10-09 – Wednesday	10	13,14,15,16
2013-10-10 – Thursday	11	17,18
2013-10-11 – Friday	12	19

Table 1. Field survey dates and survey lines. The survey line locations can be seen in figure 27.

Date	Survey Day	Survey Line
2014-02-04 – Tuesday	1	-
2014-02-05 – Wednesday	2	20
2014-02-06 – Thursday	3	21
2014-02-07 – Friday	4	Reference

Table 2. Field survey dates and survey lines of additional measurements. The survey line locations can be seen in figure 27.

Vegetation deteriorated the GPS signal precision at several points in the wetlands and by the gravel road, where coordinates and topography could not be recorded. These point values were later interpolated prior to the modeling.

Electrode contact was good in the majority of the survey lines. Electrode points near the gravel road and in coarser sections of the filling material at the Färgaren 3 lot needed to be prepared with slurry to improve the electrode-earth contact, as did survey sections on erected lawns in e.g. Line 21 and Line 20 (which partly ran on sidewalks).



## 7 Results

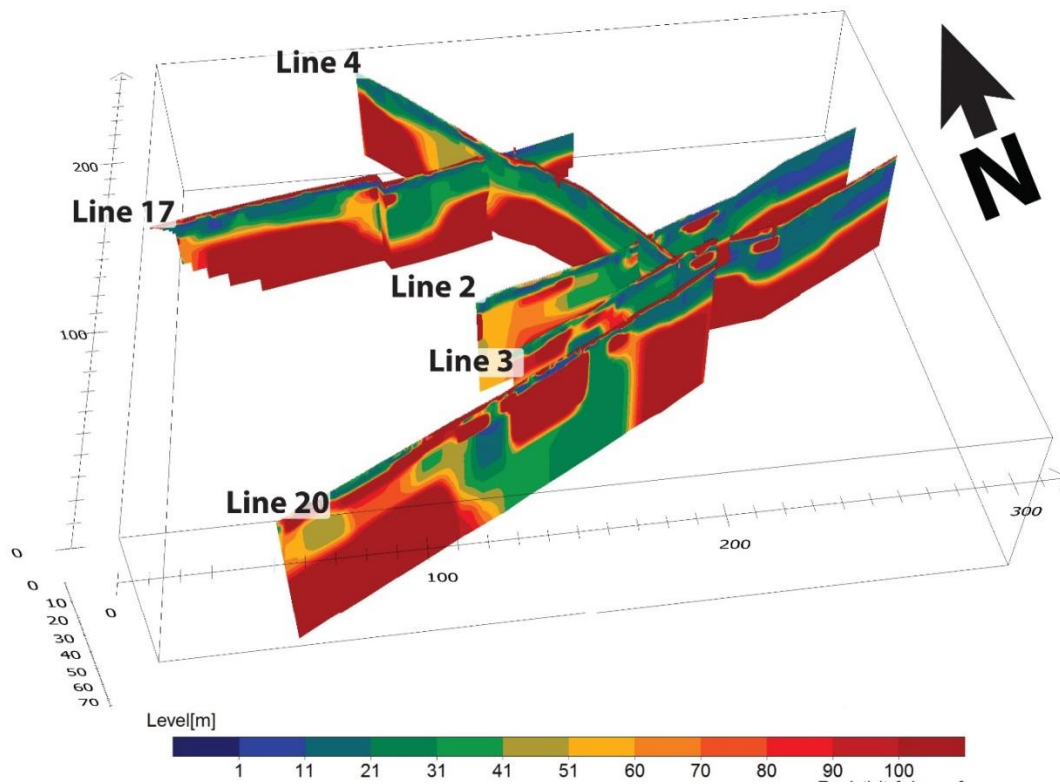


Figure 26. Fence diagram rendered in Erviz showing 2-D survey lines of main model section. The res2Dinv inversion settings used are shown in Appendix C.

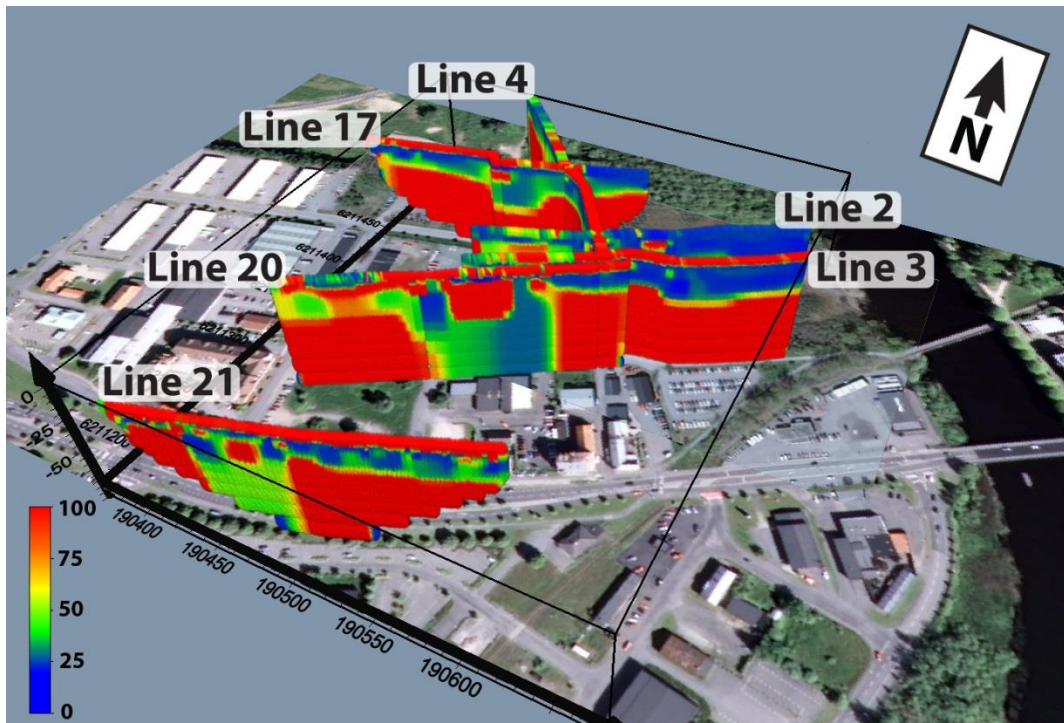


Figure 27. Voxler model showing all 2-D survey lines with GPS coordinates projected onto an orthophoto. The blocky appearance is due to the method of displaying 2-D data in Voxler.

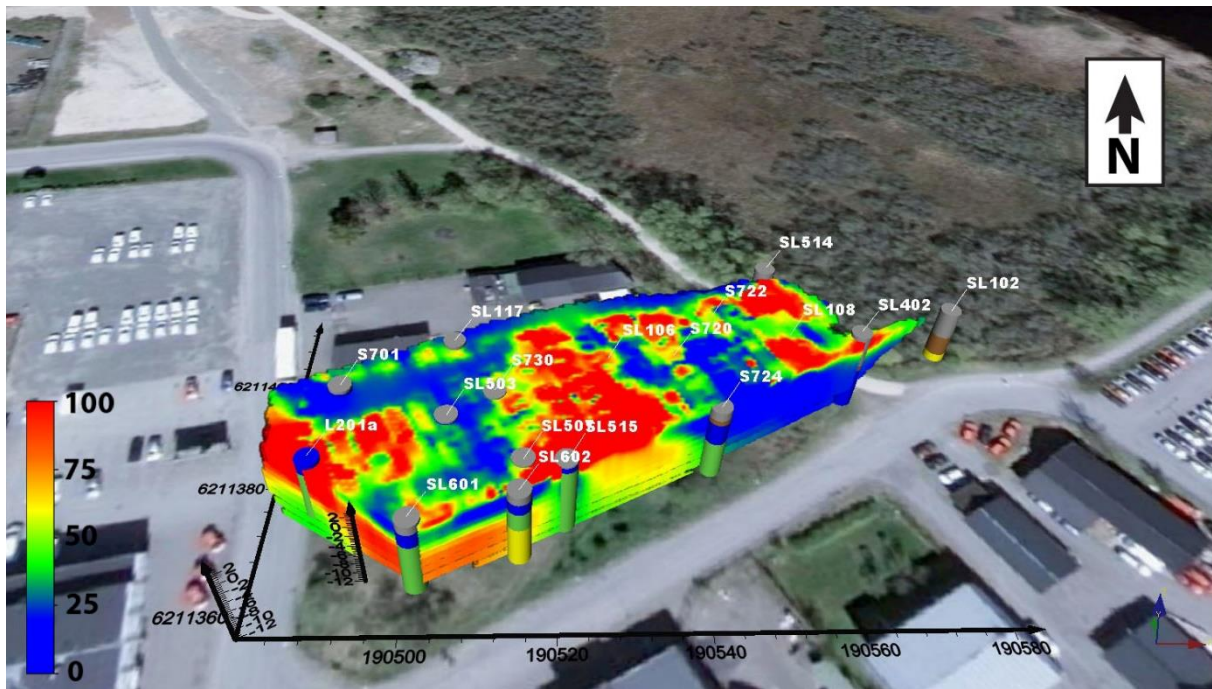


Figure 28. 3-D-resistivity model of the Färgaren 3 lot displayed in Voxler together with borehole log stratigraphies. A selection of boreholes that provided a good areal spread of deep logs were chosen and imported into the Voxler model. All straight survey lines are also shown modeled in 2D in Appendix D.

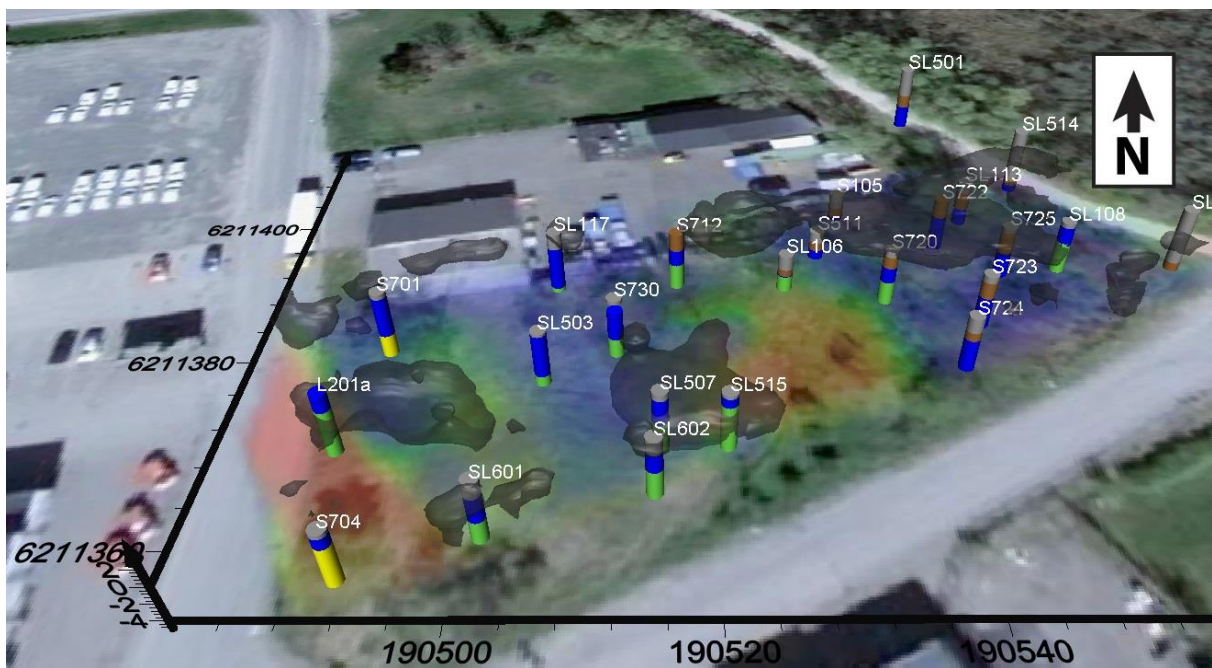


Figure 29. Voxler model showing IP-effects in the 3-D model of the Färgaren 3 lot. Areas with chargeability values of over 7 mv/V are covered with black isosurfaces. The figure also shows borehole logs and opaque resistivity values of the 3-D model (figure 28 above) in the background. A few additional shallow boreholes (3m>) in the north eastern section have been added to this model, showing the peat blanket (brown layer).



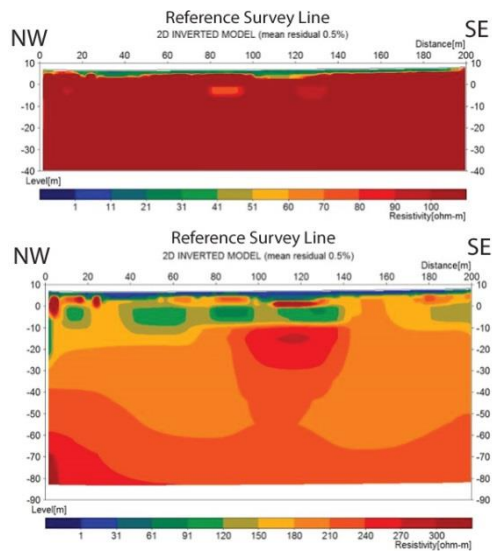


Figure 30. Off-site reference profile displayed in Erigraph shown with i) a low-depth, small scale (upper) and ii) full depth, larger scale emphasizing inter-bedrock resistivities (lower).

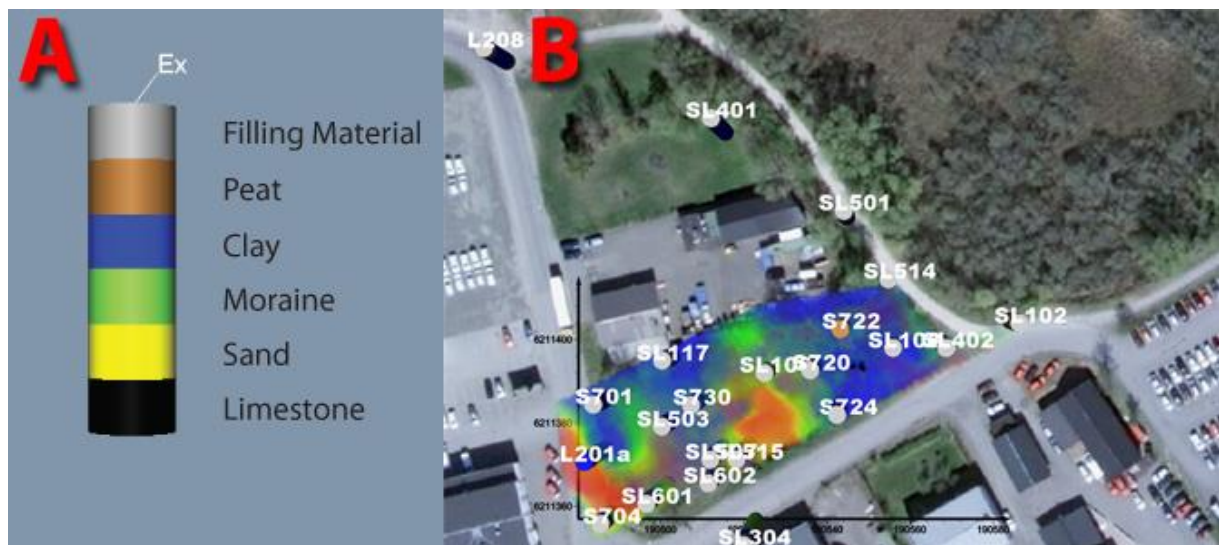


Figure 31. (A): Example of borehole log. The general stratigraphy described in section 4.3 consists of a surface layer of artificial filling material, a soil layer of clay, chalky till and a bedrock layer of limestone. Boreholes show that the thickness of fill and soil layers vary greatly and in some boreholes all are not present. There are also occurrences of peat and sorted sand. (B): Overview of Färgaren 3 showing boreholes in the model area. A borehole log excerpt is shown in Appendix E.

## 8 Interpretation

The interpretations of the results are presented in a series of illustrated figures with explanatory captions. There is more in-depth discussion and detailed reports in the texts.

### 8.1 Hydrogeological model

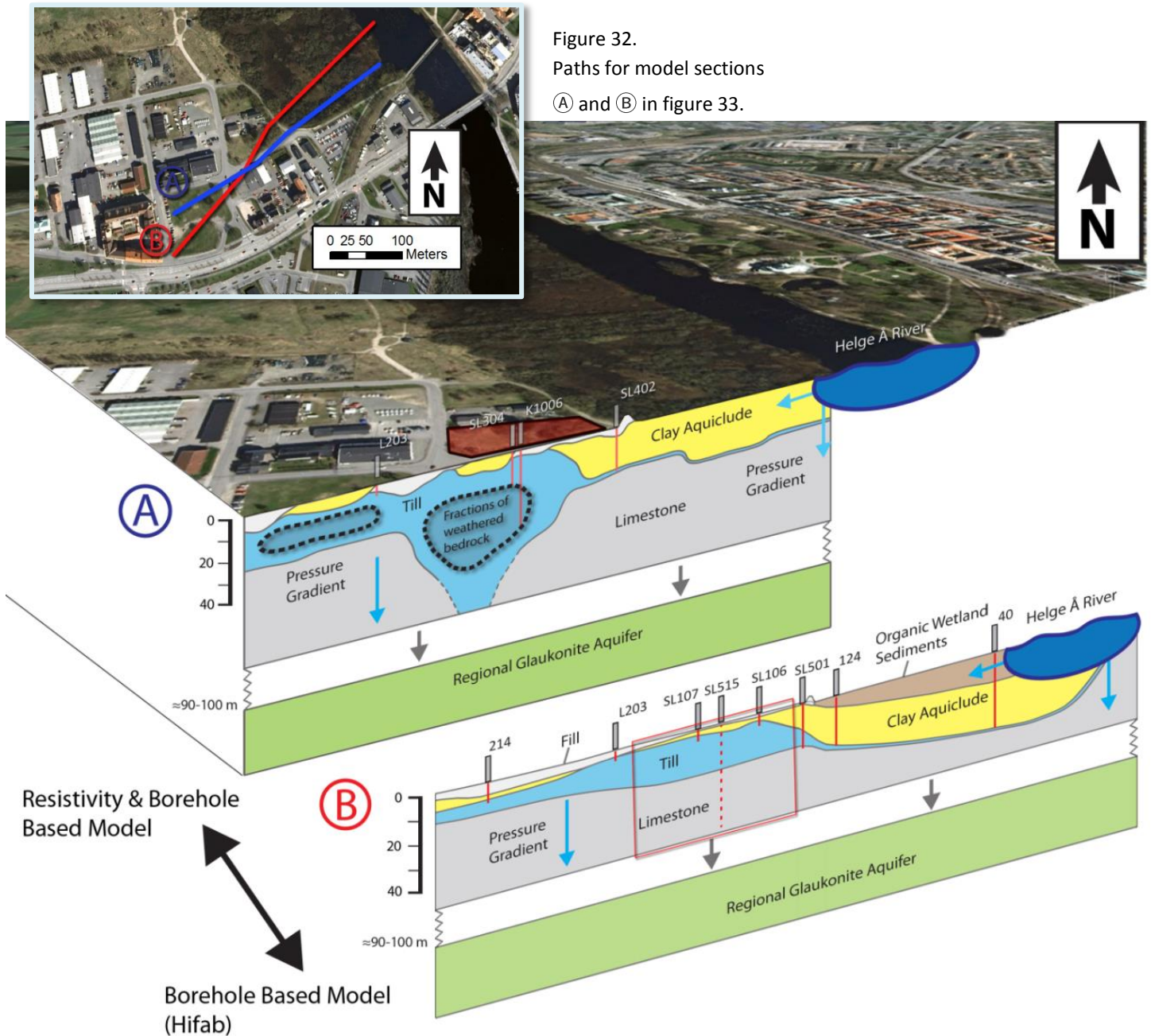


Figure 33. Hydrogeological concept model (A) interpreted using resistivity data compared to model (B) from Engdahl et.al. 2011 based solely on borehole data. The Färgaren 3 lot is marked in red. Results from the deep survey profiles (figure 26 and 27) indicate a local depression in the bedrock near the western end of the Färgaren 3 lot, which is a major difference from the prior borehole model (B). Such a depression might facilitate the vertical spread of pollutants in this heavily contaminated part of the lot. The borehole SL515 in (B) is shown as an example where an older borehole log does not correlate with the resistivity interpretation or the more recent borehole K1006 in (A). This model was created based on the modeled profiles shown in figure 34 below.

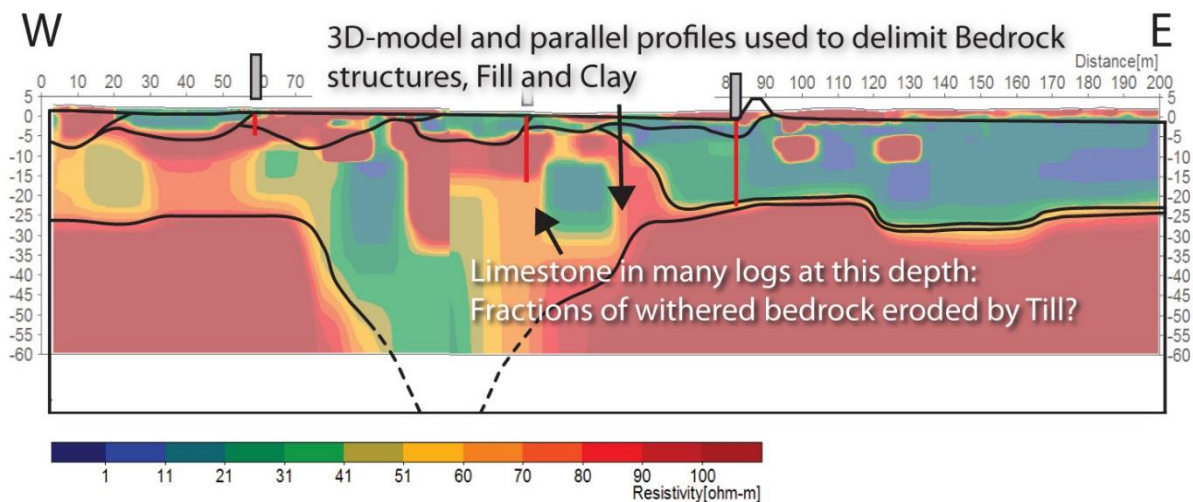


Figure 34. The model in figure 33 is based on boundaries of overlapping resistivity profiles shown here (Line 20 and Line 3), supplemented with information from the 3-D resistivity model and various borehole logs. Parallel survey Line 2 and crossing survey Line 4 (figure 26) were also taken into account during the interpretation of the bedrock structure. While the very deep data is more uncertain there is no indication of encountering bedrock in the middle of the depression.

## 8.2 Model Fit and Borehole Log Correlation

### 8.2.1 Boreholes as an independent control method

A key point in geoelectrical surveys is to identify geological boundaries and formations. Changes in resistivity can often be coupled with changes in lithology. This is usually done through co-interpretation with a small number of boreholes. In this survey the modeled data and a number of borehole stratigraphies was positioned with GPS coordinates in a 3-D Voxler model (figure 27 and 28).

Borehole correlation is an independent control method, used as one-dimensional stick-sample assessments of model reliability.

Soil logs are not completely objective, and boreholes at the field site (from different surveys) have been logged by different persons. There are some inconsistencies mainly regarding pedogenesis and sometimes interpreting the till as sand (its main fraction) or post glacial flood plain deposits.

Furthermore, the position of the solid bedrock is noted as uncertain in most boreholes. The previous surveys (Engdahl et.al. 2010. Engdahl et.al. 2011) have experienced continued problems with separating weathered material from crushed rock in core samples, and have had above material collapsing into samples. There has also been drilling issues preventing probing through the rock to any greater extent. This may in some places have led to fractions of loose bedrock in the till being interpreted as the bedrock surface, which could explain inconsistencies at the western part of the lot with the resistivity surveys and later studies (Figure 33).



### 8.2.2 Borehole - 2-D line fit and model interpretation

The sharp resistivity contrasts in the 2-D survey profiles generally fit well with the borehole stratigraphies in the surrounding area. Boundaries are highlighted with sketches around e.g. borehole L209, SL401, SL 501 (figure 35) and SL108, SL402 and SL102 (figure 36). There are unfortunately not a large number of borehole logs extending to the bedrock surface.

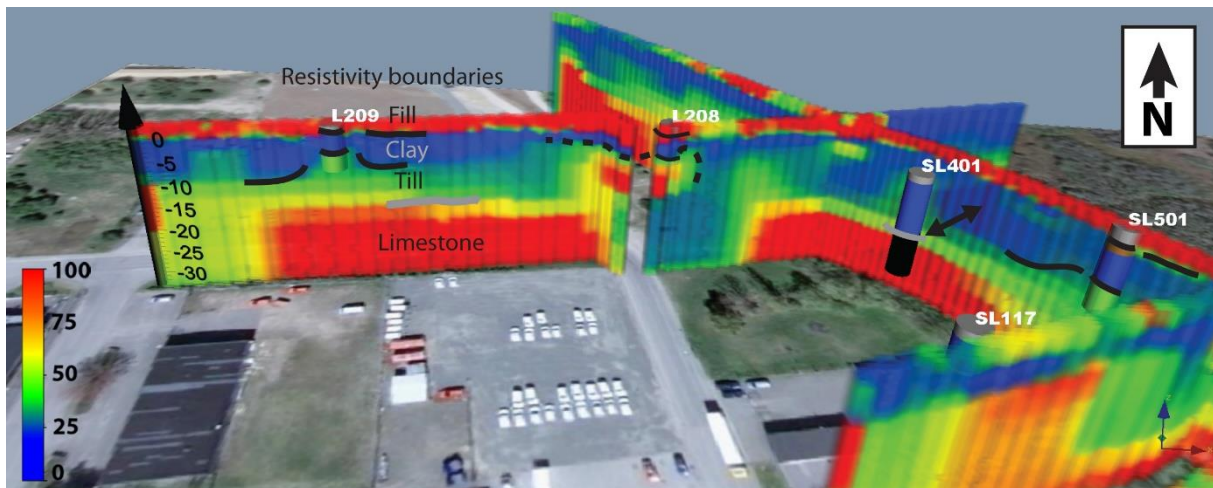


Figure 35 showing survey lines 17, 4, and 3. The figure illustrates the interpreted soil stratigraphy based on the observed resistivity gradients, and shows comparisons against borehole logs. High-resistive fill, the low-resistive clay, the intermediary till and the underlying high-resistive limestone bedrock correspond with most boreholes. The clay-till border is diffuse in some areas while other boundaries are sharper. A more detailed account of the resistivity values of the soil layers are given in section. Resistivity unit is in Ohm-m.

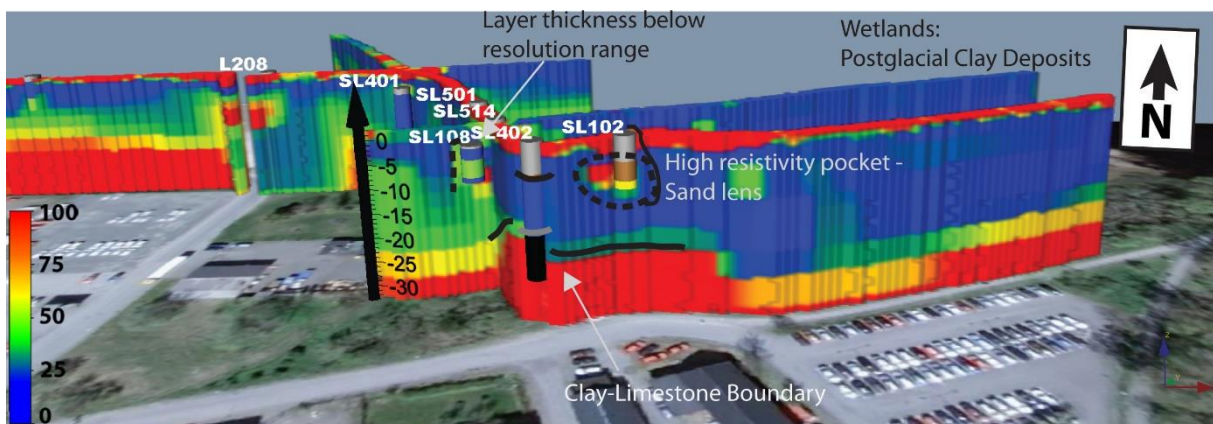


Figure 36 shows survey lines 17, 4, 3 and 2 with borehole stratigraphies. Thin layers such as the clay lens in the borehole SL108 is below the resolution of this survey and will blend into the surrounding resistivity layers. The eastern sections of line 2, 3 and 17 show thick postglacial clay that was deposited when the Helge Å River had much wider banks. The sand lenses seen in some places of the clay, e.g. borehole SL102 and SL514, might be old "shore lines" where the river has deposited sand along its banks (figure 42). Resistivity unit is in Ohm-m.

### 8.2.3 3-D Model Fit

A view of the 3-D model illustrating interpreted layer boundaries is shown in figure 37. The till which dominates the soil beneath the fill in the western part of the model has a varying resistivity, and a varying composition noted in borehole logs of this area. There are blocks of limestone bedrock noted in high resistivity sections in the westernmost end of the model, and sections in the middle that (e.g. logs SL602 and SL515) consists of more or less sorted sand. Boreholes that extend beneath the 3-D model encounter limestone fractions recently below around 15 m, however later drillings and the results of the deep resistivity profile indicate that this is not the bedrock surface (figure 33).

Some in-depth borehole correlations are shown in figure 38. Complete pictures are shown in appendix F. The level of detail and coherence with boreholes in the 3-D model is generally very high. The model in figures 37 and 38 shows mixed, somewhat messy resistivities, yet even small layers are captured. The resistivity in the model can be assumed to accurately resemble the resistivity of the ground and by extension the geology.

The geological relationship between the model values and the soils are discussed further in section 8.3.

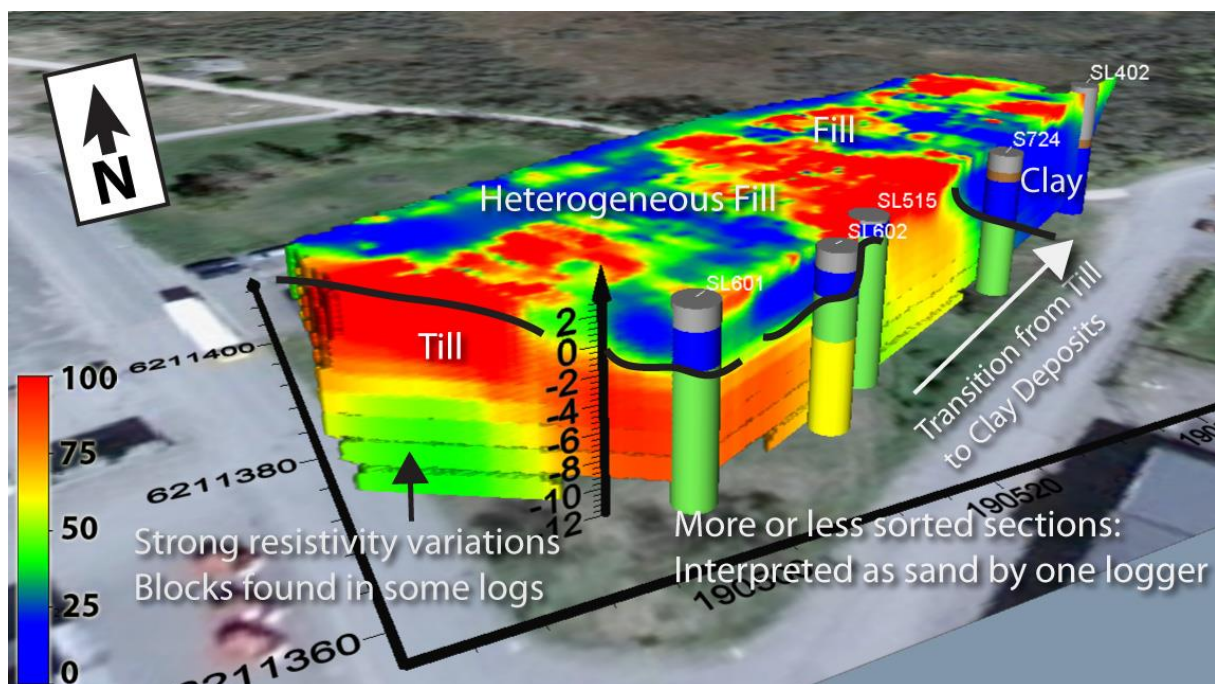


Figure 37. Illustrated interpretation of 3-D model. The model correlates the low resistivity areas with clay sections in the borehole logs well. The fill layer on the Färgaren 3 lot has a highly variable resistivity after the demolition of the main building. The till varies in fraction composition (and resistivity) in the lot and in some boreholes samples have been interpreted as sand. Resistivity unit is in Ohm-m.

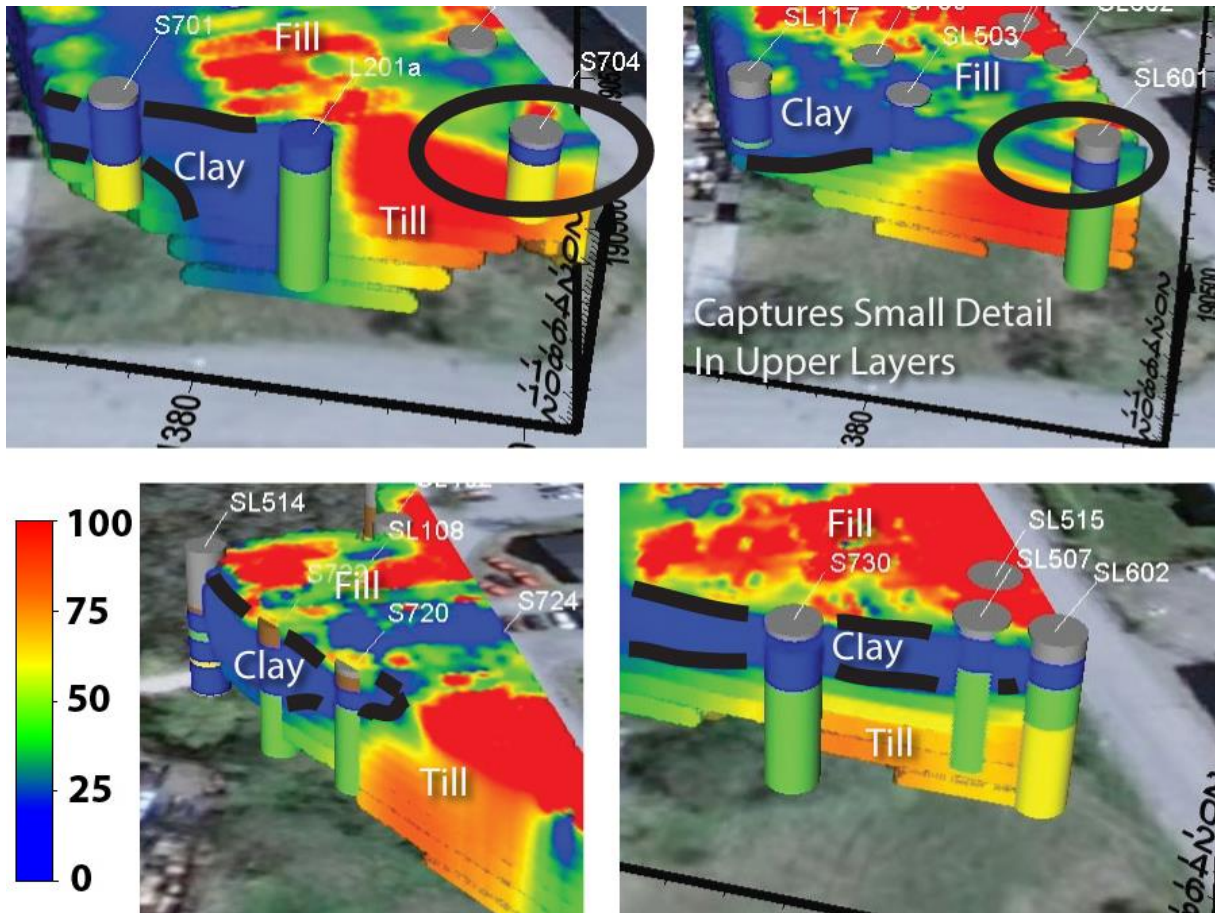


Figure 38. Pictures show several examples of detailed 3-D model sections with positioned borehole logs. There is generally a very strong correlation between:

- i) Higher and mixed resistivity zones and borehole fill layers (shallow)
- ii) Low resistivity zones and borehole clay layers.
- iii) Higher resistivity zones and borehole till/sand presence (deep)

Resistivity unit is in Ohm-m. Larger images are shown in Appendix F.



#### 8.2.4 Numerical Fit and Model Resolution

The only numerical uncertainty available in Res2Dinv and Res3Dinv is the global residual misfit in percent between the observed and modeled apparent resistivities (Loke 2004). The values are presented in table 3 below.

Survey Line	Residual Misfit	Extended Profile	Notes
2	1,9	Yes	
3	1,1%	Yes	
4	0,7%	Yes	
17	1,9	No	
20	5,2%	Yes	Electrode holes drilled on sidewalk
21	5,7%	No	Measured on erected lawn by road and parking site
3-D-Model	3,56%	-	
3-D-Model IP	4,52	-	
Reference Profile	0,5%	Yes	Measured in nature reserve - low electrical interference

Table 3. Residual values for the resistivity models in figure 27 and the resistivity and IP residual for the 3-D-model in figure 28.

Increasing electrode spacings will increase the depth of investigation and decrease resolution. This means that resolution decreases with depth.

The electrode spacings used were between 2,5 and 100 meters and the median depth of investigation was down to 73,32 meters. The lateral resolution is given as roughly  $\approx 1/2$  a-spacing and would be between 1,25 to 50 m.

Practical depth of investigation and resolution will also be influenced by local resistivity contrasts.

The maximum spacing and depth of investigation can only be reached in the middle of the survey line. In other words the sensitivity (or quality) of deep data in a profile also decreases away from the middle. The two lower corners are usually omitted from the model grid in 2-D-models for this reason. Extended 2-D-sections that include the information in the lower corners should only be used with arrays that yield strong signal strengths.

These spatial variations in resolution and data quality should be kept in mind during interpretation of deep formations and structures at model edges.

An example of anomalies caused by interference coupled with poor depth resolution can be seen in the midsection of Line 20 in figure 26 where the formation that is interpreted as the bedrock boundary seemingly bends vertically.

Line 20 had holes for electrodes drilled through concrete, and the data (see residuals in table 3) was likely affected by underground structures beneath the sidewalk. The parallel Line 3, located on the Färgaren 3 lot (c:a ten meters north of Line 20) displays what is probably a more realistic representation of the sloping formation, shown in figure 34.

## 8.3 Soil resistivities and layer characteristics

### 8.3.1 Filling

Filling material is usually, but not exclusively highly resistive. This upper layer could be e.g. a blanket of gravel placed for drainage purposes under erected lawns or roadsides (often practical location for survey lines). In the survey profiles the fill layer is often easily distinguishable because of its strong resistivity contrast to the underlying low resistivity clay, as seen in figure 35.

The coarse grained construction fill at the Färgaren 3 lot is mixed in some places with components such as fine grained humus, which is low-resistive and hard to delimit from the below clay layer in the 3-D-model (figure 37).

In areas like the wetlands in the nature reserve (easternmost parts of Line 2 and 17 in figure 36) there is no filling material. The top soil layer is only covered by a thin natural bed of humus.

### 8.3.2 Clay

Clay is a very low-resistive soil. The varvey clay at the field site is internally a relatively homogeneous unit with a narrow resistivity range that will fall on the lower range of the scale (figure 12). This usually makes it easy to identify in a resistivity profile, and the postglacial clay deposits transitions from a patchy blanket into thick deposits in the wetlands in the eastern parts of the survey profiles (figure 39). There is known to be a blanket of organic materials overlying the clay in the wetlands (figure 33 ⑥), but its high saturated porosity makes it difficult to distinguish in the resistivity model.

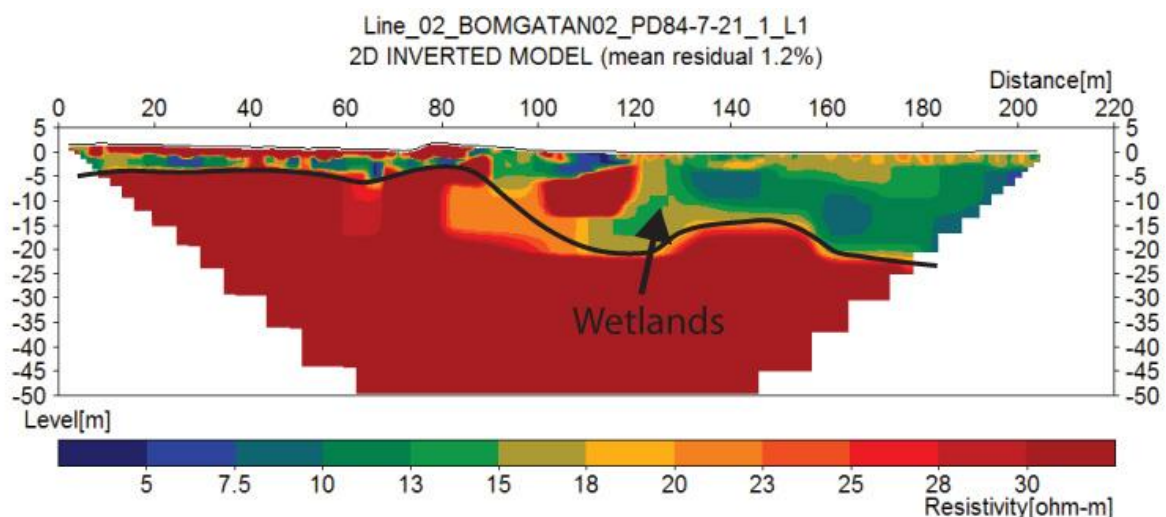


Figure 39 showing range of clay layer resistivities (non-red areas) in survey line 2 which are typical for the area. Clay resistivities matched with boreholes generally vary between c:a 5-30 ohm-m. The thickness of the post glacial clay increases significantly under the wetlands (arrow).

### 8.3.3 Till

Till, containing clay and sand fractions but also pebbles, and potentially rocks and boulders, is a geological generalization that is based on pedogenesis. This makes it hard to define resistivity ranges outside of broad estimates such as the ones given in figure 12, even for local surveys.

Till deposition is a destructive process where glaciers erode and deposit a mix of local and remote material. Till can also contain ripped off chunks of preserved bedrock which is common in Swedish regions with soft bedrock like limestone. Since glacial processes are cyclical it is also possible to find imbedded remnants of more sorted inter-periodical (i.e. postglacial) sediments.

This somewhat chaotic geology is a complication that can be seen in the strong resistivity variations of the 3-D model (figure 37). It may also have attributed to the inconsistency in the borehole logs of the Färgaren 3 lot and the resulting difficulties of determining the true position of the bedrock surface. This has made it difficult to dimension the extent of the free phase PCE pollution.

The local till varies between 30, which is unexpectedly low for Tills, to over a 100 Ohm-m. The low resistivity sections are likely made up of the small fractioned chalky till most commonly found in the wider survey area. Blocky sections and more sorted fractions dominated by sand are noted in logs from the more high resistive areas (figure 37) (Engdahl et.al. 2011).

#### 8.3.4 Limestone

Heavily weathered limestone and coarse sections of till can very well have overlapping resistivity ranges, and couldn't be separated based on their conductance. However, in the deep sections of the 2-D-survey profiles there is generally a distinct, sharp resistivity boundary which is interpreted as the likely boundary between soil and bedrock. This boundary is perhaps distinguished more clearly in the render illustrated below in figure 40, but is also illustrated in e.g. figure 35 which shows comparisons with boreholes. In the Erviz fence diagram (figure 26) the boundary can easily be distinguished across the entire survey area.

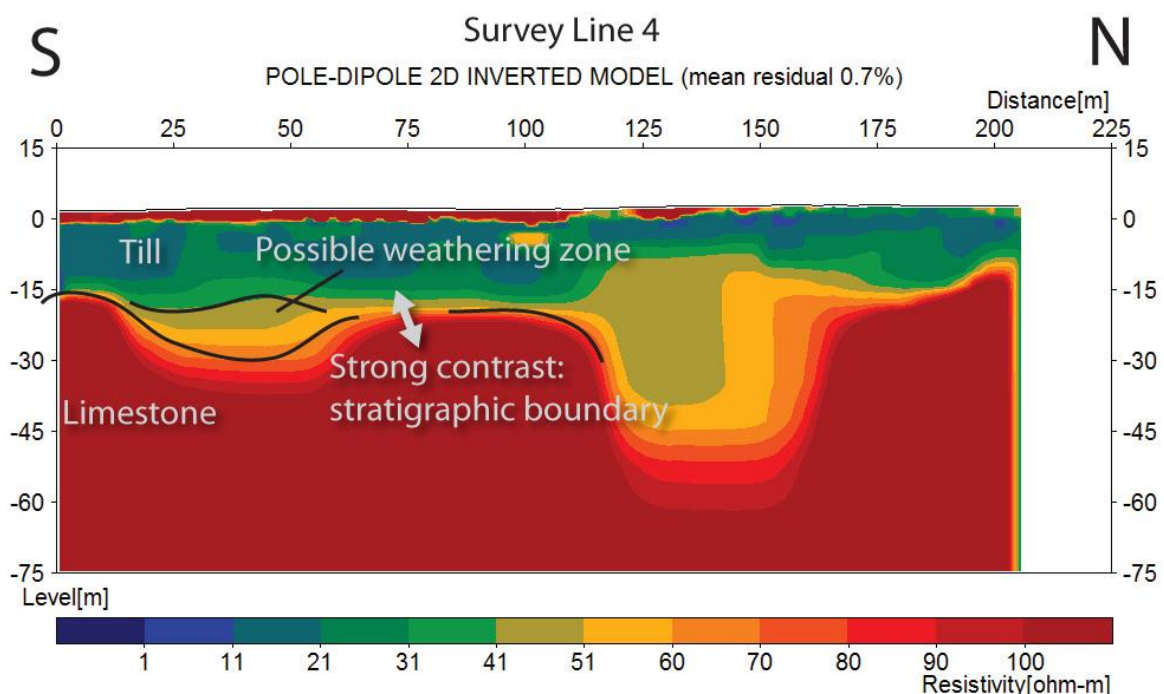


Figure 40 showing survey profile Line 4 with illustrated interpretations. Resistivities of up to c:a 40 Ohm-m in the till shows a sharp contrast to the underlying limestone which displays resistivities of around 100-300 Ohm-m. This resistivity boundary is easily identifiable in the Erviz fence diagram (figure 26).

Within 100 m of the Färgaren 3 lot the depth to bedrock varies between 5 to 30 meters (Engdahl et.al. 2011), and as can be seen in figure 26 the bedrock surface undulates in the area with many local depressions. The more gradual resistivity change seen in these local bedrock depressions (figure 40) may in part be caused by the presence of heavily weathered limestone fragments remaining in place (however it may also partly be an effect of smoothed gradients created by the inverse modelling).

## **8.4 Local model formations and anomalies**

### *8.4.1 External reference survey profile*

In addition to the 21 survey profiles in the Färgaren 3 field site area, one reference profile was measured (figure 41).

A reference profile should be done in a non-polluted setting where the same geological stratigraphy can be recorded under ideal measuring conditions. Although it would not be located within the field site, a reference profile would aid in making a correct interpretation and reduces uncertainties regarding connections between resistivity and the contaminants:

A 2-D line with perfect electrode-surface contact and an extremely good fit can be a useful tool when it comes to recognizing and interpreting anomalies and model errors e.g. such as those generated by interferences in the urban environment of the field site area.

The reference profile's location was chosen based on several factors:

- Borehole log availability
- Remoteness from electrical interferences (e.g. heavy train traffic or subsurface structures)
- Proximity to and similar local geological history and depositional environment as Färgaren 3

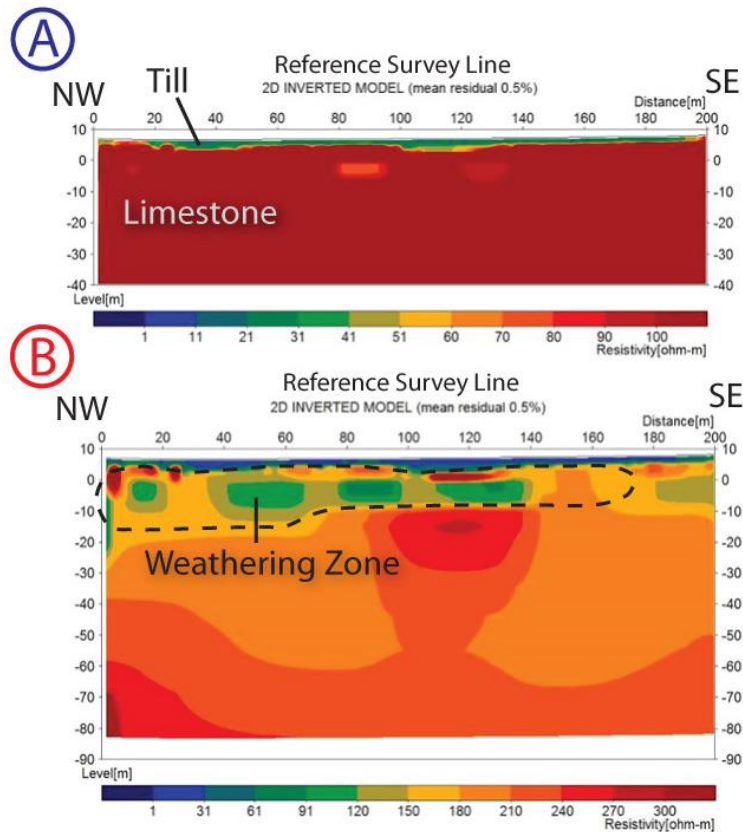


Figure 41. A: Reference survey profile showing upper till layer with relatively low resistivities (c:a 30 Ohm-m) and underlying limestone bedrock. B: Same profile shown including a greater depth and a color scale that highlights internal bedrock resistivities. Upper low-resistivity zone is interpreted as highly weathered bedrock with resistivities from just above 100 Ohm-m, compared to over 200 Ohm-m at lower depths.

The reference profile was matched with a nearby borehole log. Ideally a location containing some amount of clay should have been used. Due to the shallow position of the bedrock at the location and the high data quality, there were also hopes of recording the underlying regional glauconite sand aquifer. Unfortunately there is no clear sign of an additional strata in the deeper section of the figure 41.

The unpolluted till layer still shows unexpectedly low resistivity values. This indicates that any potential chloride production from PCE degradation in the pollution plume is not significant enough to have a detectable effect on the saturated soil's resistivity.

There is a distinct boundary to limestone close to the surface in figure 41, with a low resistivity zone in the upper layers of the limestone. This is most likely due to weathering of the uppermost bedrock, where an increased porosity and water content causes a lower resistivity.

#### 8.4.2 Buried postglacial river banks

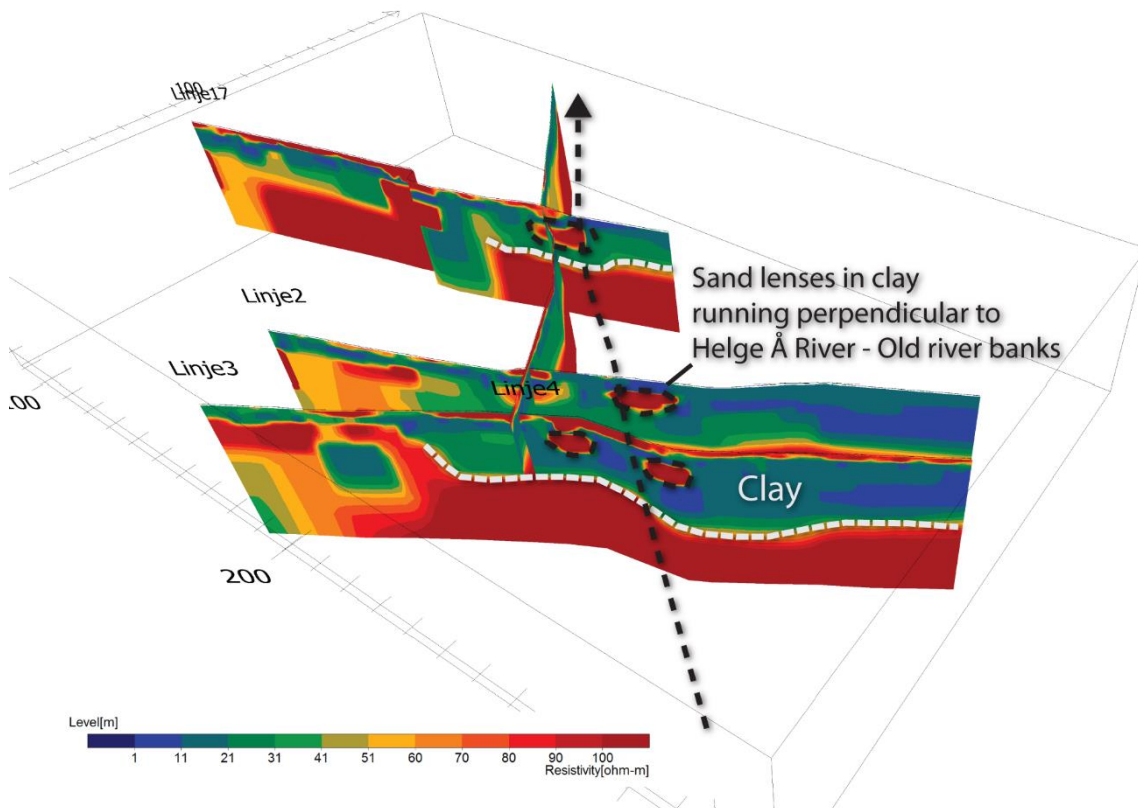


Figure 42. Fence diagram of survey lines 2, 3, 4 and 17 highlighting interpreted elongated shoreline running alongside the river and perpendicular to the survey profiles.

In the postglacial clay deposits in the eastern parts of the survey area there are several buried high-resistivity lenses that appear at roughly the same distance from the river (figure 42).

In the borehole SL514 one of these is described to contain sand fractions. This is likely postglacial “svallsand” or “swelling sand” and could be the position of an old shoreline of the postglacial Helge Å River has deposited sorted sand fractions.

#### 8.5 IP interpretation and contaminants

Both soil samples and IP-effects indicate the presence of heavy pollutants in the western part of the lot (figure 43 and 44). The samples show values in the range of hundreds and thousands of mg/kg, which seems to be the general concentrations detectable through IP effects in this survey.



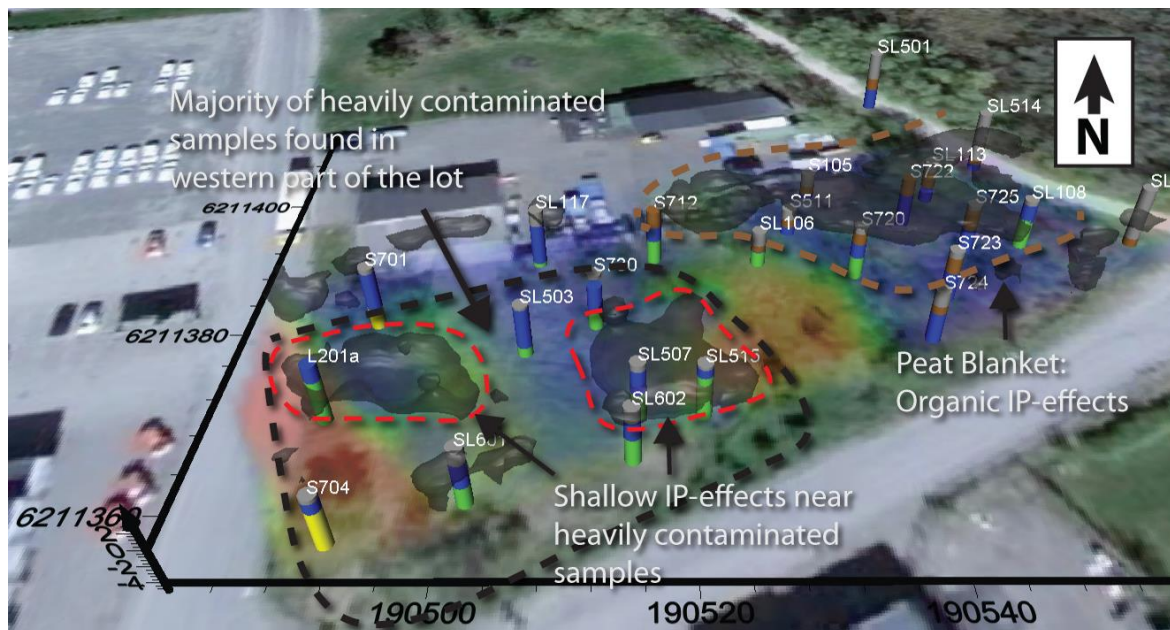


Figure 43. Illustration of the IP 3-D-model (figure 29) showing one large IP-effect (isosurfaces above 7mv/V) in the northeastern part of the model (encircled in brown). It is likely in part generated organic components in the peat bed noted in boreholes logs there (brown layer). There are two interesting IP-effects generated in the western part of the model (encircled in red) that are in the proximity of the most heavily contaminated samples and the suspected main source of PCE at the site (figure 44 and 45 below).

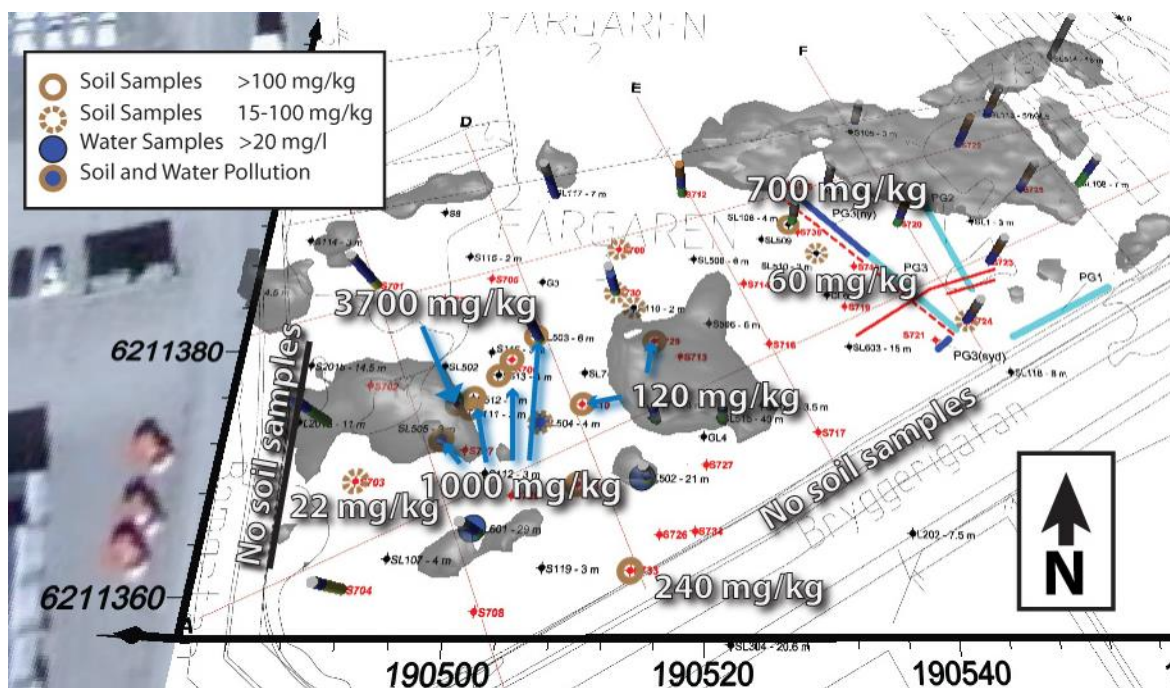


Figure 44. Illustrated survey map from Cowi 2013, georeferenced into the 3-D-model. The figure highlights all of the most heavily contaminated samples on the lot in relation to the IP-effects (isosurfaces above 7mv/V). Most soil samples with concentrations above 100 mg/kg of chlorinated aliphatics have been found in the proximity of the IP-effects in the western part of the lot where the dry cleaning building was located. Soil samples have not been made for all boreholes. Naturvårdsverket's threshold for what is considered safe is 1,2 g PCE/kg soil (Engdahl et.al. 2011).

### 8.5.1 PCE extent and pollution sources



Figure 45. Georeferenced historical orthophoto (modified from Länsstyrelsen Skåne 2005) of the main dry cleaning building (red) and a small garage and storage shed (blue) prior to demolition, together with the globally positioned 3-D IP-effects. The location of the PCE storage tank and the dry cleaning machines' exhaust pipes are marked. The IP effects correlate with these pollution sources, indicating that PCE contamination on the lot occurred mainly outside of the building. There are IP responses in relation to the PCE tank on the yard and accumulation under the exhaust pipes on the eastern side of the house (figure 46).



Figure 46. (A) Exhaust pipes of the dry cleaning machines on the main building prior to demolition. (B) PCE storage tank on the yard outside of the main building (figure 45). This is believed to have been the main storage location for PCE throughout the business's operation. A full building plan from Engdahl et.al. 2011 is shown in figure 7.

There seems to be a correlation between the IP effects of the 3-D-model and the discovered pollution sources of the dry cleaning operation presented in Hifab's report (figure 45) (Engdahl et.al. 2011). The IP effect on what used to be the yard west of the building might be due to long time leakage and spilling from handling the outdoor storage of large volume tanks containing



concentrated PCE. This is where the single largest concentration (above 3700 mg/kg) was sampled (figure 44).

There are also PCE concentrations in the soil near the exhaust pipes of the dry cleaning machines, which is the likely cause of the IP-effect seen there (figure 44).

There are not any IP-effects of similar strength on the building grounds itself, suggesting that the tank and exhausts were the main pollution sources. There are however high concentrations in some soil samples directly below the building (figure 44).

Waste water was released from a pipe in the eastern part of the lot (figure 45), but it is difficult to separate IP-effects due to organic materials from any IP-effects due to PCE concentrations. Soil samples in figure 44 shows that there is also some pollution there.

#### *8.5.2 Why do borehole samples and IP show different pollution extents?*

The borehole samples show very strong variation (factors of ten) in side-by-side PCE concentrations, making it difficult to delimit cohesive areas of polluted soil, i.e. there could be high concentrations next to negative samples and vice versa (figure 44). The IP survey would rather detect high volumes of pollutants in a 3-D area and might not reflect e.g. small pockets or clusters of very heavily polluted soil.

There is also an uncertainty involved in the IP results. In general the IP model should be expected to be of lower quality than the resistivity model since the recorded effects of 7 mV/V are not very strong with concern to local interference. The position of the IP-effects in relation to the pollutant source might not fit with the same accuracy seen e.g. in the resistivity model (figure 38). It is not unreasonable to interpret the result with an inaccuracy on the scale of 1-2 m.

## 9 Discussion

During the field survey in October (table 1) pressure head levels was measured continuously using divers in four wells in the Färgaren 3 lot (figure 47):

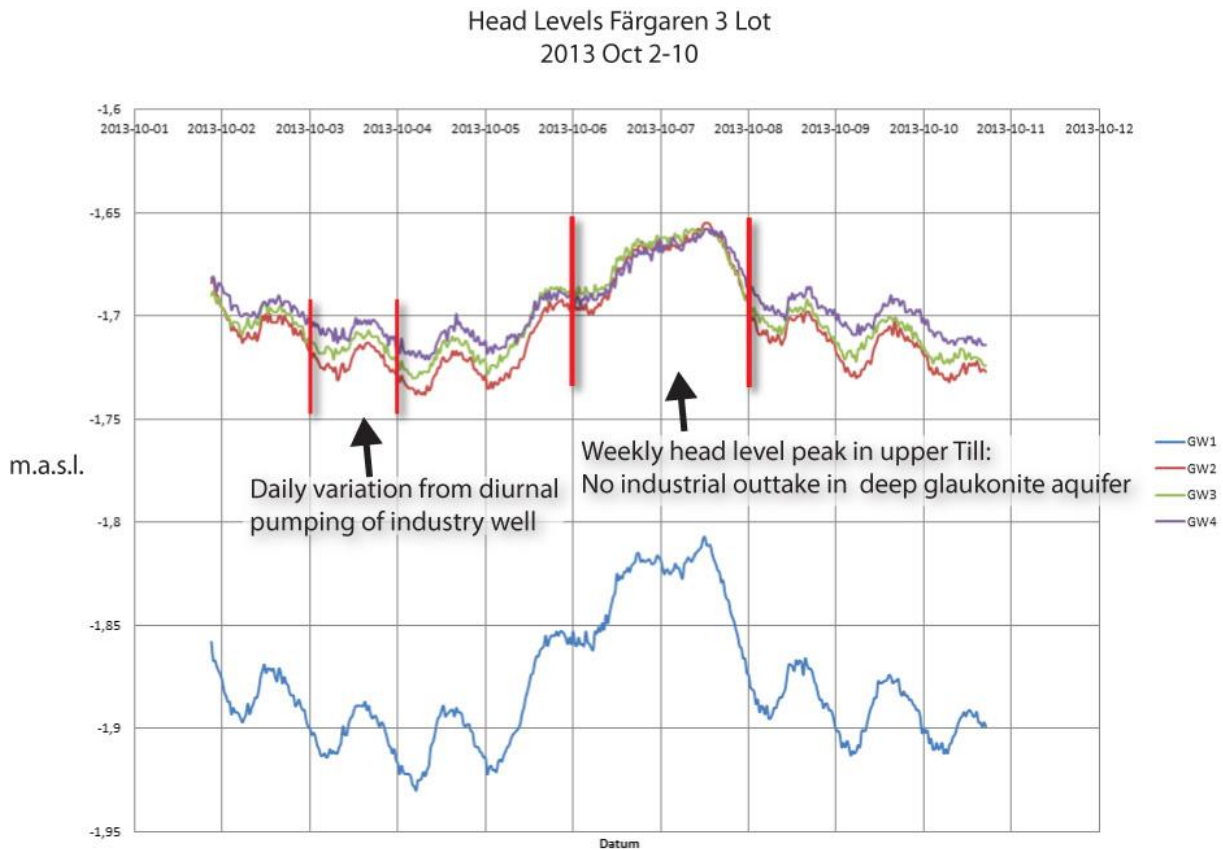


Figure 47. Table showing groundwater levels recorded by four diver logs (meters above sea level) placed in four wells in the Färgaren 3 field site during this thesis survey. There is a diurnal and weekly cycle correlating with industrial outtake in the deep glauconite aquifer. The well depth filters are GW1: 24 m (below surface), GW2: 9 m, GW3: 21 m, GW4: 14 m (Johansson et.al 2013).

There is a nightly and weekly pressure correlation between the shallow groundwater of the till and the industrial outtake from the 100 m deep well in the glauconite aquifer (south of the extended field site). This rapid response which was originally noted using divers in Engdahl et.al. 2011, and further explored through test pumping in Johansson et.al 2013, shows that there is a close connection between the shallow groundwater in the till and the deep glauconite aquifer.

### 9.1 Decontamination and future plans for Färgaren 3

Decontamination is estimated to begin sometime in 2014 (Engdahl et.al. 2011). It will likely consist of a sheet piling (retaining wall) and excavation of the upper meters of most heavily polluted soil, with a supplementary in situ sanitation of PCE that is already dissolved in the identified groundwater pollution plume.

The field studies made on behalf of the municipality have placed a large effort on mapping the bedrock surface below the Färgaren 3 lot due to PCE's tendency to sink vertically through soil layers.

It is uncertain how much the apparent bedrock depression in the heavily contaminated western part of the lot will affect the planned decontamination. It is possible that the shallower loose fragments of bedrock may also have acted as vertical boundary for the PCE contaminants.

The lack of deeper samples and logs to draw conclusions from is due to the high cost and time effort of drilling in the deeper sections in the site. One complication was that loose material in the cores collapsed which made interpretation difficult (Engdahl et.al. 2011).

### **9.2 3-D ERT and infrastructure: Färgaren 3 and Apennine (Italy)**

The article "Three-dimensional Electricity Resistivity Tomography to control the injection of expanding resins for the treatment and stabilization of foundation soils" (Santarato et.al. (2011)) includes examples from one case study in Italy and describes the use of time lapse (repeated measurements over time showing changes in resistivity over time) 3-D ERT to map the replacement of pore water with injected polyurethane resin in soils. The resin functions as a soil stabilizer around building foundations and is characterized by a very high electrical resistivity through which it can be detected in the measurements.

The survey records the soil pore stabilization of a stress-fractured two story residential building in the northern Apenninic foothills (northwestern Italy). The authors conclude that they have developed a methodology for subsurface 3-D ERT to accurately map and track a highly resistive polyurethane substance using time lapse inversion. The article mentions several considerations that should be made specifically regarding surveying around infrastructure. It was possible to apply non-invasive electrode arrays in obstructive environments to provide accurate "on-the-fly" optimization of resin injection for restoration work.

#### ***9.2.1 Urban surveying and alternate geophysical methods***

Though Santarato et.al. (2011) favor ERT as the "fast, non-invasive, three-dimensional monitoring approach" they also mention seismic and ground penetrating radar (GPR) as possible survey methods for monitoring the resin distribution. They make some observations about the main disadvantages: Full seismic 3-D processing requires a lot of computational power and risks severe noise from nearby foundation structures. GPR primarily does not have sufficient penetration ability through high conductivity soils such as clays.

In the Färgaren 3 survey, the biggest concern of the ERT method has been electrical interferences and conductive underground structures which can degrade data quality. Infrastructure projects and contaminated areas tend to be in urban locations where there is large potential for electrical noise.

It is also not possible to separate adjacent materials that have the same resistivity. One example of this is the organic sediments overlying the clay in the wetlands (figure 33 ⑥, Line 2 in figure 26). They are known from previous surveys but their low resistivity due to their water content makes them indistinguishable from the clay in the survey models.

### *9.2.2 Three-dimensional ERT – Advantages and procedure*

2-D ERT is a widely used method for subsurface imaging, and has been used assessing soil stabilization and material consolidation. However Santarato et.al. 2011 stress that 2-D sections do not fully reflect complex 3-D subsurface variations of water content and porosity in foundation soils, requiring 3-D imaging. The complex geology evident in the 3-D Färgaren 3 model is a good example of the detail and breadth of information that 3-D modeling offers.

Santarato et.al. (2011) discusses procedures for urban geoelectrical surveys such as building sites where conventional array paths are often obstructed and impractical, similar to the survey lines used in the 3-D model at the Färgaren 3 field site. Bended (L, C, S or circular) paths allows for diagonal modeling through corners e.g. basements.

## **9.3 Observing and modeling PCE degradation in aquifers: Dover, Delaware (US)**

The article Natural Attenuation of Chlorinated Ethene Compounds (Clement et.al. 1999) describes simulating a tetrachloroethylene (PCE) contamination based on a field example.

A hydrogeological MODFLOW and an RT3D chemical transport model based on a contaminated site at the Dover Air Force Base, Delaware (US) was constructed. The pollutants originate from a longtime use of chlorinated aliphatics as solvents for military aircraft and equipment.

The RT3-D software was used to simultaneously simulate degradation and distribution of the chlorinated aliphatics in the model of the field site.

The article describes and discusses the procedure of defining a conceptual model and setting up boundaries and initial parameters based on the geology and water chemistry. The permeable soil in the area is c:a 12 meters deep consisting of mixed fractions ranging between silt to gravel (not unlike the till at the Färgaren3 field site). An impermeable clay layer at the Dover field site act as a lower boundary that prevents deeper PCE spreading.

Clement et.al. 1999 describes how the simulated spread of pollution plumes was compared and calibrated to observed data. The authors stress the difficulties with the parameterization of the complex multispecies reaction system involved. They suggest that these reaction pathways need to be understood and implemented in more detail to use the model for predictive purposes.

### *9.3.1 PCE degradation and Chloride – Färgaren Chemical Samples and Resistivity*

PCE and its derivatives degrade through aerobic or anaerobic dehalogenization (figure 1), processes which releases chloride. Depending on the environment there are also several secondary degradation pathways with different decay rates. The samples at the Dover field site showed high chloride concentrations of up to 30 mg/L. The simulated PCE degradation raised chloride levels to 20 mg/L above background levels (after 32 years).

Chloride concentrations increases in ranges of 20 mg/L could very well be visible and distinguished in resistivity profiles, although they would have to be separated from resistivity variations in geology during interpretation. The heterogeneous till at the Färgaren 3 site would make this extra difficult.

Background chloride levels from water samples at Färgaren 3 also seem to vary due to other factors (one analyzed water samples outside of the contamination plume had a chloride concentration of over 120 mg/L) (Appendix F).

## 10 Conclusions

Geoelectrical field surveys at the heavily polluted Färgaren 3 lot field site and surrounding area in Kristianstad were conducted. A total of 22 electrical resistivity tomography (ERT) profiles was measured using a pole-dipole array. From these data a high resolution 3-D model and several deeper 2-D sections of induced polarization (IP) and resistivity were modeled in Res2Dinv and Res3Dinv. The resistivity models were generally very consistent when compared to borehole logs and it was possible to interpret the geology of the Färgaren 3 field site and surrounding area in high detail (e.g. flow impeding clay formations, undulations in the bedrock and withered areas).

There appeared to be a 60 meters wide depression in the limestone bedrock under the western part of the Färgaren 3 lot (figure 33). Initial borehole surveys (2008-2010) likely misinterpreted shallow loose bedrock fractions in the till of this area as the bedrock surface, and attempts at extracting intact deeper soil cores have been met with difficulty.

Samples from the western part of the Färgaren 3 lot show extremely high concentrations of the cancerogenic solvent Tetrachloroethylene (PCE) and other chlorinated aliphatics. PCE generally accumulates on low-permeable surfaces such as bedrock. An unexpected depression in the bedrock might have implications for the municipality's planned decontamination of Färgaren 3.

IP effects in the 3-D model indicate two major PCE soil concentrations in the western part of the Färgaren 3 lot, and an organic peat bed in the eastern section. The PCE IP effects correlate with the pollution sources of the previous dry cleaning facilities: spill from a large tank with concentrated PCE on the yard, and condensed PCE fumes accumulated under the exhaust pipes in the garden. These are illustrated on the historical orthophoto in figure 45.

3-D modeling of the data was required to obtain interpretable IP results. This is likely due to the "3-D effect" of the relatively weak IP responses in the 2-D models. Globally positioned 3-D data also allowed for intuitive visualization in relation to samples and pollution sources (e.g. figure 44 and 45).

The concentrations of PCE and its degradation products in groundwater of soil in the surrounding area were probably too small compared to other factors affecting resistivity or IP to be detected in the survey. There was electrical interference recorded from the frequency used by trains with rails approximately 1 km from the field site.

While the data acquisition is simple and effective, the procedure of processing and modelling 3-D data was time consuming and somewhat complicated. This will likely become more streamlined in the near future. There are alternatives to the Res3Dinv and e.g. Santarato et.al. (2011) describes a 3-D resistivity survey in similar conditions using "ERT Lab".

The extensive and accurate results from the Färgaren 2-D and 3-D models show the possibilities for urban ERT surveying as a non-intrusive, cost- and time-efficient method for subsurface imaging. ERT can be used in combination with traditional sampling methods to provide very extensive and detailed information about underground formations, greatly reduce the number of necessary boreholes, and guide a more effective placement of boreholes.

## 11 Acknowledgements

I would like to thank my supervisor Torleif Dahlin for the opportunity for doing the thesis and for his great patience and knowledge throughout the work. I would also like to thank my supervisors Lars Nielsen and Peter Knudegaard Engesgaard for their advice and support.

I thank Carl-Henrik Månsson whose hard work day and night made the field work possible, and Per-Ivar Olsson, Sara Johansson and Marcus Wennermark for their work and advice throughout the process of writing this thesis. I also thank Erik Dahlin, Henrik Kristoffersson and Björn Andersson for much appreciated field assistance.

Magnus Johansson and Tyréns in Kristianstad kindly lended usage of their garage for equipment storage during the field survey.

Finally I would also want to thank Susanne Weidemanis and Anders Bank who allowed us to conduct the survey on the Färgaren 3 lot, and shared background material which was essential to the interpretation of the resistivity and IP data.

## 12 References

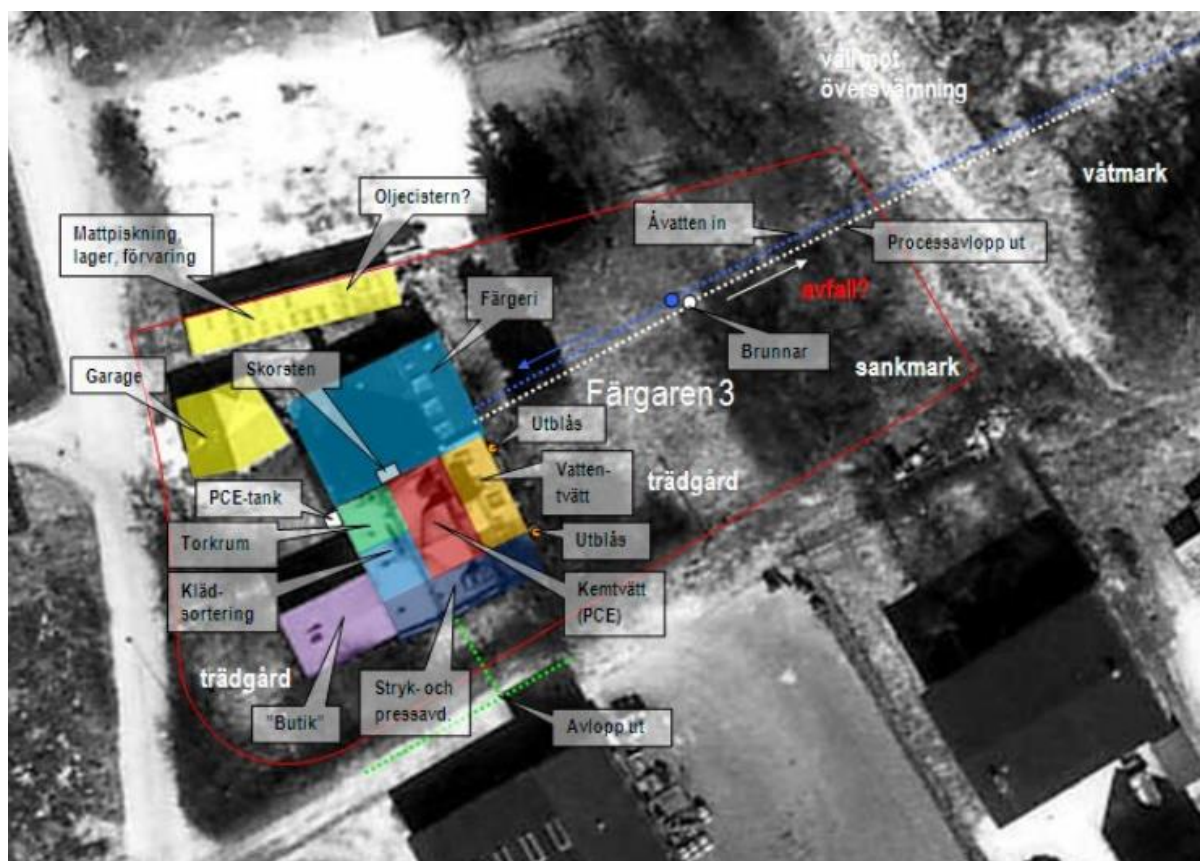
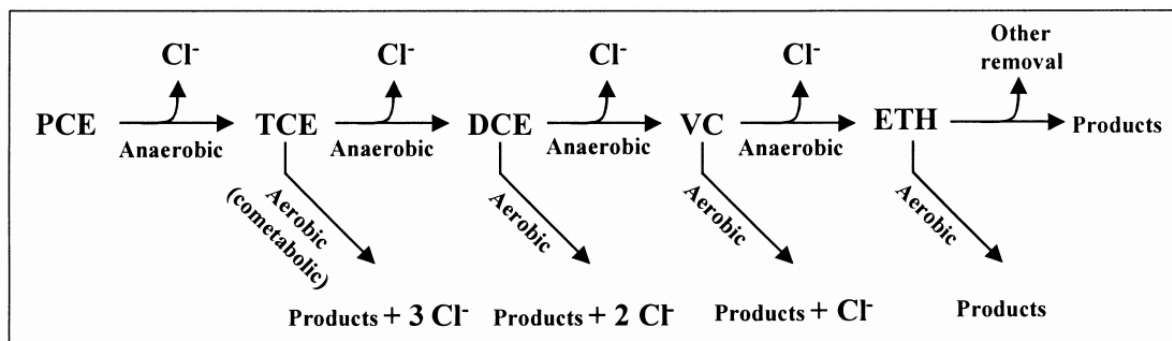
- ABEM Instrument AB (PDF). Terrameter LUND Imaging System, [www.abem.se](http://www.abem.se), version December 2013
- Agency for Toxic Substances and Disease Registry, Division of Toxicology and Human Health Sciences. 2013. Tetrachloroethylene UN# 1897 Material Safety Data Sheet. Atlanta, Georgia.
- Barker, R., 2004. The first use of geophysics in borehole siting in hardrock areas of Africa. Geological Society, Special Publications, vol. 225, issue 1, p 263-269
- Butler, D., 2005. Near Surface Geophysics. 1<sup>st</sup> ed. Society of Exploration Geophysicists. ISBN: 978-1560801306, 732 pp
- Christensen, W.K. 1984. The Albion to Maastrichtian of southern Sweden and Bornholm, Denmark; a review. Cretaceous Research 5, 313-327.
- Clement, P., Johnson, C., Sun, Y., Klecka, G., Bartlett, C., 1999. Natural attenuation of chlorinated ethane compounds: model development and field-scale application at the Dover site. Journal of Contaminant Hydrology 42, 2000, 113–140
- COWI (author not specified). 2013 (Work in progress). Färgaren 3 Kristianstad Resultatrapport Detaljerade Miljötekniska Undersökningar. Client: Kristianstad Municipality. Consult: COWI, Lyngby, Unpublished
- Dahlin, T., Leroux, V., 2012. Improvement in time-domain induced polarisation data quality with multi-electrode systems by separating current and potential cables. Near Surface Geophysics, 10(6), p.545-565
- Dahlin T., Rosqvist H., Leroux V. 2010. Resistivity-IP for landfill applications. First Break, 28(8), 101-105
- Dahlin, T., Zhou, B., 2004. A numerical comparison of 2D resistivity imaging with 10 electrode arrays. Geophysical prospecting, 52, p. 379-398.
- Engdahl, D., Larsson, N., Follin, S., Bank, A., 2010. Resultatrapport, fd Kemtvätt Färgaren 3. Report Number: 314881. Client: Kristianstad Municipality. Consult: Hifab AB, Stockholm. Unpublished.
- Engdahl, D., Larsson, N., Follin, S., Bank, A., 2011. Fördjupad riskbedömning och åtgärdsutredning, fd kemtvätt Färgaren 3. Report Number: 314881. Client: Kristianstad Municipality. Consult: Hifab AB, Stockholm. Unpublished.
- Fox, R., Hohmann, G., Killpack, T., Rijo, L., 1980. Topographic effects in resistivity and induced polarization surveys. Geophysics, Volume 45, 75-93.
- Furman, A., Ferré, T., Warrick, A., 2004. A Sensitivity Analysis of Electrical Resistivity Tomography Array Types Using Analytical Element Modeling. Vadose Zone Journal 2, p416-423.

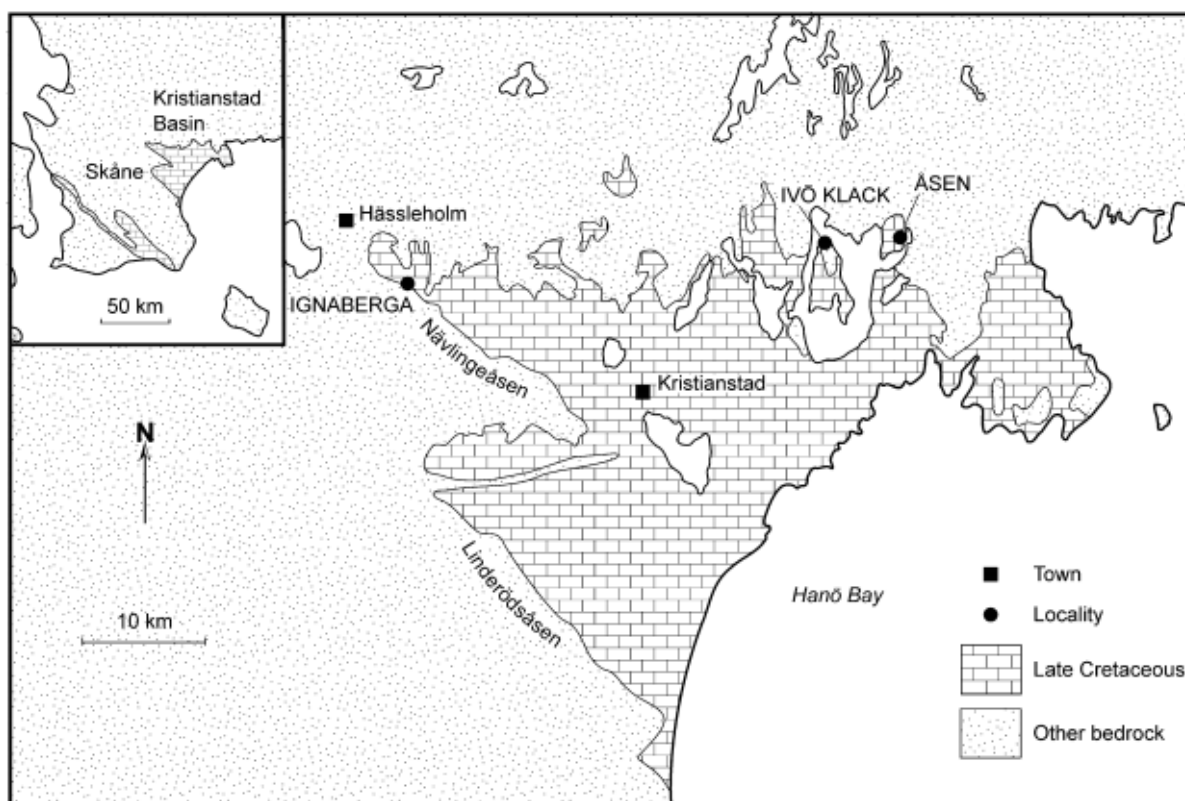


- Guha, N., Loomis, D., Grosse, Y., Lauby-Secretan, B., El Ghissassi, F., Bouvard, V., Benbrahim-Tallaa, L., Baan, R., Mattock, H., Straif, K., 2012. Carcinogenicity of trichloroethylene, tetrachloroethylene, some other chlorinated solvents, and their metabolites. *Lancet Oncology*, vol. 13, issue 12, p1192-1193.
- Gustafsson et.al 1979 – Gustafsson, O., Andersson, J.-E., De Geer, J., 1979. Sammanställning av hydrogeologiska data från Kristianstadsslätten. Sveriges Geologiska Undersökning. Rapporter serie C, Ca, RM.
- Johansson, M., Martinsson, S., Sundlöf, B., 2013. Provpumpning Färgaren 3. Report Number: 246236. Client: Kristianstad Municipality. Consult: Tyréns AB, Kristianstad. Unpublished.
- Knödel, K., Lange, G., Voigt, H.-J., 2007. *Environmental Geology: Handbook of Field Methods and Case Studies*. Ed: Bundesanstalt für Geowissenschaften und Rohstoffe. New York: Springer Berling Heidelberg. ISBN 978-3540746690.
- Lindgren, J., Siverson, M., 2002. *Tylosaurus ivoensis*: A giant mosasaur from the Early Campanian of Sweden. *Transactions of the Royal Society of Edinburgh: Earth Sciences*, 93:73–93.
- Loke, M., 2004 (PDF). Tutorial: 2-D and 3-D electrical imaging surveys, [www.geoelectrical.com](http://www.geoelectrical.com), version December 2013
- Länsstyrelsen Skåne. 2005. *Förorenade Områden* (PDF). [wp.renaremark.se](http://wp.renaremark.se)
- Menke, W., 1989. *Geophysical Data Analysis: Discrete Inverse Theory*. Academic Press, New York, ISBN: 0 12 490921-3, 289 pp
- Nordin, A., 2014. *Lägesbeskrivning av arbetet med efterbehandling av förorenade områden*. Naturvårdsverket, Stockholm.
- Palacky, G., 1987. Resistivity characteristics of geologic targets. *Geosciences Journal*, 3, 138-144.
- Waxman, M., Smits, L., 1968. Electrical conductivities in oil-bearing shaly sands. *SPE Journal*, vol. 8, p. 107–122.
- Reynolds, J., 2011. *An introduction to Applied and Environmental Geophysics*. 2nd ed. Chichester: Wiley-Blackwell. ISBN: 978-0-471-485360
- Ringberg, B., 1991. *Beskrivning till jordartskartarn Kristianstad SO*. Sveriges Geologiska Undersökning. Ae 88.
- Santarato, G., Ranieri, G., Occhi, M., Morelli, G., Fischanger, F., Gualerzi, D., 2011. Three-dimensional Electrical Resistivity Tomography to control the injection of expanding resins for the treatment and stabilization of foundation soils. *Engineering Geology*, Volume 119, Issue 1-2, p 18-30
- Transparent Underground Structure. 2014. 2.1 Geoelektrisk Kartläggning för förundersökning av underjordisk infrastruktur i urban miljö. [www.trust-geoinfra.se](http://www.trust-geoinfra.se), version May 2013

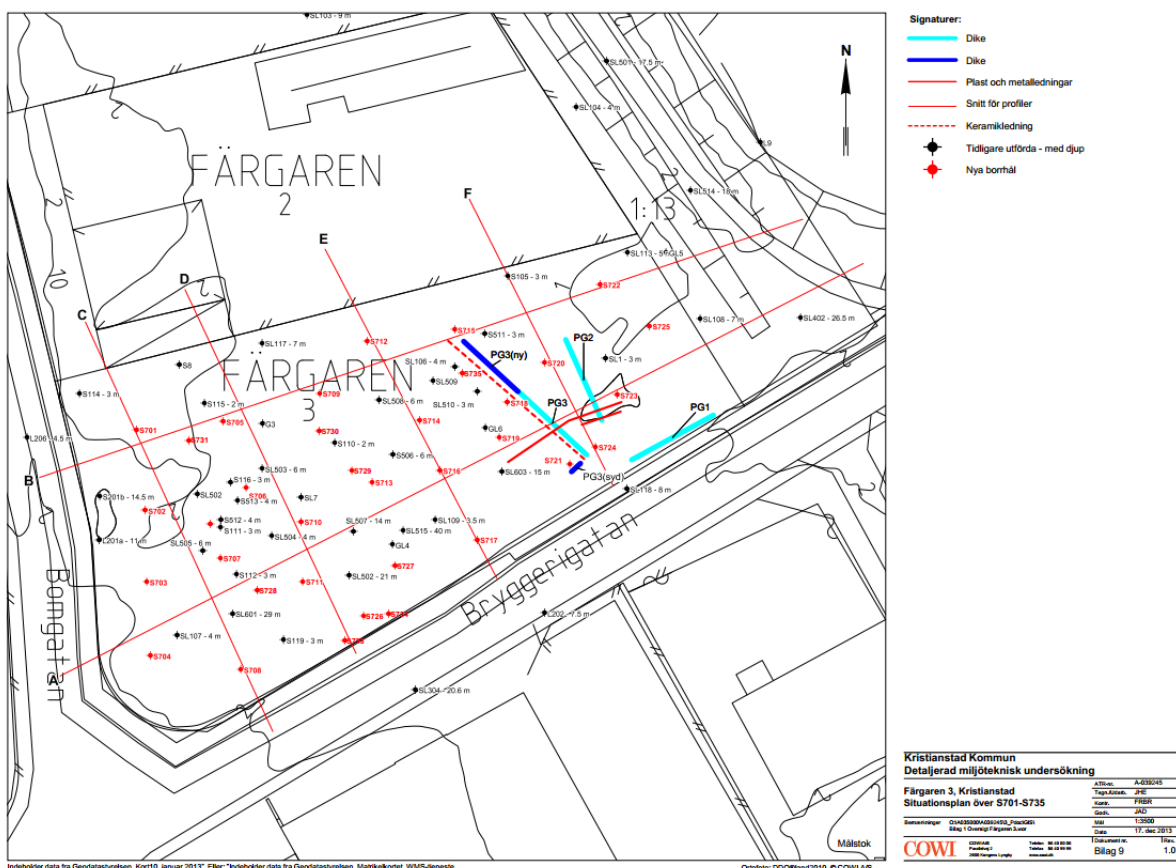
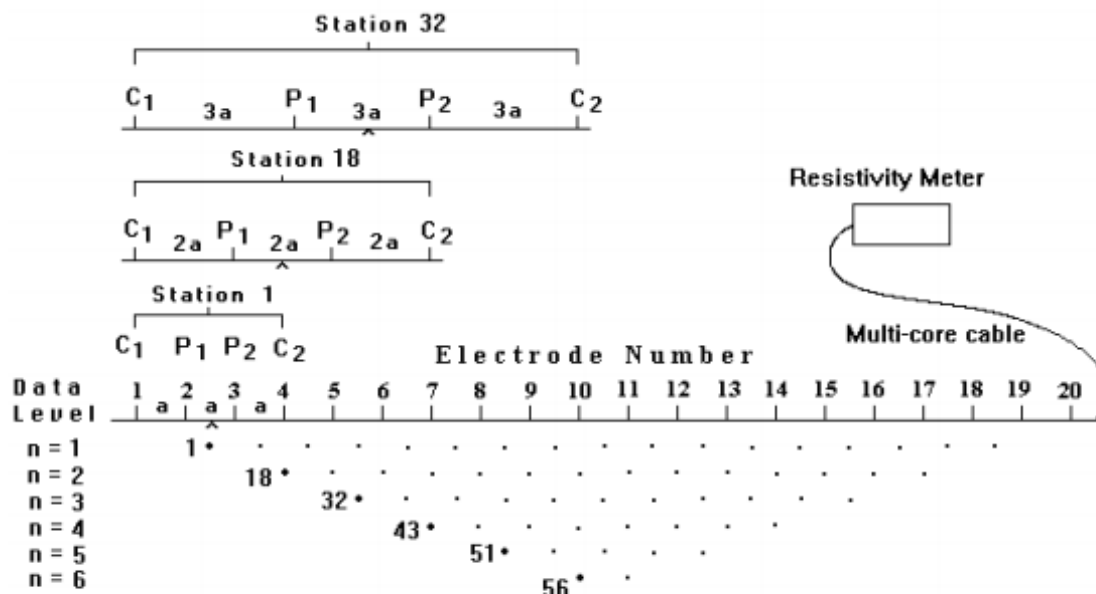
## Appendices

### Appendix A – Unmodified Figures













## Appendix B – Res2Dinv .dat file excerpt

Contains apparent resistivity data with added coordinates and topography.

```
FARGAREN2_PD84-7-21_2 Dag_3_GL - Notepad
File Edit Format View Help
PD84-7-21_2
2.5
11
6
Type of measurement (0=app.resistivity,1=resistance)
1
3354
2
1
Chargeability
mv/V
0.01 1.02
3 137.5 0 100 0 80 0 0.251138752 5.188582544
3 160 0 167.5 0 170 0 0.390957772 1.302129821
3 147.5 0 110 0 70 0 0.345283554 5.091002995
3 135 0 137.5 0 142.5 0 1.801326161 1.128319309
3 190 0 192.5 0 195 0 1.508981308 2.004071843
3 190 0 205 0 207.5 0 0.203995862 2.753344813
3 75 0 162.5 0 207.5 0 0.12762251 4.992893271
3 130 0 167.5 0 187.5 0 0.218691156 3.375338879
3 162.5 0 145 0 125 0 0.587760503 2.733290979
3 172.5 0 157.5 0 155 0 0.143356002 2.984396896
3 10 0 52.5 0 97.5 0 0.284851018 4.031975612
3 30 0 40 0 42.5 0 0.195166362 1.640037627
3 120 0 177.5 0 207.5 0 0.170842581 3.824280245
3 160 0 177.5 0 187.5 0 0.400407776 2.799298748
3 167.5 0 110 0 90 0 0.120819001 5.417362141
3 30 0 107.5 0 187.5 0 0.200876305 5.77952237
3 67.5 0 57.5 0 55 0 0.273483633 1.593159473
3 192.5 0 125 0 90 0 0.127189595 6.809069842
3 212.5 0 125 0 35 0 0.154175223 7.553140406
3 45 0 77.5 0 112.5 0 0.341830769 3.574964761
3 92.5 0 60 0 55 0 0.089247956 3.411352345
3 152.5 0 80 0 55 0 0.103225886 9.186277569
3 25 0 62.5 0 82.5 0 0.22453635 2.861272263
3 100 0 117.5 0 120 0 0.102366241 1.774391603
3 50 0 77.5 0 82.5 0 0.091050821 1.646548197
3 15 0 132.5 0 192.5 0 0.104201845 8.064095522
3 45 0 162.5 0 202.5 0 0.075145093 4.281725684
3 137.5 0 122.5 0 120 0 0.116141063 2.246996243
3 137.5 0 135 0 132.5 0 1.365597628 1.357930502
3 125 0 167.5 0 182.5 0 0.151249406 4.588301719
```



FARGAREN2\_PD84-7-21\_2 Dag\_3\_GL - Notepad

File Edit Format View Help

Topography in separate list

2  
84  
0  
7.33  
2.523661451 7.32  
5.068638538 7.031  
7.438892743 7.026  
9.908838694 7.044  
12.38528857 7.006  
14.92114858 6.997  
17.38573131 6.929  
20.04175842 6.929  
22.40005632 6.899  
24.95170637 6.876  
27.38129996 6.937  
29.9518855 6.92  
32.43447568 6.897  
35.02397814 6.942  
37.46552376 6.972  
39.94687621 6.893  
42.30342687 6.902  
44.84078169 6.902  
47.34302074 6.902  
50.06618177 6.908  
52.50982537 6.905  
54.99275025 6.961  
57.42315989 7.042  
60.00508882 7.058  
62.45066564 7.029  
64.92634156 7.159  
67.35042709 7.07  
69.77604866 7.13  
72.46880413 7.106  
74.9991869 7.044  
77.45469622 7.045  
80.11366011 7.099  
82.59704807 7.0495  
85.03765777 7.219  
87.48096926 7.17  
90.12479867 7.158  
92.49921629 7.215  
94.94687742 7.198  
97.64840828 7.211  
100.0568939 7.264  
102.706658 7.268  
105.28487 7.272  
107.7064608 7.314  
110.2077903 7.3524  
112.7108232 7.3396  
115.2221626 7.3652  
117.7254573 7.3268  
120.2089391 7.4036  
122.7094155 7.3908  
125.1911511 7.4164  
127.6952443 7.378  
130.1866953 7.442  
132.3921524 7.49  
134.9860857 7.525  
137.4814105 7.5634  
139.9885347 7.5442  
142.4860391 7.6018  
144.9754511 7.5826  
147.47402 7.621  
150.3025335 7.623  
152.4973889 7.668  
155.0795171 7.663  
157.6089334 7.75  
160.1899121 7.787  
162.4509501 7.823  
165.146664 7.827  
167.6364194 7.888  
170.1524874 7.949  
172.5210104 7.953  
175.317576 8  
177.6321357 7.947  
180.2349285 7.946  
182.6005713 7.947  
185.5513429 8.033  
187.5381454 8.115  
190.4409419 8.153  
192.8783504 8.211  
195.3050874 8.269  
197.5672078 8.377  
200.2826662 8.44  
202.5847059 8.503  
205.2779037 8.524  
207.5973198 8.567  
1  
Global coordinates present  
Number of coordinate points  
84  
Local Longitude Latitude  
0 190282.2185 6215257.796  
2.523661451 190283.6291 6215255.704  
5.068638538 190285.041 6215253.606  
7.438892743 190286.597 6215251.818

## Appendix C – 2D Inversion Settings

### Inversion settings

Initial damping factor (0.01 to 1.00)

0.1500

Minimum damping factor (0.001 to 0.75)

0.0200

Line search option (0=Never, 1=Sometimes, 2=Always)

2

Convergence limit for relative change in RMS error in percent (0.1 to 20)

5.0000

Minimum change in RMS error for line search in percent (0.5 to 100)

0.5000

Number of iterations (1 to 30)

10

Vertical to horizontal flatness filter ratio (0.25 to 4.0)

1.0000

Model for increase in thickness of layers(0=default 10, 1=default 25, 2=user defined)

2

Number of nodes between adjacent electrodes (2 or 4)

2

Flatness filter type, Include smoothing of model resistivity (0=model changes only,1=directly on model)

1

Reduce number of topographical datum points? (0=No,1=Yes. Recommend leave at 0)

0

Carry out topography modeling? (0=No,1=Yes)

1

Type of topography trend removal (0=Average,1=Least-squares,2=End to end)

0

Type of Jacobian matrix calculation (0=Quasi-Newton, 1=Gauss-Newton, 2=Mixed)

1

Increase of damping factor with depth (1.0 to 2.0)

1.1000

Type of topographical modeling (0=None, 1=No longer supported so do not use, 2=uniform distorted FEM, 3=underwater, 4=damped FEM, 5=FEM with inverse Swartz-Christoffel)

0

Robust data constrain? (0=No, 1=Yes)

1

Cutoff factor for data constrain (0.0001 to 0.1)

0.0500

Robust model constrain? (0=No, 1=Yes)

1

Cutoff factor for model constrain (0.0001 to 1.0)

0.0050

Allow number of model parameters to exceed datum points? (0=No, 1=Yes)

1

Use extended model? (0=No, 1=Yes)

0

Reduce effect of side blocks? (0=No, 1=Slight, 2=Severe, 3=Very Severe)

0

Type of mesh (0=Normal,1=Fine,2=Finest)

0

Optimise damping factor? (0=No, 1=Yes)

1

Time-lapse inversion constrain (0=None,1=Least-squares,2=Smooth,3=Robust)

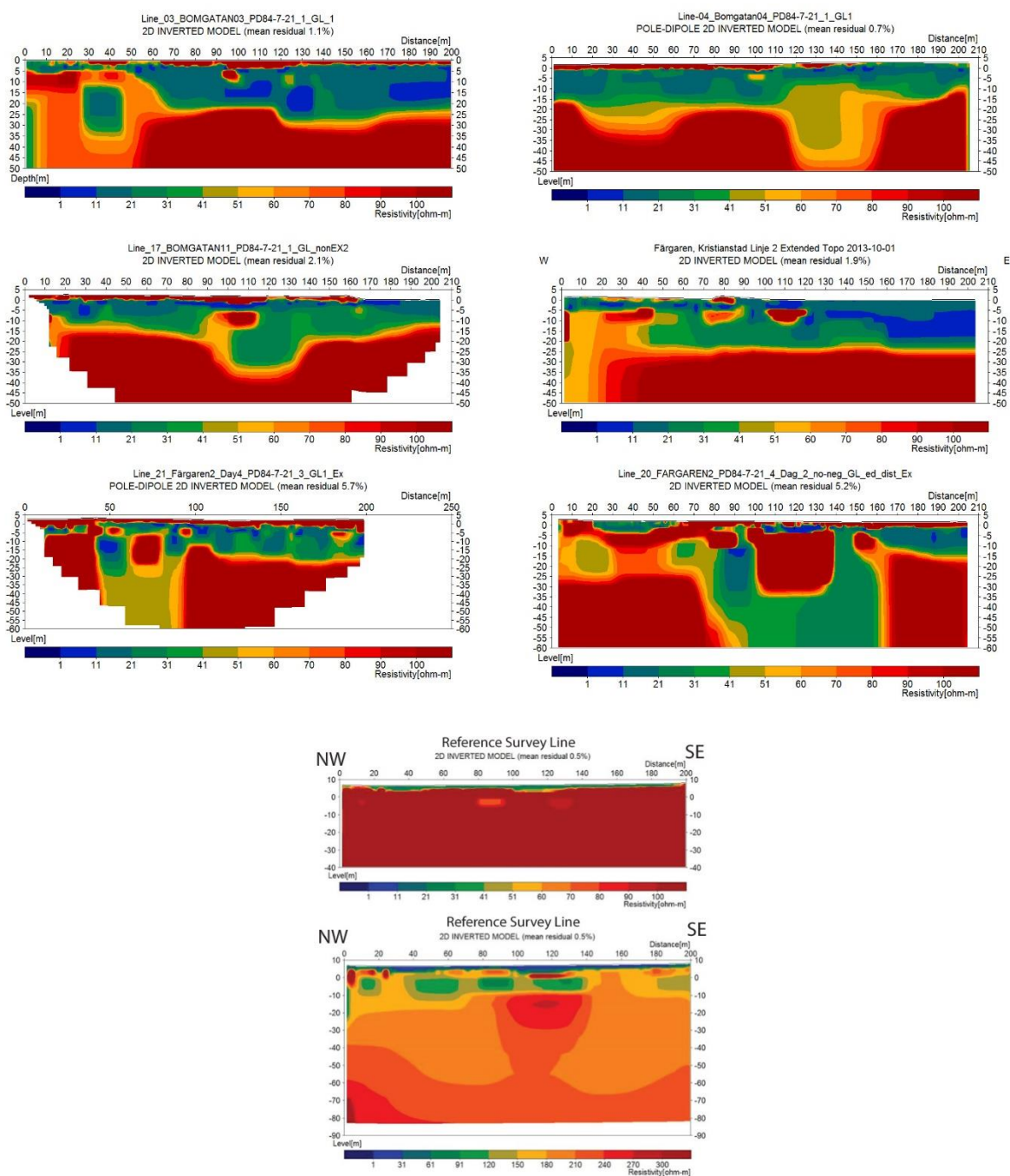
3

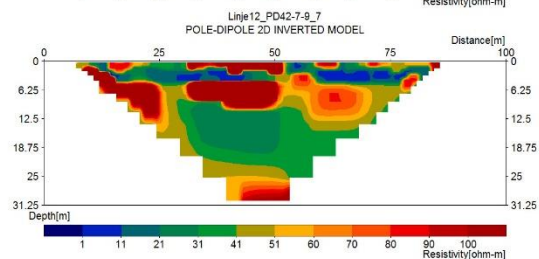
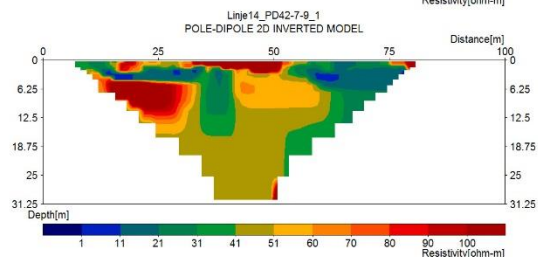
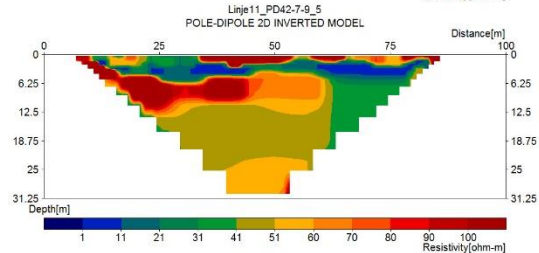
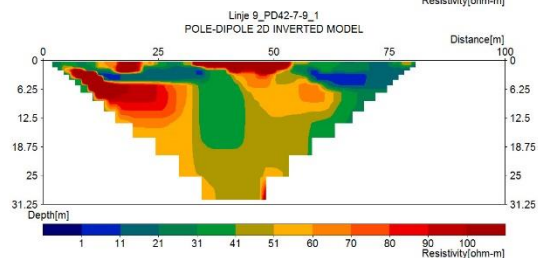
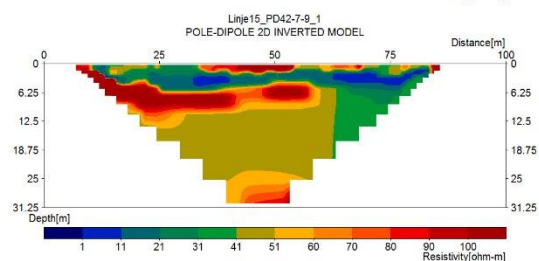
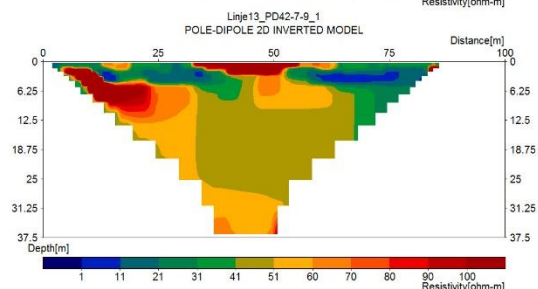
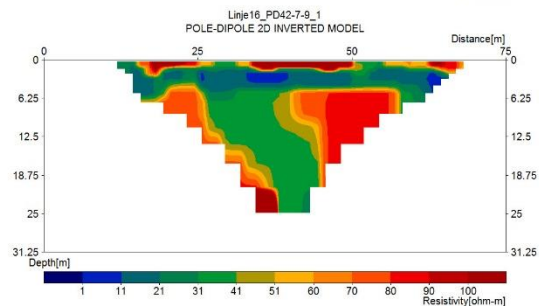
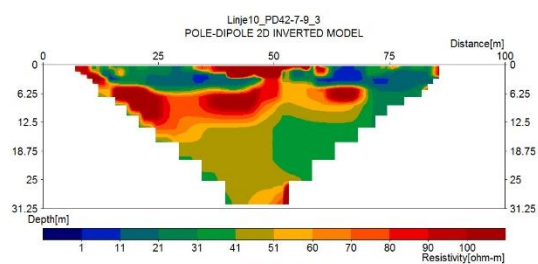
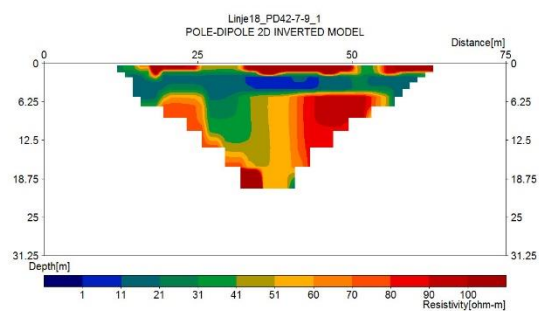
Type of time-lapse inversion method (0=Simultaneous,1=Sequential)

0  
 Thickness of first layer (0.25 to 1.0)  
 0.3750  
 Factor to increase thickness layer with depth (1.0 to 1.25)  
 1.2000  
 USE FINITE ELEMENT METHOD (YES=1,NO=0)  
 0  
 WIDTH OF BLOCKS (1=NORMAL WIDTH, 2=DOUBLE, 3=TRIPLE, 4=QUADRAPLE, 5=QUINTIPLE)  
 1  
 MAKE SURE BLOCKS HAVE THE SAME WIDTH (YES=1,NO=0)  
 1  
 RMS CONVERGENCE LIMIT (IN PERCENT)  
 0.050  
 USE LOGARITHM OF APPARENT RESISTIVITY (0=USE LOG OF APPARENT RESISTIVITY, 1=USE RESISTANCE  
 VALUES, 2=USE APPARENT RESISTIVITY)  
 0  
 TYPE OF IP INVERSION METHOD (0=CONCURRENT,1=SEQUENTIAL)  
 0  
 PROCEED AUTOMATICALLY FOR SEQUENTIAL METHOD (1=YES,0=NO)  
 0  
 IP DAMPING FACTOR (0.01 to 1.0)  
 0.250  
 USE AUTOMATIC IP DAMPING FACTOR (YES=1,NO=0)  
 0  
 CUTOFF FACTOR FOR BOREHOLE DATA (0.0005 to 0.02)  
 0.00010  
 TYPE OF CROSS-BOREHOLE MODEL (0=normal,1=halfsize)  
 0  
 LIMIT RESISTIVITY VALUES(0=No,1=Yes)  
 0  
 Upper limit factor (10-50)  
 50.000  
 Lower limit factor (0.02 to 0.1)  
 0.020  
 Type of reference resistivity (0=average,1=first iteration)  
 0  
 Model refinement (1.0=Normal,0.5=Half-width cells)  
 0.50  
 Combined Combined Marquardt and Occam inversion (0=Not used,1=used)  
 0  
 Type of optimisation method (0=Gauss-Newton,2=Incomplete GN)  
 2  
 Convergence limit for Incomplete Gauss-Newton method (0.005 to 0.05)  
 0.005  
 Use data compression with Incomplete Gauss-Newton (0=No,1=Yes)  
 0  
 Use reference model in inversion (0=No,1=Yes)  
 1  
 Damping factor for reference model (0.0 to 0.3)  
 0.01000  
 Use fast method to calculate Jacobian matrix. (0=No,1=Yes)  
 1  
 Use higher damping for first layer? (0=No,1=Yes)  
 1  
 Extra damping factor for first layer (1.0 to 100.0)  
 5.00000  
 Type of finite-element method (0=Triangular,1=Trapezoidal elements)

1  
 Factor to increase model depth range (1.0 to 5.0)  
 1.050  
 Reduce model variations near borehole (0=No, 1=Yes)  
 0  
 Factor to control the degree variations near the boreholes are reduced (2 to 100)  
 5.0  
 Factor to control variation of borehole damping factor with distance (0.5 to 5.0)  
 1.0  
 Floating electrodes survey inversion method (0=use fixed water layer, 1=Incorporate water layer into the model)  
 1  
 Resistivity variation within water layer (0=allow resistivity to vary freely, 1=minimise variation)  
 1  
 Use sparse inversion method for very long survey lines (0=No, 1=Yes)  
 0  
 Optimize Jacobian matrix calculation (0=No, 1=Yes)  
 0  
 Automatically switch electrodes for negative geometric factor (0=No, 1=Yes)  
 1  
 Force resistance value to be consistent with the geometric factor (0=No, 1=Yes)  
 0  
 Shift the electrodes to round up positions of electrodes (0=No, 1=Yes)  
 0  
 Use difference of measurements in time-lapse inversion (0=No, 1=Yes)  
 1  
 Use active constraint balancing (0=No, 1=Yes)  
 0  
 Type of active constraints (0=Normal, 1=Reverse)  
 0  
 Lower damping factor limit for active constraints  
 0.4000  
 Upper damping factor limit for active constraints  
 2.5000  
 Water resistivity variation damping factor  
 8.0000

## Appendix D – 2D Profiles





# Appendix E – Borehole Log Example

From Engdahl et.al. 2010

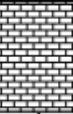
Resultatrapport, huvudstudie fd Kemtvätt Färgaren 3  
Kristianstads kommun

314881  
Bilaga 4

Beskrivning av borrhålets läge:  PID-mätning har skett inomhus.				Uppdragsnummer: 314481		Datum: 2009-06-09		borrhål nr:  SL402 1(2)			
				Uppdragsnamn: Färgaren 3, Kristianstad							
				Fältingenjör: Per Hübinette				Uppdragsledare: David Engdahl			
				Borrenprepnrör: Skånska Energi				Bormetod: Konv. ODEX			
Jordlagerföljd, egenskaper, kommentarer					Provtagning		Brunnsdata				
Djup (mumy)	Jordlagerföljd (skiss)	Jordart	Beskrivning och kommentarer	Nivå (mumy)	PID (ppm)	Brunnsinstallation (skiss)		Kommentarer (filtertag, täm etc)			
0											
		F; sa gr	Brun, torr		20			Läsbar däck			
		F; si sa	Brun, fuktig, organiskt material, ingen tydlig föroreningslukt								
2		F; sa si le	Grå, relativt torr, "lermoränkaraktär"								
					12						
4											
					19						
6											
		T	Mörkbrun, siltkaraktär		16						
8		si le	Grå, ngt vattenförande, osäker bedömn. geologi								
					11						
10		le	Grå, lös, "smäcklert"								
12											
14											
16											
18		Mn/B?	Nivå för övergång lösa jordlager till berg är osäker								
20		B	Kalksten, grå, vattenförande		7			2 m filter			
22					8						
								1 m filter			
24			fortsätter på sida 2		9						

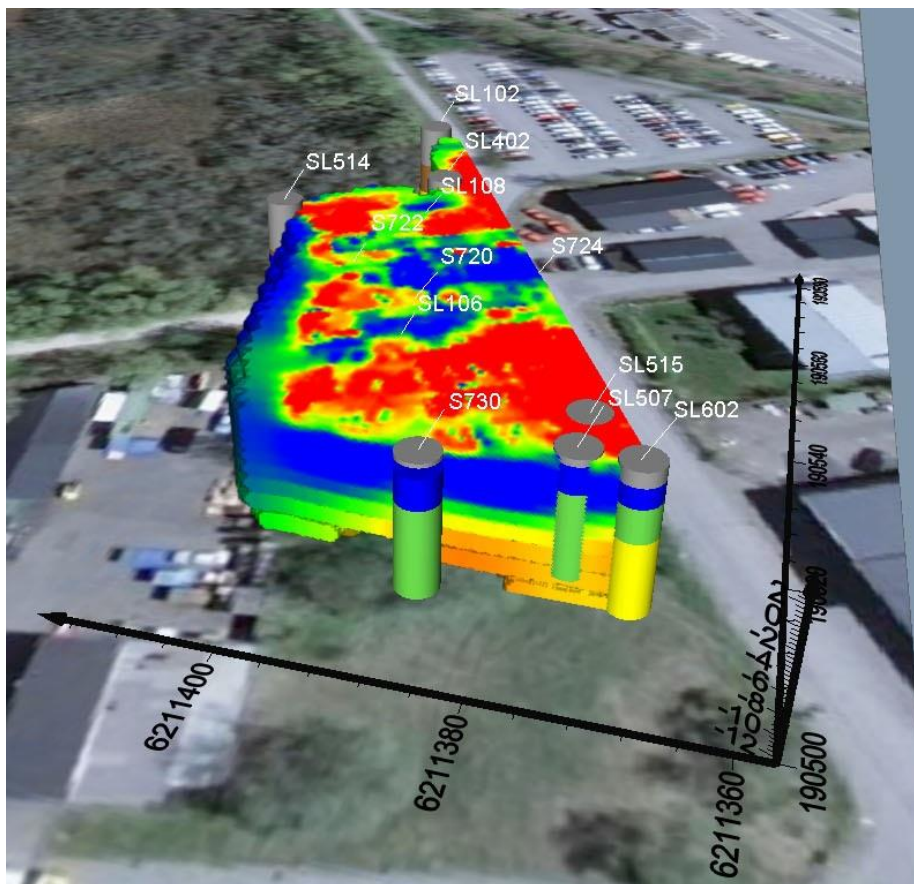
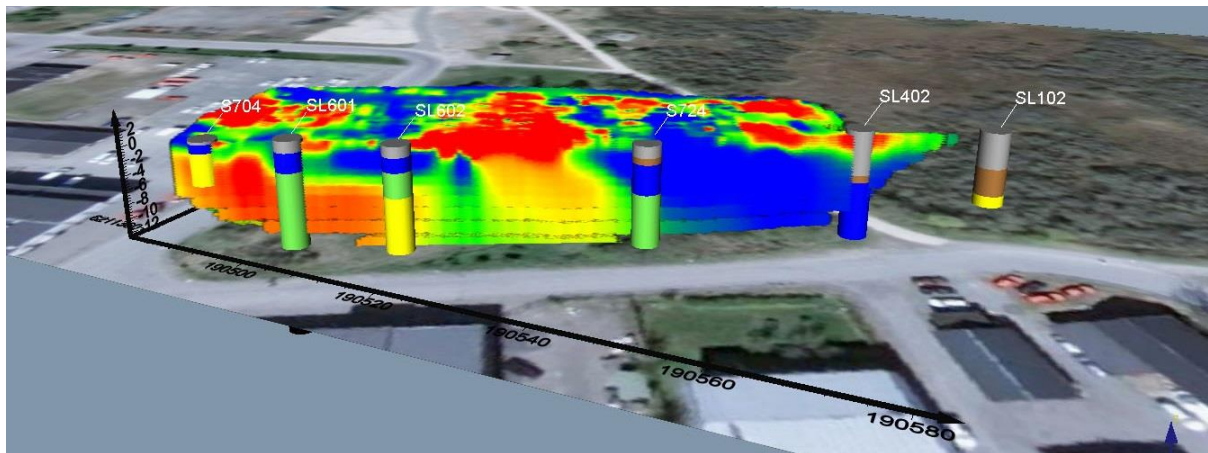
Hifab AB

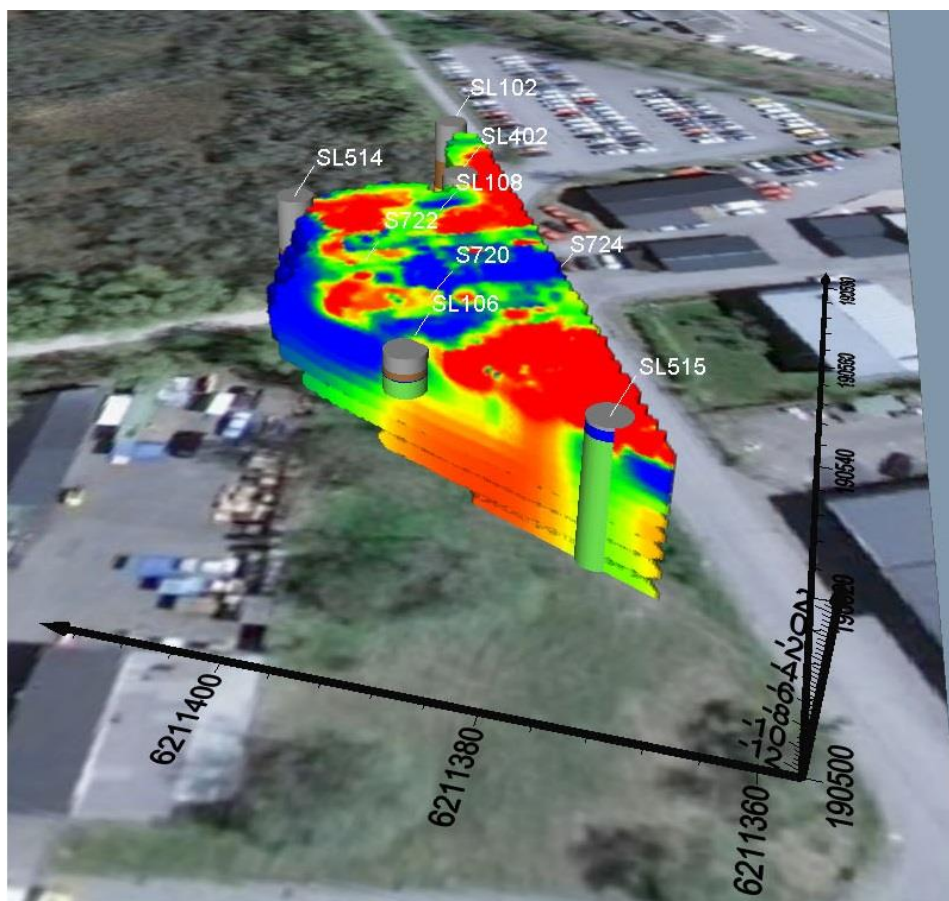
8 (12)

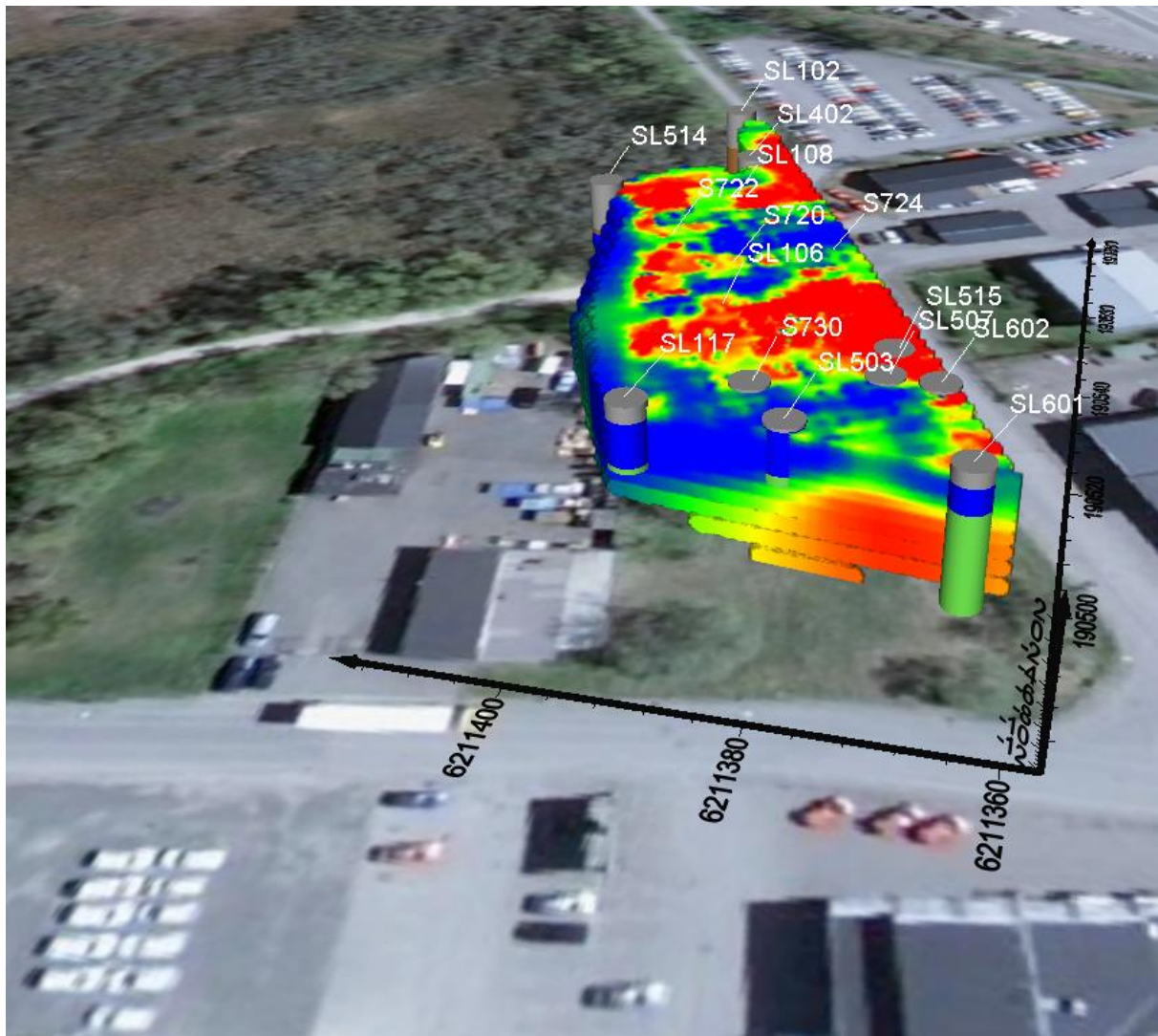
Beskrivning av borrhålets läge:  PID-mätning har skett inomhus.				Uppdragsnummer: 314481	Datum: 2009-06-09	Borrhål nr:  SL402 2 (2)	
				Uppdragsnamn: Färgaren 3, Kristianstad		Uppdragsledare: David Engdahl	
				Fältingenjör: Per Hübinette		Borremetod: Konv. ODEX	
				Borrentreprenör: Skånska Energi			
Jordlagerföljd, egenskaper, kommentarer				Provtagning		Brunnsdata	
Djup (mumy)	Jordlagerföljd (skiss)	Jordart	Beskrivning och kommentarer	Nivå (mumy)	PID (ppm)	Brunnsinstallation (skiss)	Kommentarer (filterlag, tätning etc)
24							
		forts.	forts.		9		forts.
26			Grå, sannolikt skikt med låg vattenföring		9		1 m filter
			26,5 m. Stopp i kalksten				
28							
30							
32							
34							
36							
38							
40							
42							
44							
46							
48							



Appendix F – Full 3D model images










# Appendix G – Chemical Analysis Excerpt

	A	B	C	D	E	F	G	H	I	J	K
1		Provnnummer	177-2013-10150213	177-2013-10150214	177-2013-10150215	177-2013-10150217	177-2013-10150218	177-2013-10150317	177-2013-10150318	177-2013-10150319	
2		Provtagningsdag	2013-10-14	2013-10-14	2013-10-14	2013-10-14	2013-10-14	2013-10-14	2013-10-14	2013-10-14	
3		Provpunkt	921456	921456	921456	921456	921456	921456	921456	921456	
4		Ankomstdag	2013-10-14	2013-10-14	2013-10-14	2013-10-14	2013-10-14	2013-10-14	2013-10-14	2013-10-14	
5		Provets märkning	SL 401	SL 302 4,5 m	SL 302 15 m	SL 402	SL 6018 m	SL 60114 m	SL 6037 m	SL 60312 m	
6											
7	Ämne	Ämnes-ID	Enhet								
8	Lukt, styrka, vid 20 °C	312000018037		ingen	svag	svag	svag	svag	svag	tydlig	
9	Lukt, art, vid 20 °C	312000018037		ingen	obestämd	obestämd	obestämd	obestämd	obestämd	järnliknande	
10	Turbiditet	312000011522	FNU	28	96	17	30	120	27	82	
11	Färg (410 nm)	312000011321	mg P/l	62	270	110	100	32	91	210	
12	pH	312000011516		7.1	6.6	7.5	7	7.2	7.4	7	
13	Alkalinitet	312000010878	mg HCO3/l	420	480	360	520	520	480	560	
14	Konduktivitet	312000011358	mS/m	120	100	73	130	100	120	160	
15	Klorid	312000011206	mg/l	84	120	57	61	49	84	78	
16	Sulfat	312000011208	mg/l	200	1.4	7.6	240	96	110	370	
17	Fluorid	312000011209	mg/l	0.47	< 0.20	0.5	0.45	0.6	0.42	0.37	
18	COD-Mn	312000006051	mg O2/l	2.5	9.4	1.7	4.3	2.4	2	5.7	
19	TOC	312000011522	mg/l	4.4	7.4	3.5	7.1	4.5	4.4	7.6	
20	DOC	312000011345	mg/l	4	5.8	3	7	4.3	3.5	7.1	
21	Ammonium	312000014852	mg/l	0.37	2.7	0.48	1.2	0.19	0.27	0.45	
22	Ammonium-nitrogen (NH4-N)	312000011044	mg/l	0.29	2.1	0.37	0.97	0.15	0.21	0.35	
23	Fosfat (PO4)	312000014852	mg/l	0.064	0.86	0.13	0.04	0.043	0.04	< 0.020	
24	Fosfatfosfor (PO4-P)	312000011320	mg/l	0.021	0.28	0.044	0.013	0.014	0.013	< 0.0050	
25	Nitrat (NO3)	312000014852	mg/l	< 0.44	< 0.44	< 0.44	< 0.44	< 0.44	< 0.44	< 0.44	
26	Nitrat-nitrogen (NO3-N)	312000011047	mg/l	< 0.10	< 0.10	< 0.10	< 0.10	< 0.10	< 0.10	< 0.10	
27	Nitrit (NO2)	312000014852	mg/l	< 0.0070	< 0.0070	< 0.0070	< 0.0070	< 0.0070	< 0.0070	< 0.0070	
28	Nitrit-nitrogen (NO2-N)	312000011202	mg/l	< 0.0020	< 0.0020	< 0.0020	< 0.0020	< 0.0020	< 0.0020	< 0.0020	
29	NO3/50+NO2/0.5	312000014852	mg/l	< 1.0	< 1.0	< 1.0	< 1.0	< 1.0	< 1.0	< 1.0	
30	Totalhärdhet (°dH)	312000013224	°dH	32					15	42	
31	Natrium Na (end surgjort)	312000013013	mg/l						120	60	
32	Natrium Na (uppslutet)	312000003262	mg/l	34	75	83	49	110	84	60	
33	Kalium K (uppslutet)	312000003271	mg/l	4.4	6.2	3.4	8.7	5.4	5.5	12	
34	Kalium K (end surgjort)	312000012937	mg/l						5.4	13	
35	Kalcium Ca (end surgjort)	312000012936	mg/l						32	260	
36	Kalcium Ca (uppslutet)	312000003271	mg/l	180	130	59	220	92	130	240	
37	Järn Fe (end surgjort)	312000012931	mg/l						10	12	
38	Järn Fe (uppslutet)	312000003271	mg/l	4.4	27	2	4.6	7.9	3.1	9.5	
39	Magnesium Mg (end surgjort)	312000012939	mg/l						11	20	
40	Magnesium Mg (uppslutet)	312000003262	mg/l	17	7	9.2	19	10	14	19	
41	Mangan Mn (end surgjort)	312000013005	mg/l						0.28	0.34	
42	Mangan Mn (uppslutet)	312000003262	mg/l	0.53	1.5	0.14	0.55	0.28	0.33	0.31	
43	Bor B (end surgjort)	312000016385	mg/l						0.082	0.22	
44	Bor B (uppslutet)	312000016385	mg/l	0.19	0.066	0.097	0.25	0.078	0.091	0.24	
45	Kisel Si (end surgjort)	312000013058	mg/l						10	10	
46	Kisel Si (uppslutet)	312000013059	mg/l	13	11	9.1	9	11	13	10	
47	Koppar Cu (uppslutet)	312000003271	mg/l	< 0.020	< 0.020	< 0.020	< 0.020	< 0.020	< 0.020	< 0.020	
48	Koppar Cu (end surgjort)	312000012939	mg/l					0.00027	0.00088		
49	Järn Fe (II)	312000000026	mg/l	2.3	14	0.11	2	0.76	0.12	5.3	
50	Brom Br	312000016384	mg/l	< 0.50	< 0.50	< 0.50	< 0.50	< 0.50	< 0.50	< 0.50	
51	Summa anjonekvivalenter	312000027202	mekv/l	13.4	11.2	7.71	15.3	11.8	12.6	19.1	
52	Summa kationekvivalenter	312000027203	mekv/l	13.1	10.3	7.39	15	10.3	11.6	17.8	
53	Totalhärdhet (°dH)	312000027596	°dH	30	19	10	36	15	22	38	